WL-TR-97-2011

THERMAL MANAGEMENT RESEARCH STUDIES
VOLUME 1 - ELECTRONICS COOLING

Rengasamy Ponnappan, Ph.D.
UES, Inc.
4401 Dayton-Xenia Road
Dayton, OH 45432-1894

18 November 1996

Final Report for the period: June 1991 - January 1996

Approved for Public Release; Distribution is Unlimited

AERO PROPULSION AND POWER DIRECTORATE
WRIGHT LABORATORY
AIR FORCE MATERIEL COMMAND
WRIGHT-PATTERSON AIR FORCE BASE, OH 45433-7251

NOTICE

USING GOVERNMENT DRAWINGS, SPECIFICATIONS, OR OTHER DATA INCLUDED IN THIS DOCUMENT FOR ANY PURPOSE OTHER THAN GOVERNMENT PROCUREMENT DOES NOT IN ANY WAY OBLIGATE THE US GOVERNMENT. THE FACT THAT THE GOVERNMENT FORMULATED OR SUPPLIED THE DRAWINGS, SPECIFICATIONS, OR OTHER DATA DOES NOT LICENSE THE HOLDER OR ANY OTHER PERSON OR CORPORATION; OR CONVEY ANY RIGHTS OR PERMISSION TO MANUFACTURE, USE, OR SELL ANY PATENTED INVENTION THAT MAY RELATE TO THEM.

THIS REPORT IS RELEASABLE TO THE NATIONAL TECHNICAL INFORMATION SERVICE (NTIS). AT NTIS, IT WILL BE AVAILABLE TO THE GENERAL PUBLIC, INCLUDING FOREIGN NATIONS.

THIS TECHNICAL REPORT HAS BEEN REVIEWED AND IS APPROVED FOR PUBLICATION.

JOHN E. LELAND
Project Engineer
Mechanical Branch

PHILLIP G. COLEGROVE
Chief
Mechanical Branch

MICHAEL A. MARCINIAK, Major, USAF
Deputy Chief
Aerospace Power Division

IF YOUR ADDRESS HAS CHANGED, IF YOU WISH TO BE REMOVED FROM OUR MAILING LIST, OR IF THE ADDRESSEE IS NO LONGER EMPLOYED BY YOUR ORGANIZATION PLEASE NOTIFY WL/ POOS WRIGHT-PATTERSON AFB OH 45433-7251 TO HELP MAINTAIN A CURRENT MAILING LIST.

Do not return copies of this report unless contractual obligations or notice on a specific document requires its return.

REPORT DOCUMENTATION PAGE

Form Approved
OMB No. 0704-0188

1. AGENCY USE ONLY *(Leave blank)*	2. REPORT DATE	3. REPORT TYPE AND DATES COVERED
	18 November 1996	Final June 1991 - January 1996

4. TITLE AND SUBTITLE

Thermal Management Research Studies Volume 1 - Electronics Cooling

5. FUNDING NUMBERS

C F33615-91-C-2104
PE-62203F
PR-3145
TA-20
WU-00

6. AUTHOR(S)

Rengasamy Ponnappan, Ph.D.

7. PERFORMING ORGANIZATION NAME(S) AND ADDRESS(ES)

UES, Inc.
4401 Dayton-Xenia Road
Dayton, OH 45432-1894

8. PERFORMING ORGANIZATION REPORT NUMBER

UES-255-TR-96-1
(Vol. 1)

9. SPONSORING/MONITORING AGENCY NAME(S) AND ADDRESS(ES)

Aero Propulsion and Power Directorate
Wright Laboratory
Air Force Materiel Command
Wright-Patterson AFB, OH 45433-7251
POC: John E. Leland, WL/POOS (937) 255-2922

10. SPONSORING/MONITORING AGENCY REPORT NUMBER

WL-TR-97-2011

11. SUPPLEMENTARY NOTES

The other volumes of this report are: Volume 2 - Rotating Heat Pipe (WL-TR-97-2002)
Volume 3 - Heat Pipe in High-G Environment: Analysis, Design and Testing (WL-TR-96-2128)

12a. DISTRIBUTION/AVAILABILITY STATEMENT

Approved for public release; distribution is unlimited

12b. DISTRIBUTION CODE

13. ABSTRACT *(Maximum 200 words)*

An innovative cooling concept called "venturi flow cooling" has been introduced and developed for potential use in the thermal management of the advanced high-power electronic devices. Single phase cooling medium is effectively used to create very high velocities in localized region of interest to improve heat transfer. Several different test apparatus have been built to investigate the heat transfer and flow phenomena. Using the venturi flow system and water, power devices, such as MCT and IGBT, were successfully tested at their rated current and frequency levels never possible with other cooling methods. Heat flux up to 257 W/cm^2 and heat transfer coefficient up to 13 W/cm^2 °C were demonstrated in this cooling system

This cooling technique is highly recommended for the future electronic cooling applications of the emerging more electric airplane systems involving very high intensity localized heat dissipation devices. This report presents the detailed descriptions of all aspects of this project.

14. SUBJECT TERMS	15. NUMBER OF PAGES
Electronics cooling, high-power electronic device, venturi cooling concept, high velocity flow, MCT, IGBT, CVD diamond wafer, load-cell, contact resistance, heat sink, localized heat dissipation	152
	16. PRICE CODE

17. SECURITY CLASSIFICATION OF REPORT	18. SECURITY CLASSIFICATION OF THIS PAGE	19. SECURITY CLASSIFICATION OF ABSTRACT	20. LIMITATION OF ABSTRACT
UNCLASSIFIED	UNCLASSIFIED	UNCLASSIFIED	SAR

TABLE OF CONTENTS

TABLE OF CONTENTS (CONT'D.)

TABLE OF CONTENTS (CONT'D.)

LIST OF ILLUSTRATIONS

LIST OF ILLUSTRATIONS (CONT'D.)

LIST OF ILLUSTRATIONS (CONT'D.)

LIST OF ILLUSTRATIONS (CONT'D.)

LIST OF TABLES

LIST OF APPLICABLE DOCUMENTS

AD1. Ponnappan, R.; Reyes, A.S.; and Beam, J.E., "Venturi Flow Cooling Concept for High Heat Flux Applications", Advances in Electronic Packaging ASME 1992, Vol. 1, pp. 143-151, ASME, New York, NY. pp. 225-234.

AD2. R. Ponnappan, and J.E. Beam, "A Novel Electronic Cooling Concept", SAE Paper No. 929478, Proc. 27th IECEC Vol. 2, pp 411-416, Aug 1992.

AD3. R. Ponnappan, J.E. Leland, W.S. Chang, and J.E. Beam,"Results of a Single Phase Venturi Flow", Proc. 6th International Symposium on Transport Phenomena in Thermal Engineering, Seoul, Korea, 9 - 13 May 1993.

AD4. R. Ponnappan, J.E. Leland, J.E. Beam, W.S. Chang, B.T. Nguyen, and J.A. Weimer, "Active Cooling of MCT Using Venturi Flow", 28th IECEC, American Chemical Society Paper No. 93457 Conf. Proc. Vol. 1 pp 769-776. 8 - 13 Aug 1993.

AD5. R. Ponnappan, and J.E. Leland, "Forced-Convection Heat Transfer in a Venturi-Type Annular Flow", Heat and Mass Transfer 94. Proc. of the 1st ISHMT-ASME Heat and Mass Transfer Conf. Ed. Balakrishnan and Murthy Tata-McGrawhill, New Delhi, India, 1994 pp 197-203.

AD6. V. Shanmugasundaram, R. Ponnappan, J.E. Leland, and J.E. Beam, "Conjugate Heat Transfer in Venturi-type Cooling System: Numerical and Experimental Studies", Paper No. AIAA 95-2114, 30th AIAA Thermophysics Conference, San Diego, CA, 19 - 22 June 1995.

AD7. R. Ponnappan, J.E. Leland, J.E. Beam, G. Fronista and J.A. Weimer, "Efficient Cooling of MCT and IGBT Using Venturi Flow," IECEC paper no. AP-87 ASME 1995. Proc. 30th IECEC Vol. 1, pp. 561-568, August 1995.

AD8. R. Ponnappan, J.E. Leland, W.S. Chang, J.E. Beam, B.T. Nguyen and J.R. Weimer, "Active Cooling of Metal Oxide Semiconductor Controlled Thyristor Using Venturi Flow," J. Propulsion and Power, Vol. 12, No. 2, pp. 398-404, March-April 1996.

AD9. R. Ponnappan, J.E. Leland, G. Fronista and J.E. Beam, "Influence of External Thermal Resistance on Forced Convective Cooling of Power Devices," 34th Aerospace Science Meeting and Exhibit, AIAA 96-0364, Jan. 15-18, 1996, Reno, NV.

FOREWORD

This final technical report was prepared as part of the contract deliverables under the "Thermal Management Research" contract F33615-91-C-2104. This contract was sponsored and administered by the Aero Propulsion and Power Directorate (APPD) of Wright Laboratory (WL) at Wright-Patterson Air Force Base (WPAFB). Dr. J.E. Leland was the Air Force Project Engineer/Technical Monitor at various stages of the program.

The present volume (Volume 1) outlines the research effort performed under Task 001: Electronics Cooling Study covering the venturi flow cooling setup development at APPD's Thermal Laboratory and steady state performance tests conducted using simulated electronics and actual power devices. The other volumes of the final report are:

Volume 2: Rotating Heat Pipe (Task 004) WL-TR-97-2002
Volume 3: Heat Pipe in High-G Environment: Analysis, Design and Testing (Task 002) WL-TR-96-2128

The technical material found in this volume under Sections 2.0 through 7.0 represents the historical progression of the research work and the evolution of various important ideas (from the basic concept to the ceramic heater, the heat concentrator and the actual electronic devices) that happened over the span of 4 years. Each section is written to be complete in itself and to reflect the overall development of the comprehensive venturi cooling concept. A certain amount of duplication in the text was inevitable. Some of the improvements or analyses done at the later stages might not be addressed in the sections describing the work done during the early stages.

The work described here was performed entirely on-site at the Thermal Laboratory (WL/POOS) by UES, Inc., Dayton, Ohio with Dr. R. Ponnappan as the Program Manager and Principal Investigator. Messrs. M. Streby (UES), J. Tennant (UES), M.D. Ryan (UES) and D. Reinmuller (WL) provided the technical support. UES' Materials and Processes Division, together with the corporate publication group, provided the administrative and documentation support. The author sincerely appreciates the services by Dr. Qun He, UES, Inc., in preparing this document.

1.0 INTRODUCTION

1.1 BACKGROUND

The development of high performance thermal systems for the current and future electronic equipment has stimulated interest in methods to enhance heat transfer [1]. There are ongoing research efforts to address the thermal problems generated by large number of small heat loads (each less than 10 W) but there is little work in progress to handle electronic components that generate high localized heat fluxes of the order of 100 W/cm^2 or more [2]. Advanced power conditioning devices require new solid state switching devices such as MCTs which can handle high currents at reasonably fast switching speeds. MCTs operate at current densities of 150-200 A/cm^2 over an active die area of <1 cm^2, resulting in a heat flux of over 400 W/cm^2. Although generally operated in a low duty cycle pulsed mode for inverters and motor controllers, the steady state heat levels for these devices will be in the 100 W/cm^2 range. If operated in a continuous mode, as a power control switch, a single MCT would generate a continuous heat load of 200 W or more [2].

For direct immersion cooling or flow through two phase cooling, Fluorinert (3M Company's) fluids are being widely considered by the electronic industry. Recent research results from the literature show that the highest heat flux (= critical heat flux) obtained in flow through boiling in curved channel using FC-72 is 141 W/cm^2 at $T_w = 92°C$ for direct contact simulated heat source [3] and 63 W/cm^2 at $T_w = 150°C$ for indirect contact actual MCT device [4]. Wadsworth and Mudawar [5] reported single phase FC-72 fluid jet impingement cooling heat flux of 80 W/cm^2 with jet velocity of 12.9 m/s and subcooling of 40°C. A CHF (two phase) value as high as 411 W/cm^2 was achieved by them using micro-groove surface enhancement in their research [5]. Even though the FC fluids have very good dielectric and thermophysical properties, they are expensive, volatile and absorbent of moisture and air. For typical applications, inexpensive fluids that are easily available are sought. Spray and jet impingement cooling are effective but relatively difficult to use. Also, the thermal instabilities associated with the spray and two-phase cooling techniques may discourage electronic packaging designers. A

simple, new approach called "venturi flow cooling concept" was introduced and some preliminary results were presented by the author [6,7].

1.2 SCOPE

The overall scope of this research task was to explore innovative cooling concepts for removing waste heat from advanced power electronic devices to be used in more electric airplane applications with very high power densities up to 200 W/cm^2 using single phase fluid flow operating in the temperature range of 0-150°C.

The specific objectives of this effort at various stages were as listed below:

1) Evaluate several available cooling fluids for use in high power systems in aircraft and select the most appropriate fluid;

   Design an experimental setup to demonstrate the feasibility of the venturi flow cooling concept with a goal to obtain a CHF of 200 W/cm^2 or higher using water first as a reference and then PAO coolant;

   Characterize the chosen fluid for heat transfer performance and establish a data base in order to provide sufficient data for the electronic packaging requirement;

2) Perform experiments in the venturi flow setup using water and ceramic strip heaters as simulated electronic devices;

   Investigate the heat transfer enhancement due to the venturi effect and compare with an equivalent system of simple pipe flow;

3) Extend the investigations mentioned in objective 2) to an improved test section involving a heat concentrator type heater design;

Corroborate the experimental results with existing heat transfer correlations for both Venturi and pipe (circular) flow cages;

4) Using the basic venturi flow setup and the modified test section, perform experiments with actual MCT device in electrical-conduction mode at maximum rated current flow;

Conduct the same electrical tests using pipe flow and commercial cold plate heat sinks and compare with venturi flow results;

5) Perform experiments on MCT and IBGT devices in high frequency switched-mode of operating using the venturi flow system;

6) Using the venturi system and the power devices, investigate the effects of external thermal resistances in mounting the devices to the heat sink;

Study the effects of contact pressure variation, electric insulators such as diamond wafer, Kapton film and thermal grease on the device's operating temperature.

2.0 VENTURI FLOW COOLING CONCEPT - DESIGN ANALYSIS

2.1 NOVEL CONCEPT

Venturi is a familiar term in fluid mechanics. Venturi flowmeter and venturi ejector pump use the converging and diverging nature of the flow. The suction effect of the throat is used in the venturi ejector pump for feed water pumping and the pressure drop across the throat is used in the venturi flowmeter for measuring flow rates. The flow velocity at the throat section is the highest. Basically, this feature is utilized here for localized cooling. The arrangement of the venturi is slightly different here. Flow through a straight circular tube is converted into a tapering annular flow by positioning a specially shaped "body of revolution" in the center of the tube directly in the flow path as shown in Figure l(a) and (b). High power dissipating devices are mounted on the flattened faces directly outside the tube at the throat section. Flow velocity at the throat can be increased beyond an order of magnitude over the upstream velocity.

Consequently, Re and Nu are increased for a given high Pr fluid ($5 < Pr < 100$). Boiling could be allowed locally at the throat (depending upon the constraints on the wall temperature and fluid properties) for further enhancing heat transfer. The idea of creating high flow velocity is the key to the success of this method. In addition, the effect is very localized to suit the localized heat source, characteristic to the MCT devices. Both direct and indirect mounting (with respect to the contact with the fluid) are feasible. By suitable design of the taper angles, the liquid pressure drop due to the venturi can be minimized. Viscosity is a major deciding factor in using this type of convective cooling as the pump power and viscous dissipation effects could outweigh the heat transfer enhancement.

The major features of the venturi flow cooling, in summary, are as follows:

1) Heat transfer coefficient enhancement using single phase flow of fluids such as PAO coolant, turbine oil, Fluorinert (FC) fluids and water. Two phase flow is possible when low temperature boiling fluids (FC) are used.
2) Very high localized (throat) fluid velocities, V = 20 to 40 m/s attainable easily.

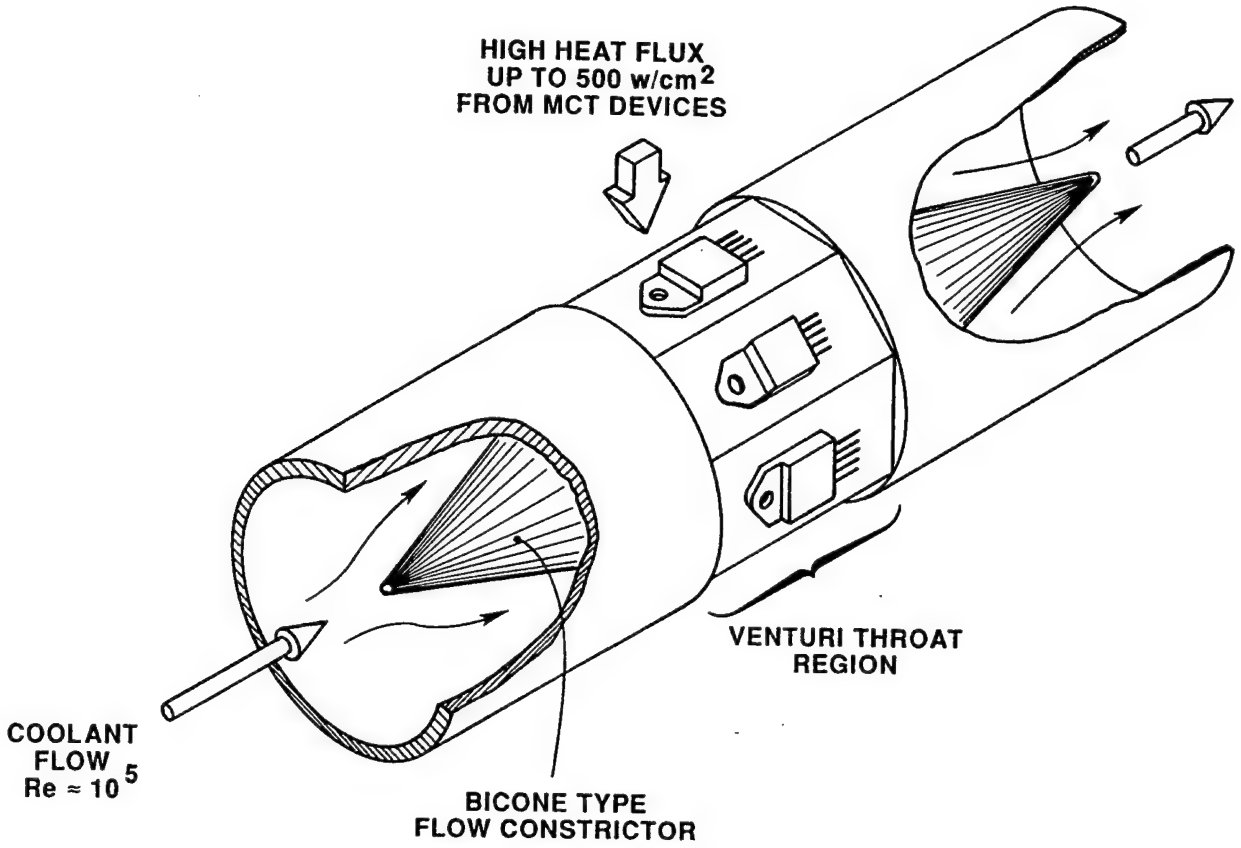

Figure 1 (a) Venturi Flow Cooling Concept - Conceptual Diagram.

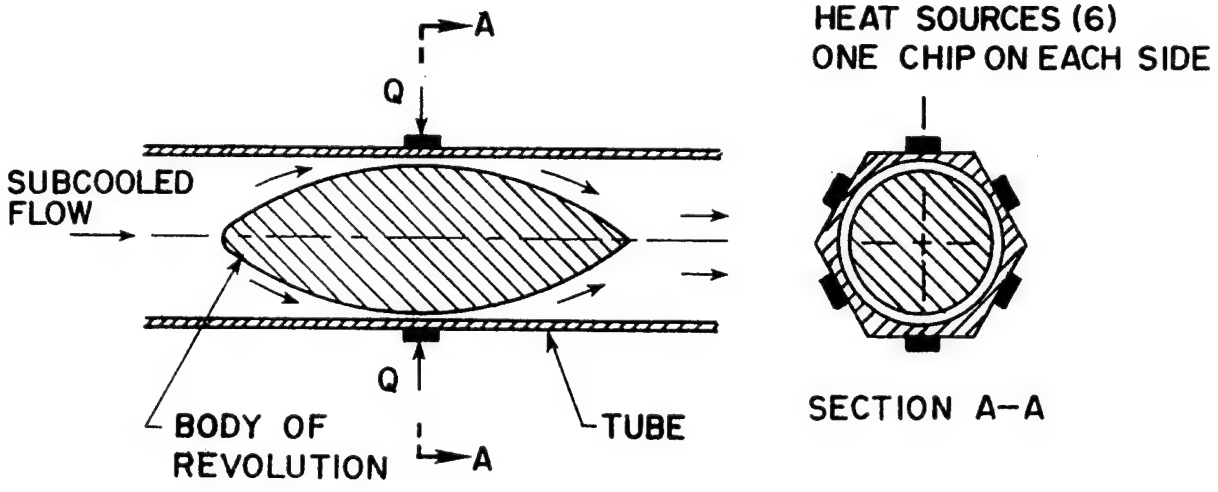

Figure 1(b). Venturi Flow Cooling Concept - Cross-Sectional Views.

3) High heat flux goals of 250 W/cm^2 (with simulated electronics heat dissipation and assuming a 45° spreading angle for wall conduction) practicable.

4) Heat flux values better than those possible for circular annulus and curved channel.

5) Heat transfer coefficient ($\bar{h}_c$) attainable is up to 30,000 W/cm^2°C with single phase flow.

2.2 ANALYSIS

2.2.1 Requirements of Electronic Cooling Application in Aircraft

The problem here is one of modeling and analyzing the flow and heat transfer aspects of the venturi flow. The requirements dictated by the aircraft electronic cooling application are:

1) The wall temperature simulating the device (MCT) temperature must be less than 150°C.

2) Fluid must be available onboard the aircraft.

3) Fluid temperature range of -40 - 100°C with a suitable primary coolant loop.

4) Prandtl number of the fluid in the operating temperature range is higher than 5.

2.2.2 Choice of Fluids

The coolant fluids considered for this application are: (1) Fluorinert (FC-72, 77, 87) fluids, (2) water (used for experimental simplicity), (3) turbine oil (MIL-L-7808J Ester based synthetic lubrication oil), and (4) PAO coolant (MIL-C-87252A dielectric cooling fluid). FC fluids are inert, dielectric and low boiling point fluids; but expensive and suffers high evaporation loss. Water is good for both single and two phase applications but it corrodes metals and freezes at 0°C. Both turbine oil and PAO coolant are used in aircraft and these fluids have high Pr. These two fluids are meant for single phase use only and their flash points are higher than the safe operating temperature of electronics. Relatively higher pumping power is required as their viscosities are higher compared to water and FC fluids. Typical property data for these fluids are listed in Table 1(a) and (b). Because of complexities in building test setup for FC fluids and turbine oil, only water and PAO coolant are chosen for investigation in this study.

Table 1(a). Property Data for Candidate Coolants

No.	PROPERTY AT 25°C		FC-72	WATER	TURBINE OIL MIL-L7808J	PAO MIL-C-87252A
1.	Boiling Point	°C	56	100	–	–
2.	Flash Point	°C	–	–	246	160
3.	Density, ρ	g/cm^3	1.68	0.997	0.94	0.789
4.	Thermal Conductivity, k	W/m °C	0.057	0.608	0.143	0.1725
5.	Specific Heat, Cp	J/g °C	1.0465	4.186	1.9256	2.2186
6.	Kinematic Viscosity, ν	m^2/s	0.4×10^{-6}	0.9×10^{-6}	18.0×10^{-6}	8.0×10^{-6}
7.	Dynamic Viscosity, μ	ns/m^2	0.672×10^{-3}	0.897×10^{-3}	16.92×10^{-3}	6.314×10^{-3}
8.	Prandtl Number, Pr	N.D.	12.34	6.18	227.8	81.2

Table 1(b). Selected Property Data for Turbine Oil and PAO Coolant

PROPERTY		TURBINE OIL MIL-L-7808J			PAO COOLANT MIL-C-87252A		
		25°C	40°C	100°C	25°C	40°C	100°C
1. ρ	g/cm^3	0.94*	0.930	0.890	0.7892	0.7793	0.7392
2. k	W/m°C	0.143*	0.1419*	0.1384	0.1725	0.169*	0.15424
3. Cp	J/g °C	1.9256*	1.9674*	2.135	2.2186	2.2437	2.4437
4. ν	m^2/s	18.0×10^{-6}*	12.0×10^{-6}	3.2×10^{-6}	8.0×10^{-6}*	5.4×10^{-6}*	1.65×10^{-6}
5. μ	Ns/m^2	16.92×10^{-3}	11.16×10^{-3}	2.848×10^{-3}	6.314×10^{-3}	4.208×10^{-3}	1.219×10^{-3}
6. Pr	N.D.	227.8	154.8	44.93	81.2	55.91	19.32
Flash Point		246°C			160°C		

*Extrapolated data

2.2.3 Convective Heat Transfer Solution

The venturi flow cooling can be modeled as a problem of forced convection through an annular tube with localized wall heat addition. Essentially, a single phase fluid flow through a circular tube converges to an annular flow at the throat section and then diffuses back to circular flow. Figure 2 shows the different parameters of the venturi flow and heat transfer model. In order to maximize the average heat transfer coefficient $\bar{h}_c$ at the throat region, the flow has to be turbulent and hence the Reynolds number at the throat (Re_t) has to be greater than at least 10^4 whereas the upper limit is set by the practical limitation of pumping capacity. Even though the converging nature of the flow damps the turbulence intensity at the throat, the increased velocity is expected to provide significant heat transfer enhancement.

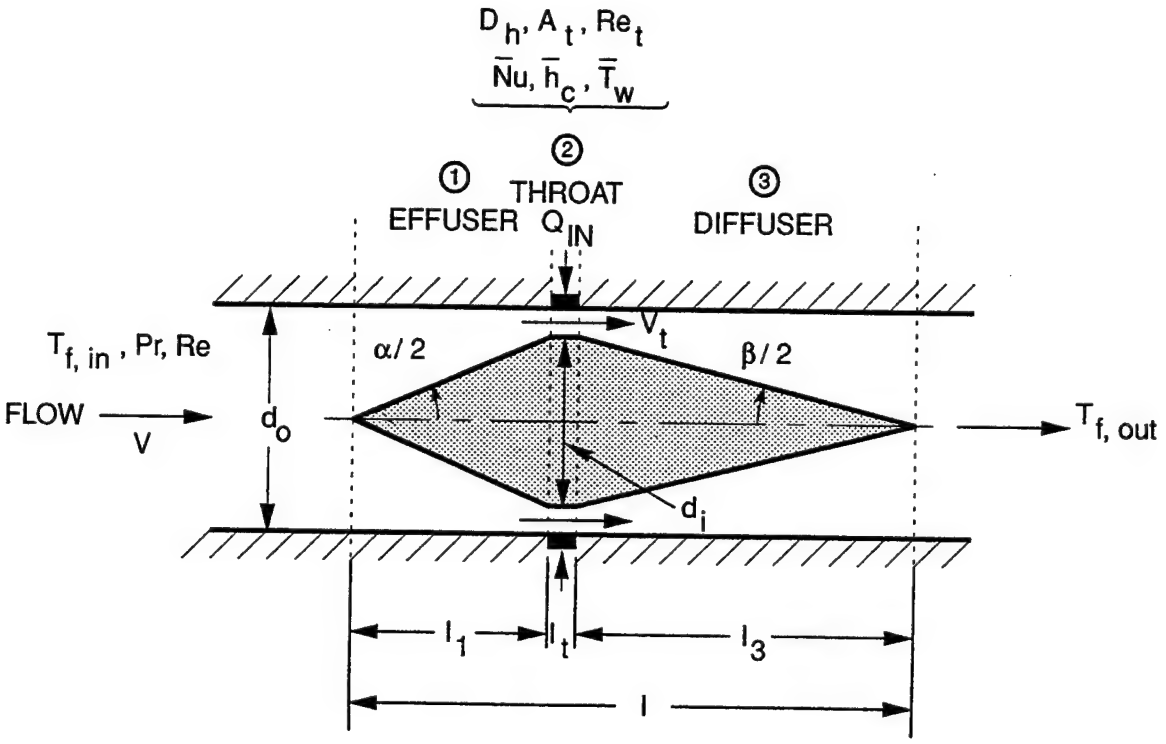

Figure 2. Flow and Heat Transfer Model Representation.

The steady state convective heat transfer from the wall to fluid is given by:

$$Q_o = Q_{in} - Q_L = \bar{h}_c A_e (T_w - T_{f,in}) \quad (1)$$

where T_w is the spatially averaged fluid side wall temperature and $T_{f,in}$ is bulk fluid temperature at the inlet to the venturi. An energy balance on the control volume of fluid at the throat region along with continuity equation for the upstream and downstream flow are,

$$Q_o = \dot{m}\, C_p\, (T_{f,out} - T_{f,in}) \quad (2)$$

$$\dot{m} = \rho A V = \rho A_t V_t \quad (3)$$

$$\text{Also, heat flux, } q = Q_o/A_e \text{ where } A_e = \pi d_o l_t \quad (4)$$

For simplicity, heat spreading due to wall-conduction is not considered here.

The dimensionless group of numbers pertinent to this problem are the upstream Re, throat Re, Pr and Nu which are defined as,

$$\begin{aligned} Re &= V\, d_o/\upsilon \quad ; \quad Re_t = V_t D_h/\upsilon \\ Pr &= \mu\, c_p/k \quad ; \quad Nu = \bar{h}_c D_h/k \end{aligned} \quad (5)$$

where $D_h = d_o - d_i$ = hydraulic diameter at throat region. The Nusselt number of a fully developed turbulent flow between parallel planes with constant rate of heat addition on one wall with the other wall insulated are given by Kays and Leung [8]. These values have been experimentally verified for air (Pr = 0.7) flow and are recommended for high Pr fluids also. Figure 3 shows the Kays and Leung results, namely Nu vs. Re for fully developed turbulent flow between parallel planes for $3 < Pr < 100$.

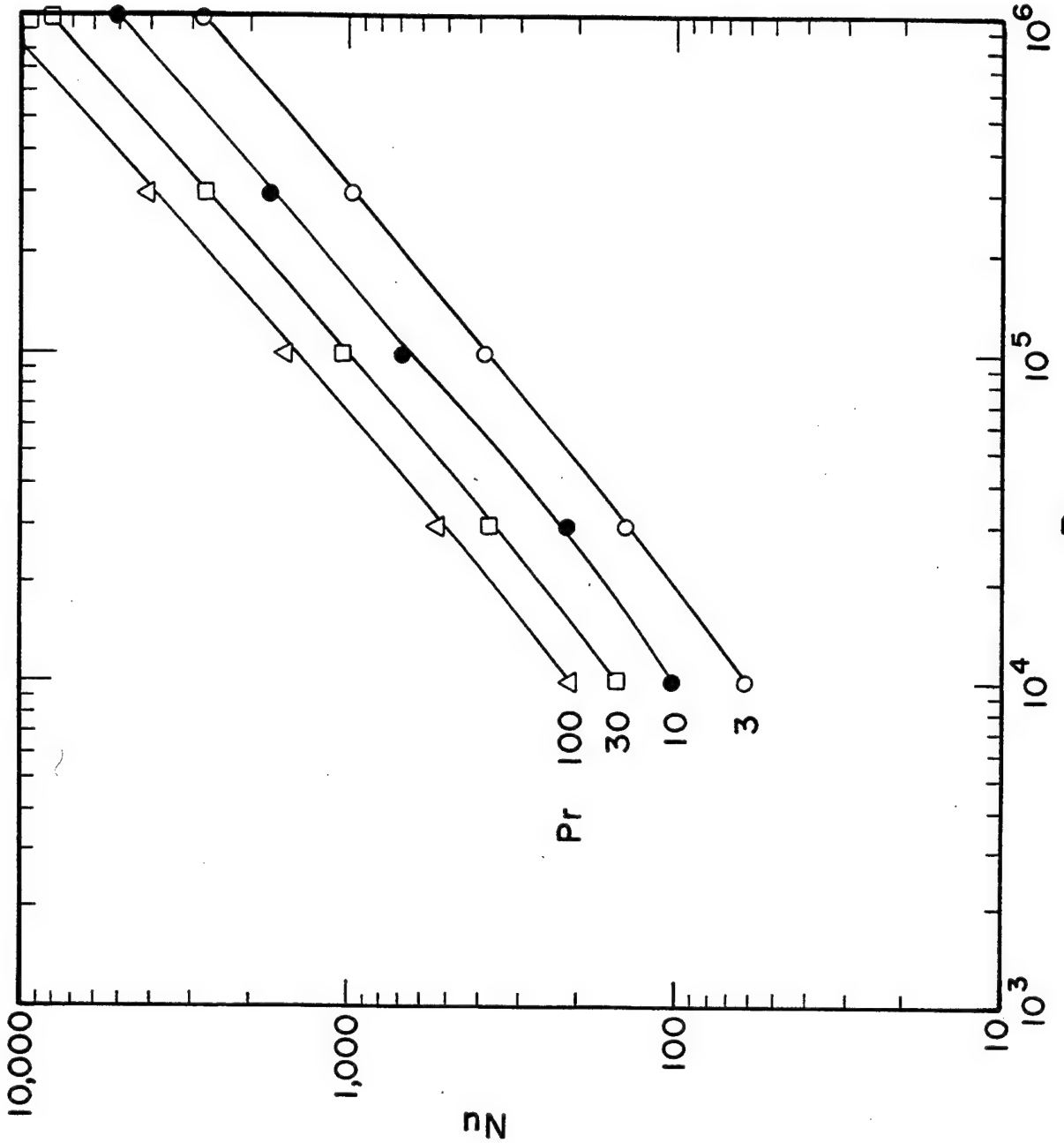

Figure 3. Nu vs. Re for Fully Developed Turbulent Flow Between Parallel Planes for 3<Pr<100.

Based on the heat flux requirement of electronic devices such as MCT and the Nusselt number solution, experimental parameters such as the physical dimensions, mass flow rate, Re, Re_t, ΔT_f, $\bar{h}_c$, etc., are determined. Typical heat transfer coefficients of practical electronic cooling systems using forced convection in existence are under 0.7 W/cm^2°C [1,4,9]. Hence, it became important to explore this new technique to augment heat transfer in electronic cooling.

2.2.4 Parametric Analysis

Based on the heat flux requirements (100-300 W/cm^2) of proposed high power electronics and the Nusselt number solution, experimental parameters such as the physical dimensions, mass flow rate, Re, Re_t ΔT_f, $\bar{h}_c$, etc., are determined.

The average heat transfer coefficient ($\bar{h}_c$) required to obtain a given heat flux for given fluid and ΔT_w is plotted for various fluids as shown in Figure 4. The useful temperature ranges for single phase operation of these fluids are shown as bar-graphs on the top portion of Figure 4 for ready reference only. The bar-graphs do not relate to the rest of the plots. Typical heat transfer coefficients of practical electronic cooling systems using forced convection in existence are under 0.7 W/cm^2°C as seen in Table 2. Hence, it is important to find new techniques to augment heat transfer in electronic cooling.

Table 2. Range of Heat Transfer Coefficients for Various Cooling Methods[a]

$\bar{h}_c$ = Heat Transfer Coefficient (W/m^{2}K)			
FLUID	MODE	RANGE	TYPICAL
Air	Free Convection	3 to 12	5
Air	Forced Convection	10 to 100	50
Fluorocarbon Liquid	Free Convection	100 to 300	200
Fluorocarbon Liquid	Forced Convection	200 to 2000	1000
Fluorocarbon Liquid	Boiling	2000 to 6000	4500
Water	Forced Convection	3000 to 7000	4500

[a]Data taken from Reference [1]

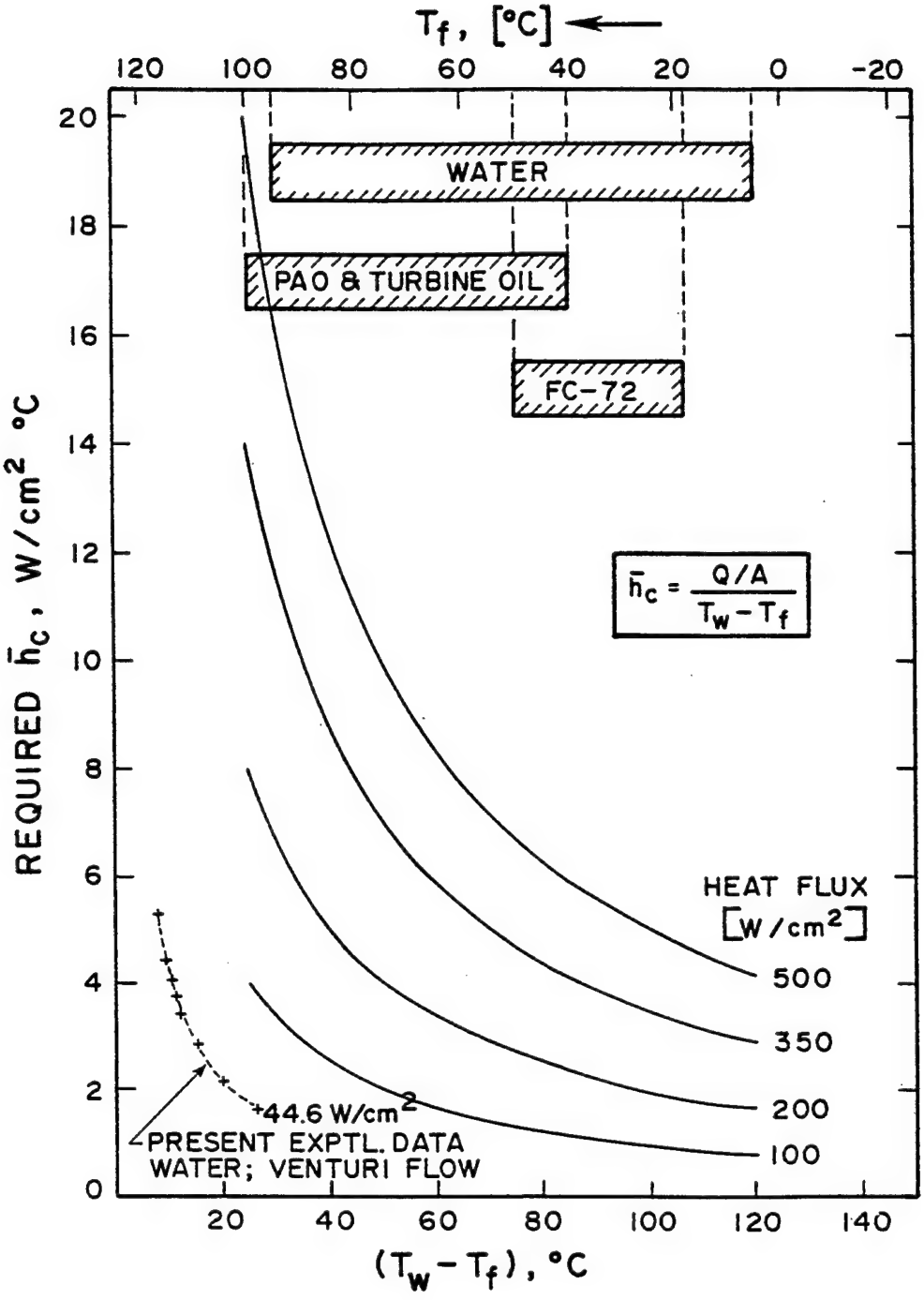

Note: The bar-graphs of T_f at the top are to illustrate the ranges of single phase operations of various fluids and do not directly relate to $\bar{h}_c$

Figure 4. $\bar{h}_c$ Required vs. T_w-T_f.

Volume flow rate required as a function of heat input for various fluids is calculated and plotted in Figure 5 using Eq. (2). The low rise in fluid temperature (ΔT_f) is assumed in order to minimize ΔT_w and maximize $\bar{h}_c$.

The design constraints of generating a 250 W/cm^2 heat flux using a wrap-around heater and velocity amplification at the throat ($V_t/V = 16.9$) leads to the selection of the tube diameter and hydraulic diameter. Accordingly, $d_o = 3.33$ cm and $D_h = 0.1$ cm are chosen. Now using the Nu values from Figure 3, possible $\bar{h}_c$ values are calculated for the candidate fluids as a function of Re_t and plotted in Figure 6. It can be seen from this graph that $\bar{h}_c$ of 3 W/cm^2°C could be achieved with the venturi flow concept using PAO coolant at 40°C and $Re_t = 10^4$. Experimental data from Gu, et al., [3] for FC-72 flow through boiling in a curved channel is plotted in Figure 6 for comparison. This shows that single phase flow through venturi can yield higher $\bar{h}_c$ than two phase flow in curved channel.

Flow rate versus Re for various fluids at the venturi throat as well as upstream are plotted for the chosen venturi dimensions in Figure 7. This chart provides the design point for selecting the pump size, once the cooling requirements ($\bar{h}_c$ and Re) are fixed.

2.2.5 Comparison of Pipe, Annular and Venturi Flows

Considering the three flow configurations illustrated in Figure 8, a comparison is made on their relative merits. For flow through circular tube of inner diameter, hydraulic diameter $D_h = d_o$.

Therefore, Nusselt number

$$Nu_1 = \frac{h_1 d_o}{k_1} \tag{6}$$

For annular flow through an annulus of diameters d_o and d_i,

$$Nu_2 = \frac{h_2 (d_o - d_i)}{k_2} \tag{7}$$

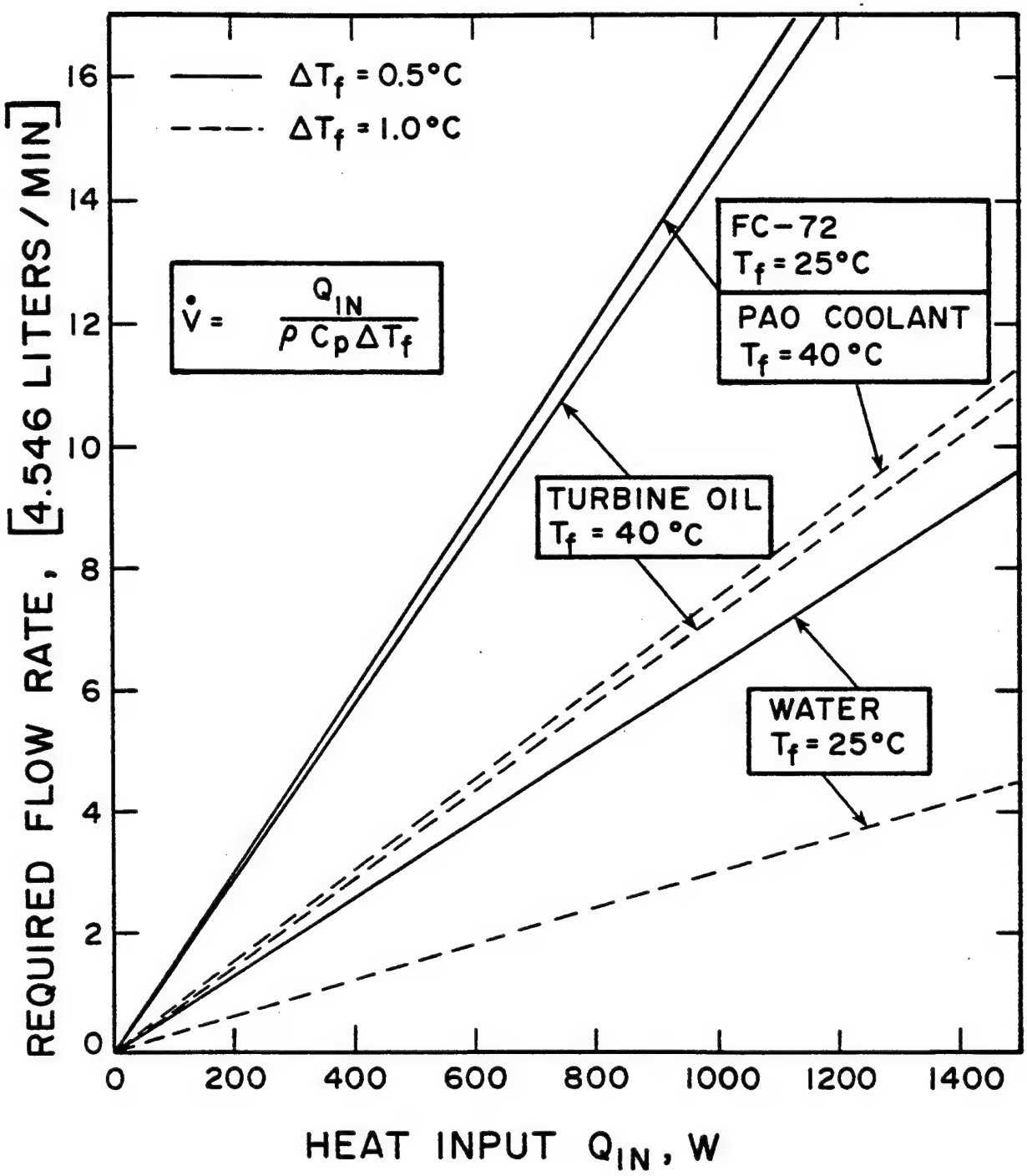

Figure 5. Required Flow Rate Versus Heat Input for Different Fluids.

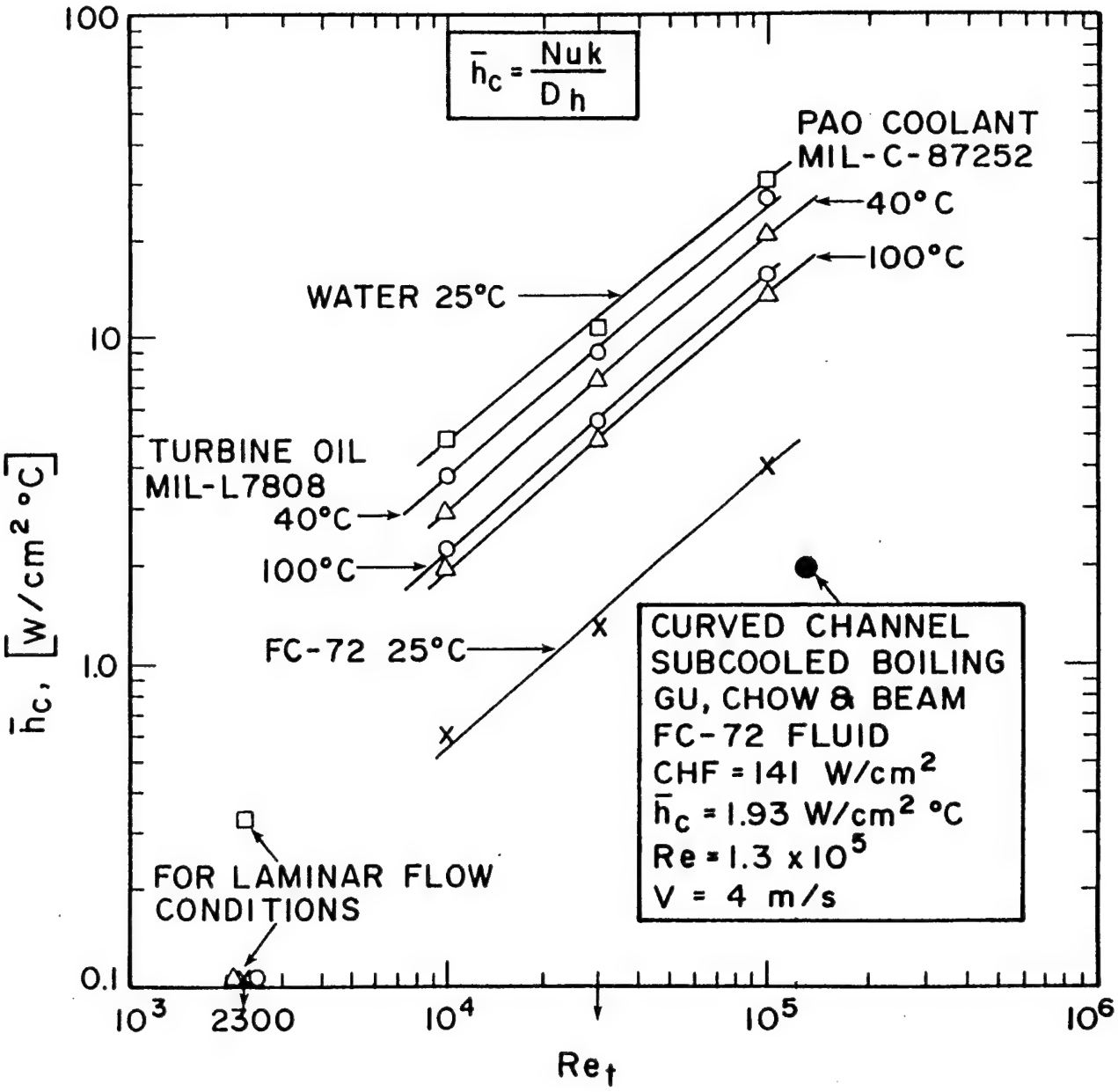

Figure 6. $\bar{h}_c$ Possible Versus Re_t for Single Phase Flow Through Venturi with $d_o = 3.33$ cm; $D_h = 0.1$ cm.

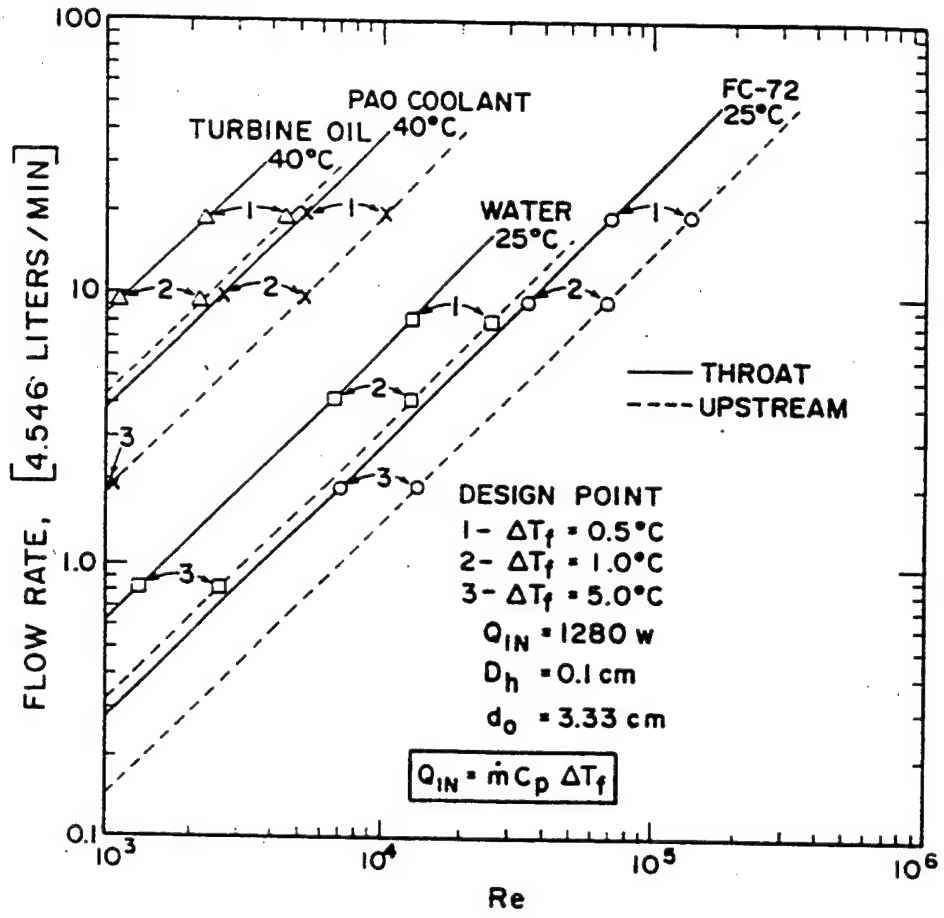

Figure 7. Flow Rate Required Versus Re for Various Fluids at Upstream and Throat Conditions.

GEOMETRY

1. STRAIGHT TUBE UNIFORM CROSS SECTION

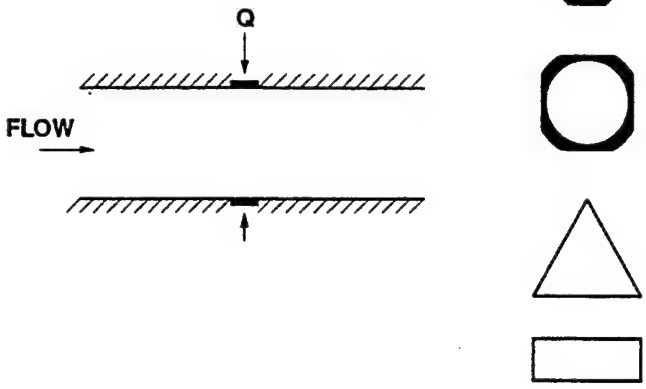

2. CIRCULAR ANNULUS

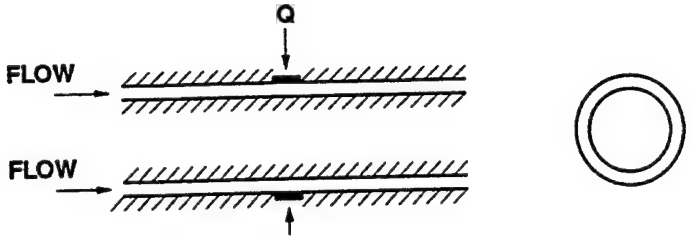

3. CIRCULAR TUBE WITH CONSTRICTION

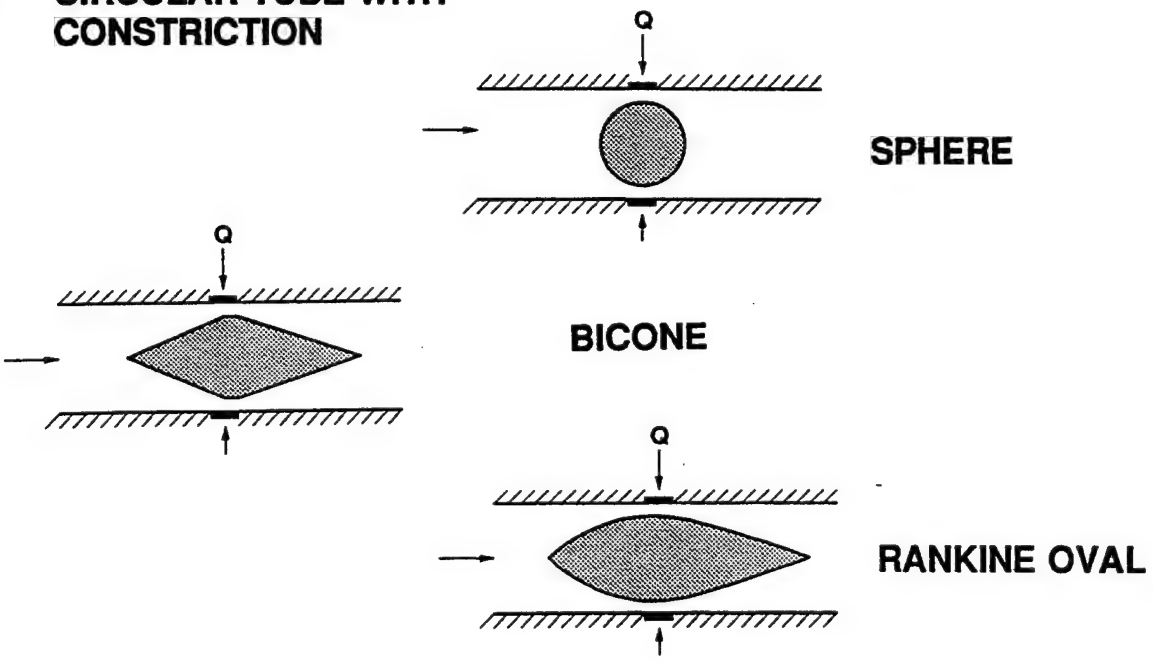

Figure 8. Comparison of Pipe (Circular), Annular and Venturi Flows.

The tabulated Nusselt number for turbulent flow regime of given Re and Pr for both cases are approximately equal within 10% [Ref. 8}. Hence $Nu_1 \simeq Nu_2$ and if we use the same fluid at the same temperature, $k_1 = k_2$. From Eqs. (6) and (7)

$$\frac{h_2}{h_1} = \frac{d_o}{d_o - d_i} = \frac{1}{1 - \left(\frac{d_i}{d_o}\right)} \tag{8}$$

A typical set of design diameters chosen here (see DESIGN Section 2.3), $d_o = 3.33$ cm and $d_o - d_i = 0.1$, 0.15 and 0.2 cm, shows that h_2/h_1 varies from 16 to 33. Even though the heat transfer coefficient advantage, for the annular and venturi flow cases over that of circular flow, is the same, the effective region for heat addition is restricted to the throat area in the venturi flow compared to the full length in the case of annular flow. However, the functional pressure drop penalty is higher for annular flow.

2.3 DESIGN

2.3.1 Test Section with Heater

In order to verify the venturi flow cooling concept, a circular tube test section with a wrapped around resistance heater is chosen. A suitable flow diameter based on the velocity amplification factor at the venturi throat is obtained from Eq. (3) for constant density as

$$F = \frac{V_t}{V} = \frac{A}{A_t} = \frac{1}{1-(d_i/d_o)^2} \tag{9}$$

Table 3 gives a range of flow diameters (2-5 cm) and radial clearance at the throat (0.5-1.0 mm) which can provide velocity amplifications from 5 to 25. A nominal 3.33 cm flow diameter has been selected for practical convenience.

Table 3. Venturi Throat Velocity Amplification Factor

d_o mm	d_i mm	d_o-d_i/2 mm	d_i/d_o	$F = V_t/V$
20	18	1.0	0.9	5.26
	18.5	0.75	0.425	6.93
	19	0.5	0.45	10.256
25.4	23.4	1.0	0.92	6.61
	23.9	0.75	0.94	8.72
	24.4	0.5	0.96	12.95
30	28	1.0	0.933	7.75
	28.5	0.75	0.95	10.25
	29	0.5	0.966	15.25
33.33	31.33	1.0	0.94	8.59
	31.83	0.75	0.955	11.37
	32.33	0.50	0.97	16.92
40	38	1.0	0.95	10.25
	38.5	0.75	0.962	13.58
	39	0.50	0.975	20.25
50	48	1.0	0.96	12.76
	48.5	0.75	0.97	16.9
	49	0.5	0.98	25.25

An electrical resistance heater is designed to generate the maximum possible uniform heat flux around the wall of the cylindrical or poly-faced test section. A minimum of 1.0 mm wall thickness is used to reduce the radial temperature difference and to minimize axial heat spreading in the wall. In a typical design, the wall is aluminum 6061-T651 alloy which is anodized to provide an average 38 μm thick electrical insulating layer for the heater. The design drawings of this test section are given in Appendix A. A 32 AWG nichrome wire coated with polyimide insulation is wrapped on the helical grooves with 0.0508 cm pitch formed on the test section. There are 4 turns of 0.335 ohm/cm nichrome wire on 0.2 cm length with 19.1 ohm total resistance. The heat flux generated at the heater is calculated by

$$q = \left(\frac{E}{\pi D \ell_t} \right)^2 \frac{P}{\rho_o} \qquad \textbf{(10)}$$

The design heat flux is 500 W/cm^2 which reduces to 250 W/cm^2 if 45° spreading of heat in the axial direction is assumed. The radial ΔT for 1 mm × 33.3 mm diameter aluminum wall is 24°C.

An alternate heater design simulating the flat base contact of the MCT device with the heat sink is also considered. In this design, thick film resistors were used as the heaters. A small rectangular ceramic chip, 21 mm long, 2.6 mm wide, and 1 mm thick with a few micron thick resistance metal film (about 25 ohms across the ends) is mounted on each of the six machined flat faces of the venturi test section in a hexagonal shape. The chips are held in place by clamps as shown in Figure 9. The resistances are connected in series-parallel combination (R_{eff}=37.5 ohms) to generate 469 W/cm^2 at the throat section using a 240 volt ac power source.

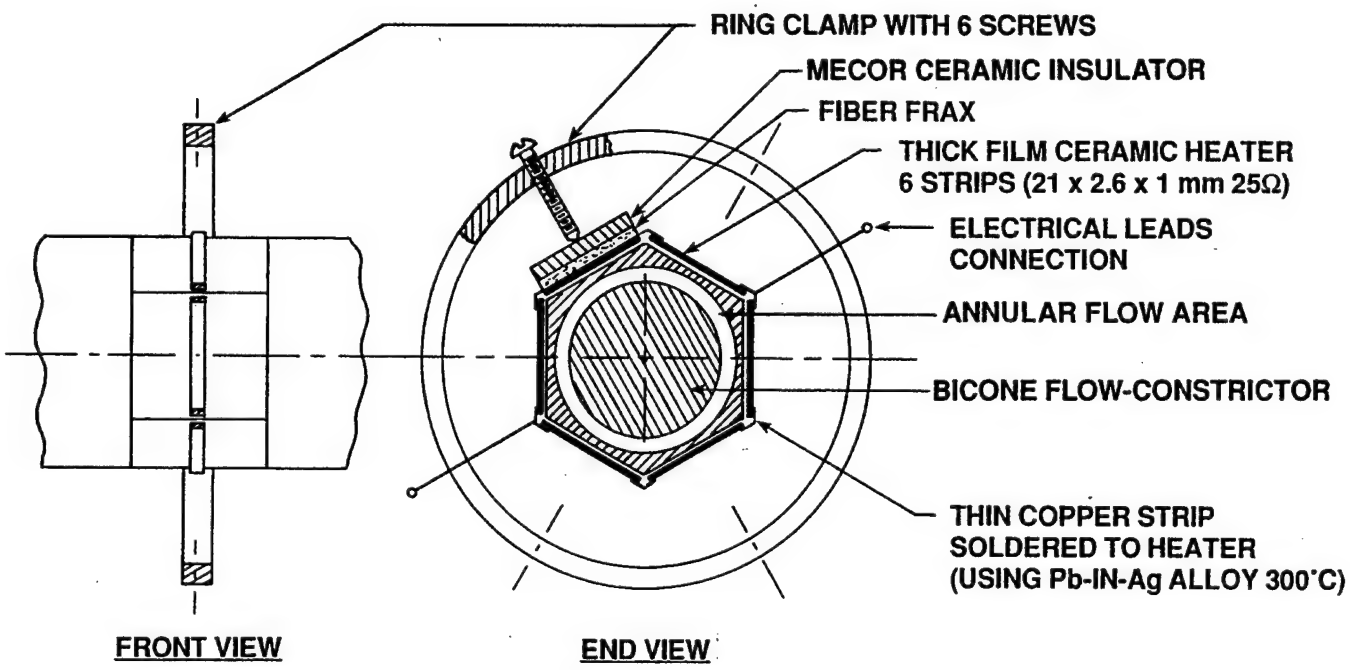

Figure 9. Ceramic Strip Heater Mounting Arrangement.

The test section is made of copper in this case to facilitate soldering of the ceramic heater strips to the base. Radial ΔT across the 1.0 mm thick ceramic (99% Al_2O_3 ; k = 29 W/m°C) is 162°C at Q = 256 W. The corresponding ΔT across the 2.96 mm average thickness of the copper is 35°C. Hence, a total radial ΔT of 197°C is expected between the heater and the fluid. Assuming 45° of axial heat spreading, it can be calculated that the maximum possible heat flux for this heater is reduced to 211 W/cm^2.

2.3.2 Flow Constrictor Design and Pressure Drop

The venturi type flow is created in the test section by a bicone shaped body placed in the center of the tube as shown in Figure 2. The design dimensions of the venturi are given in Table 4. Liquid flow pressure drop for the venturi comprising the throat-annulus and converging/diverging sections is calculated from fluid mechanics principles and known friction factor values [10]. For single-phase flow, total head loss due to friction in the test section is estimated as the sum of losses in the effuser, throat and diffuser sections in addition to the loss

Table 4. Dimensions of Venturi Test Section

Length of Venturi test section, l	:	10.5 cm
Length of converging section, l_1	:	4.13 cm
Length of throat, l_t	:	0.264 cm
Length of diverging section, l_3	:	6.35 cm
Upstream flow diameter, d_o	:	3.33 cm
Throat annulus ID, d_i	:	3.22 cm
Reference hydraulic dia., D_h	:	0.1 cm
Actual hydraulic dia. tested Bicone-2	:	0.11 cm
Velocity Amplification Factor, F	:	15.87
Cone Angles a) Effuser, α	:	40°
b) Diffuser, β	:	20°
Main flow cross section area, A	:	8.728 cm^2
Throat annulus area, A_t	:	0.516 cm^2
Heat addition area in throat, A_e	:	2.765 cm^2
Material of Bicone-2	:	SS304

due to circular pipe flow as in Eq. (12). Equations (12)-(15) give the formulas for friction losses in these flow sections. The present venturi section should be imagined as the combination of a circular pipe and a conventional venturi (where the outer wall itself converges and diverges). The wetted wall surface area in the present case is larger than that of the conventional venturi.

Total head loss,

$$H_T = H_\ell + H_{\ell 1} + H_{\ell 2} + H_{\ell 3} \tag{11}$$

Loss due to straight circular tube,

$$H_\ell = \frac{f\ell V_1^2}{2gd_o} \; ; \; \ell = \ell_1 + \ell_2 + \ell_3 \tag{12}$$

Where $\ell_2 = l_t$, length of throat.

Loss due to effuser (converging section),

$$H_{\ell 1} = \frac{f}{8 \tan \alpha/2}\left[1 - \left(\frac{A_2}{A_1}\right)^2\right]\frac{V_2^2}{2g} \tag{13}$$

Loss due to throat,

$$H_{\ell 2} = \frac{f\ell_2 \, V_2^2}{2gD_h} \; ; \; d_h = d_o - d_i \tag{14}$$

It may be noted that Eq. (14) is not necessarily applicable to such a short length of the throat section and may be ignored in comparison to the other head losses.

Loss due to diffuser (diverging section)

$$H_{l3} = \frac{K'(V_2 - V_3)}{2g} \text{ where for } \beta \leq 40^\circ$$

$$K' = \frac{f(A_2 + A_3)}{8(A_3 - A_2)\tan \beta/2} + 3.2(\tan \beta/2)^{1.25} \quad \textbf{(15)}$$

Frictional pressure drops for various fluids have been calculated for the chosen venturi geometry and flow velocities in the range $10^3 \leq Re \leq 10^5$. The results are plotted in Figure 10. PAO coolant at 25°C suffers the highest frictional pressure drop for example, 720 kPa (105 psi) at $Re = 10^4$. The diffuser section creates maximum loss and this can be reduced by reducing β.

The major disadvantage of high frictional loss is the high pumping power requirement. Available flow moving devices such as centrifugal or turbine vane pumps can easily provide the flow rates required in the present design. Positive displacement type, reciprocating pumps or gear pumps could be used if high pressures are required.

2.3.3 Viscous Dissipation

Due to high velocity flow at the throat section in a narrow annular gap, viscous dissipation is expected. Viscous dissipation per unit volume of fluid at the throat section can be estimated using,

$$\Phi = \mu\left(\frac{\Delta V_t}{\Delta y}\right)^2 \quad \textbf{(16)}$$

where $\Delta y = d_o - d_i/2$ and ΔV_t = relative velocity of fluid at the wall and the core of the annulus. Total heat generation due to viscous dissipation, Φ_T for the volume of fluid ($v_t = 0.1029 \times 10^{-6}$ m^3) at the throat is estimated for all candidate fluids and listed in Table 5.

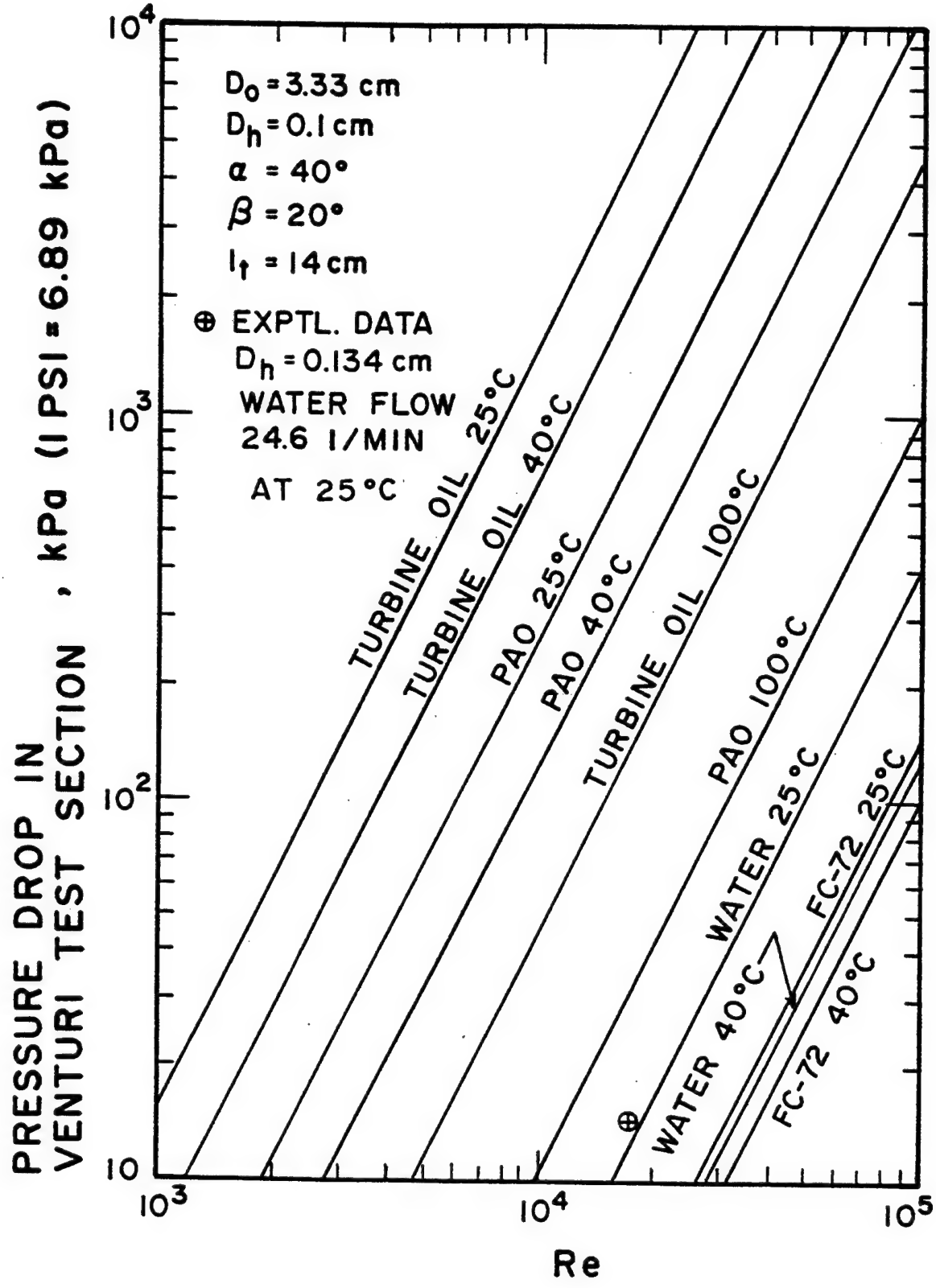

Note: See Figure 12 for additional experimental data for water.

Figure 10. Pressure Drop Versus Reynolds Number for Venturi Flow.

Table 5. Viscous Dissipation for Flow in a Venturi $D_h = 0.1$ cm ; $d_o = 3.33$ cm

No.	FLUID	TEMPERATURE [°C]	Re_t	V_t [m/s]	Φ [W/m^3]	Φ_T [W]
1.	FC-72	25	10^5	40	4.3×10^6	0.44
2.	Water	25	10^5	90	29.1×10^6	2.99
3.	Turbine Oil	40	10^4	120	643×10^6	66.15
		40	2500	30	40×10^6	4.13
		100	10^4	32	45.7×10^6	4.70
4.	PAO Coolant	40	10^4	54	49.1×10^6	5.05
		100	10^4	16.5	1.32×10^6	0.14

For PAO coolant at 40°C, $\Phi_T \approx 5$ W if $Re_t = 10^4$ and $V_t = 54$ m/s. Within reasonable limits of Re_t and V_t, viscous dissipation may not be a serious problem.

2.3.4 Velocity Amplification Factor

In order to verify the venturi flow cooling concept, a suitable flow diameter based on the velocity amplification factor at the venturi throat is obtained from Eq. (9) for constant density. A range of flow diameters (2-5 cm) and radial clearance at the throat (0.5-1.0 mm) can provide velocity amplifications from 5 to 25. A nominal 3.33 cm flow diameter has been selected for practical convenience. In the present experiment, tests were conducted in three different flow configurations with amplification factors F = 1 (circular), F = 12.6 (Bicone-1) and F = 17.5 (Bicone-2).

2.3.5 Design Summary

A novel cooling concept using single phase liquid flow has been described. This new "venturi flow cooling" technique has applications in the more electric aircraft power conditioning system involving MCT devices. Localized heat fluxes up to 200 W/cm^2 seems feasible based on the design analysis performed. Parametric calculations show that PAO coolant could be used in

conjunction with the venturi flow device for MCT cooling with minimal pressure drop penalty. Even though other fluids such as water, FC-72 and turbine oil could be used, they are not attractive for aircraft applications.

It is possible to obtain a heat transfer coefficient of 3.0 $W/cm^2°C$ for PAO flowing through the venturi at 40°C and $Re_t = 10^4$. The corresponding flow rate and $(T_w - T_f)$ are 86 liters/min and 85°C, respectively.

Commonly available flow moving devices are sufficient to circulate the fluid through the venturi. Geometry and mounting arrangements can be optimized depending upon the heat input.

3.0 COOLING STUDY USING CERAMIC HEATERS

3.1 CERAMIC HEATER TEST SECTION

A heater design simulating the flat base contact of the MCT device with the heat sink is considered. In this design, thick film resistance material on ceramic substrate is used as the heater. A small rectangular ceramic chip, 21 mm long 2.6 mm wide and 1 mm thick with a few micron thick resistance metal film (about 25 ohms across the ends) is mounted on each of the six machined flat faces of the venturi test section in a hexagonal shape. The chips are held in place by clamps as shown in Figure 9.

3.2 EXPERIMENTAL WORK

An experimental setup as shown in Figure 11 was built for verifying the venturi flow cooling concept. The setup consisted of a copper test section with the venturi arrangement, cool bath, centrifugal pump, filter, flowmeters power measuring and data logging equipment. Foil type and thin bead copper-constantan thermocouples were mounted on the heater strips and on the wall of the test section close to the heater. Probe type thermocouples were fitted in the flow stream to measure the inlet and outlet temperatures. The heater strips were tightly pressed on the flat faces of the test section by screw clamps. Fiberfrax insulation was wrapped over the test section to minimize heat losses. Flow control valves were adjusted to set a desired flow rate in the system. Power was applied to the heater in steps of 25W until the conservatively established safe operating temperature (215°C) of the silver solder used on the heater strips was not exceeded and the test section was allowed to attain steady state condition. This typically took 10-15 minutes. Tests were repeated for various flow rates from 2 to 38 liters/min. for each of the three flow configurations.

Whenever the bicone was to be incorporated in the system, the gasket-sealed test section flanges were dismantled and the bicone was installed concentrically in the flow path. A specially designed flange support with a lock screw rigidly held the bicone in place and a visual inspection on the bench ensured concentricity of the annulus. Calorimetric measurements showed that Q_o was 80% of Q_{in} and 20% of the power was lost through the insulation.

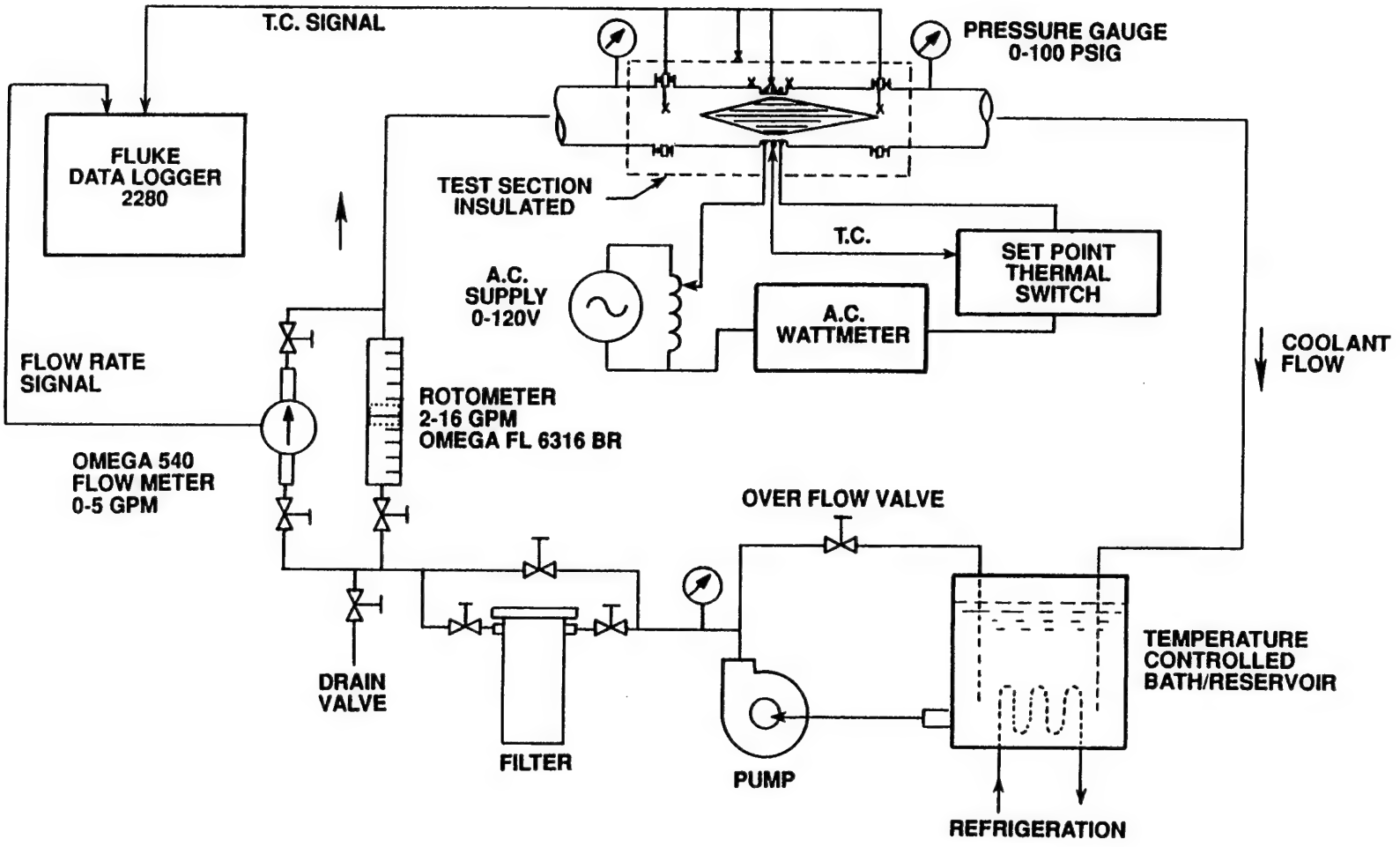

Figure 11. Schematic of the Experimental Setup.

3.3 RESULTS AND DISCUSSIONS

The steady state test results for water are summarized for the cases of minimum and maximum flow settings as given in Table 6 for the three physical flow configurations tested. The average heater temperatures $\bar{T}_H$ are high because the thick film resistance layer is separated from the wall by 1 mm thick ceramic substrate.

3.3.1 Pressure Drop

Liquid flow pressure drop in the venturi test section was measured using absolute pressure sensors mounted on the upstream and downstream of the venturi. The measured values are plotted along with the calculated values as a function of Re as shown in Figure 12. It can be seen that the experimental data and the theoretical estimates using Eqs. (11-15) match very closely. This validates the efficacy of these equations in predicting the pressure drop. Bicone-2 with narrower throat suffered the maximum pressure loss of 37 kPa at $Re = 2.55\times10^4$. Pump power required to offset the pressure drop caused by the venturi over the 10.5 cm test section can be calculated using Eq. (17).

$$P = \dot{V}\Delta\rho \qquad (17)$$

As seen from Table 6, at maximum flow rate tests, the excess pump power consumed by venturi amounts to 11.3 W or 22.1W.

3.3.2 Effect of Heat Spreading

Due to the finite thickness of the wall, the apparent area of heat addition to the fluid is different from the actual area of the heater-to-wall interface. This is illustrated in Figure 13 schematically. Pending a rigorous numerical analysis, for the purposes of preliminary estimates, intuitively, a 45° axial conduction spreading on either side is assumed. Hence, there is about one-third reduction of heat flux at the wall-to-fluid interface as seen in Table 6 data. For example, a wall thickness of 2.96 cm reduces the heat flux from 130 W/cm^2 to 40 W/cm^2 due to spreading. A numerical analysis on this aspect was carried out during the later stages of this research and the results are presented in Section 5.5.2.

Table 6. Summary of Test Results - Ceramic Heater Test Section

Fluid: Water
Physical Dimensions: Upstream flow dia. $d_o = 3.33$ cm
Test section length $l = 14$ cm
Flow Configurations:

I. Circular
$D_h = d_o = 3.33$ cm

II. Venturi Bicone-1
$D_h = 0.123$ cm
$\alpha = 40°$ $\beta = 20°$
$F = 12.6$

III. Venturi Bicone-2
$D_h = 0.0965$ cm
$\alpha = 40°$ $\beta = 20°$
$F = 17.5$

Heat Losses: 20% $Q_o = 0.8\ Q_{in}$

Parameter		Circular		Venturi Bicone-1		Venturi Bicone-2	
		Min Flow	Max Flow	Min Flow	Max Flow	Min Flow	Max Flow
1. Heat Flow, Q_O	W	240	240	360	360	360	360
2. Coolant Flow, $\dot{V}$	ℓpm	1.97	30.29	2.31	37.8	2.31	35.9
3. $\bar{T}_f$, avg.	°C	30.3	24.7	27.2	25.0	27.1	25.2
4. $\bar{T}_w$, avg.	°C	83.1	50.5	61.8	41.6	59.7	41.0
5. $\bar{T}_H$, avg.	°C	211.7	178.5	214.9	192.4	209.5	189.4
6. Flow Velocity, V	m/s	0.04	0.58	0.044	0.73	0.044	0.69
7. Re		0.14×10^4	2.15×10^4	0.16×10^4	2.69×10^4	0.16×10^4	2.55×10^4
8. Throat Vel., V_T	m/s	--	--	0.56	9.17	0.78	12.1
9. Re_T		--	--	0.08×10^4	1.37×10^4	0.08×10^4	1.29×10^4
10. ΔT_{Wf}	°C	44.5	17.5	25.1	7.1	23.1	6.3
11. $\bar{h}_C$	W/cm^2 °C	0.65	1.53	1.61	5.68	1.74	6.39
12. Heat Flux, q	W/cm^2						
A) Without wall conduction spreading		87	87	130	130	130	130
B) With wall conduction spreading (45°)		27	27	40	40	40	40
13. Pressure Drop, kPa		0	~7	0	18	0	37

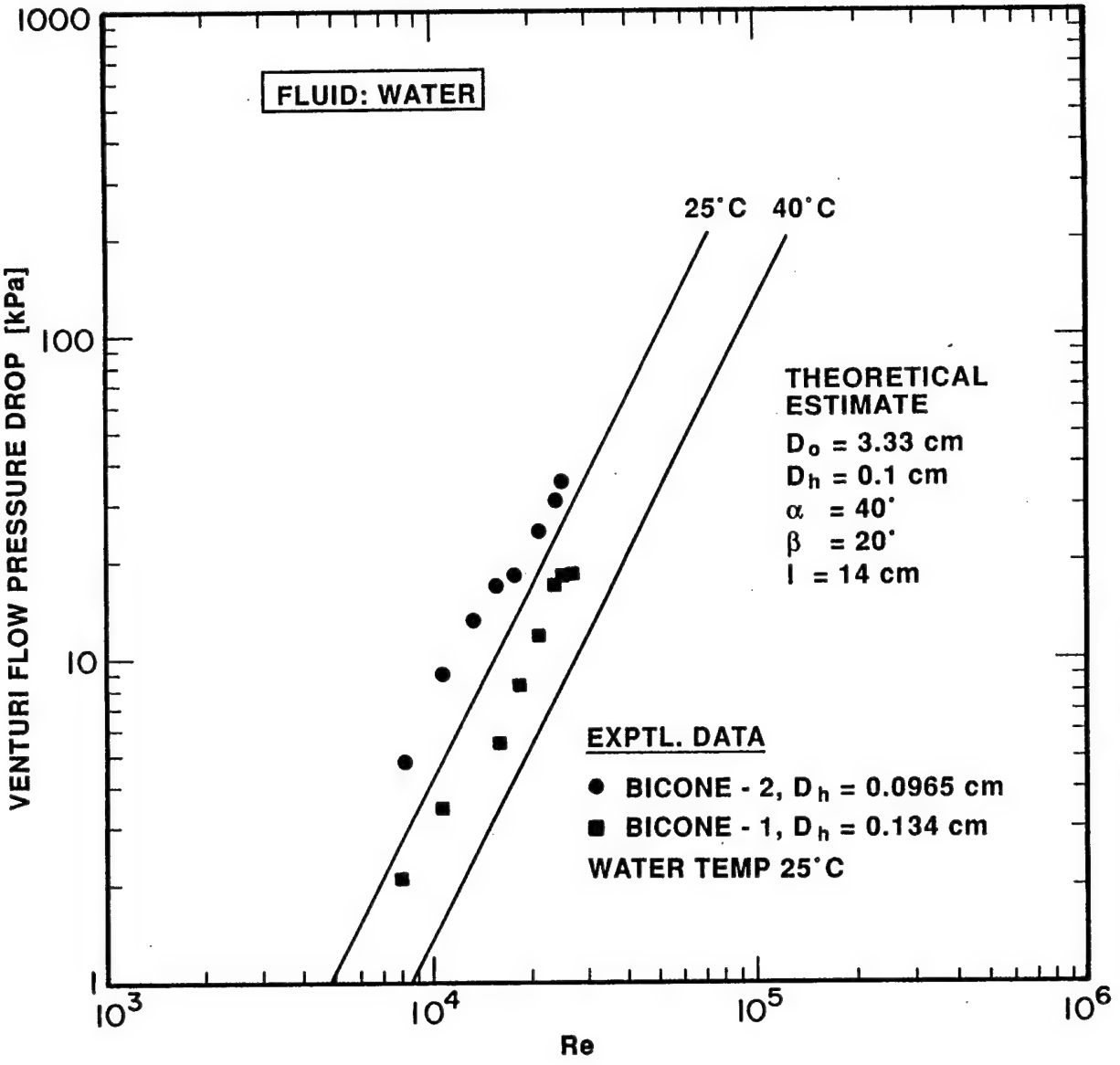

Figure 12. Measured and Calculated Pressure Drop for Water Flow Through Venturi Test Section.

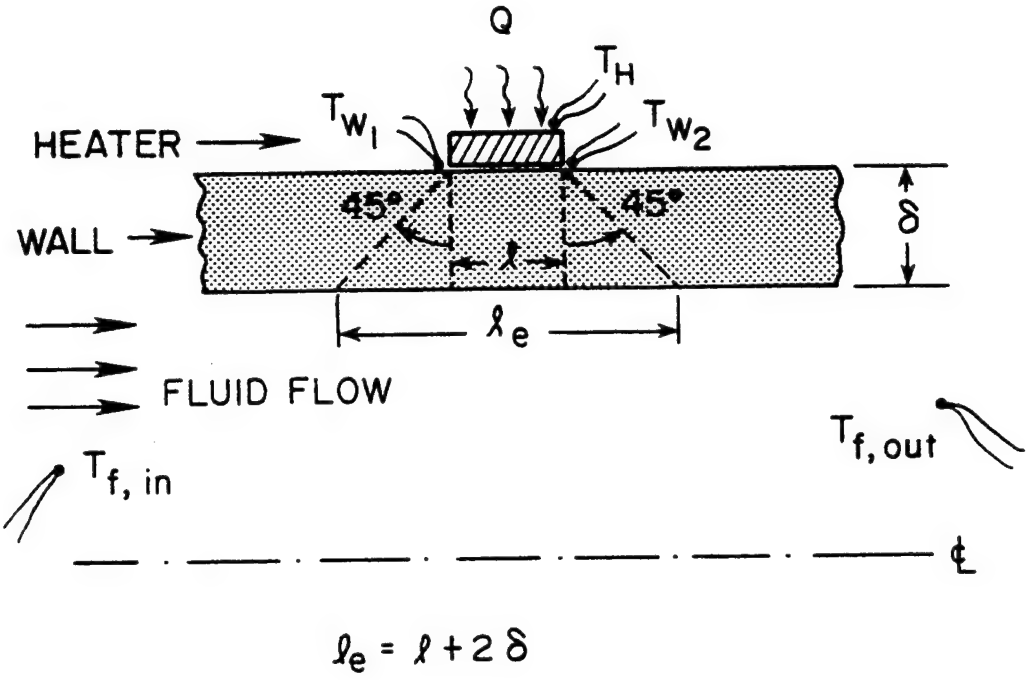

Figure 13. Effective Area of Heat Addition and Thermocouple Locations.

3.3.3 Heat Transfer Coefficient and Wall Temperature Variation

Average heat transfer coefficient ($\bar{h}_c$) and the average wall temperature ($\bar{T}_w$) are plotted as functions of Reynolds number in Figure 14. The wall temperature is the average of the measured temperatures from the thermocouples mounted on the wall on either side of the heater strips as seen in Figure 13. Even though spatially-averaged fluid-side wall temperature would be ideal to have, it is practically difficult to install thermocouples to make such measurements. The thermocouples were attached so close to the heater, it was of concern that the heater might influence the readings to be higher than the actual T_w. This concern was exemplified by the experimental discrepancy that the upstream side sensor showed ~5 °C higher than that of the downstream. However, the average of these two measurements was used for calculations. True fluid-side T_w was obtained by subtracting the temperature drop in the wall (ΔT_w) which was 9.5 °C for Q_o = 360 W as calculated from Eq. (18) and allowing for 20% heat loss to the ambient. For $Re < 10^4$ the wall temperature variation for circular and venturi flow are higher than those for $Re > 10^4$. Wall temperatures in both cases drop drastically up to $Re = 10^4$ and then show gradual decrease. Venturi flow with bicone-1 and bicone-2 show only marginal difference in $\bar{T}_w$.

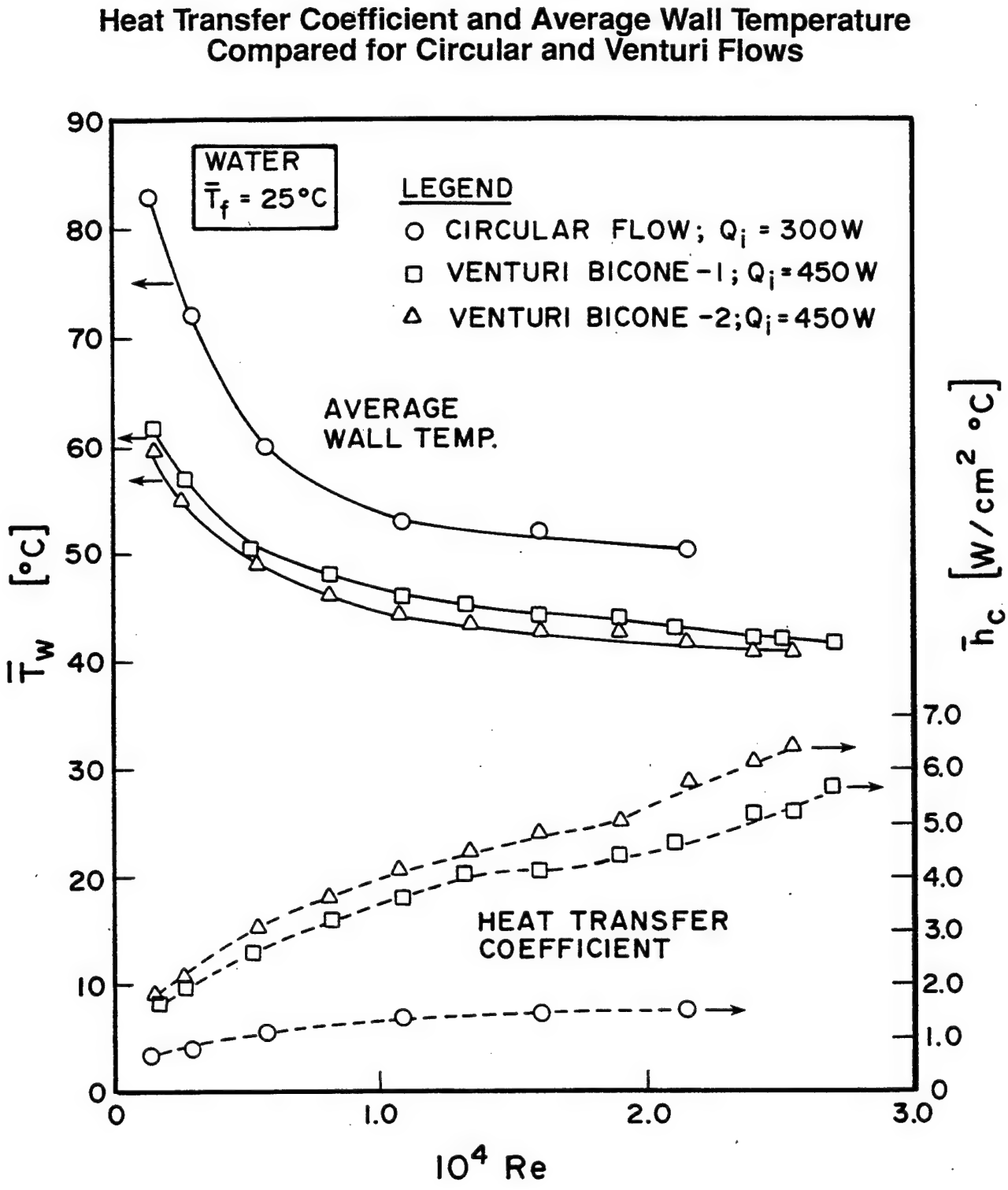

Figure 14. Wall Temperature and Heat Transfer Coefficient for Circular and Venturi Flows.

$$\bar{h}_c = \frac{0.8Q_{in}}{A_e \Delta T_{wf}} \tag{18}$$

where $\Delta T_{wf} = \bar{T}_w - \bar{T}_f - \Delta T_w ; Q_o = 0.8Q_{in}$

and $$\Delta T_w = \frac{0.8Q_{in} \ln\left(1 + \frac{2t_w}{d_o}\right)}{2\pi k l_t}$$

Because of the hexagonal exterior, the pipe wall thickness is not uniform and, hence, an average value of $t_w = 2.98$ mm was used here. Other data are as given in Tables 4 and 6.

For circular flow, $\bar{h}_c$ does not vary much with Re whereas for venturi flow it varies appreciably with increase in Re. The maximum $\bar{h}_c$ value attained is 6.39 W/cm^2 °C which is quite large for single phase flow. The $\bar{h}_c$ curves for venturi flow show increasing trend beyond Re = 2.0×10^4 which means that one could get higher $\bar{h}_c$ if Re can be increased.

3.3.4 Verification of Experimental Results with Theory

Figure 15 shows the theoretical heat transfer coefficients based on single phase fully developed turbulent flow through a circular annulus for various fluids. Experimental data for water are also plotted. It is apparent that experimental data match those predicted very well in the turbulent regime of flow. Higher $\bar{h}_c$ values in the laminar regime (Re < 2300) is due to the short entrance length and bends in the line contributing to the consequent turbulence effects of the present experiment setup. Also, it can be seen that the present experiment, using water, out-performed the two phase data of Gu, et al., where FC-72 was used. However, this is not a fair comparison because ΔT_w is much less for two-phase. Figure 16 shows the Nusselt number variation with Re_t for $3 < Pr < 100$. Present experimental data for water with Pr = 6.18 match very well with the theory. Experimental data for $Re_t > 2.5\times10^4$ is not available due to limitation in the circulating pump capacity.

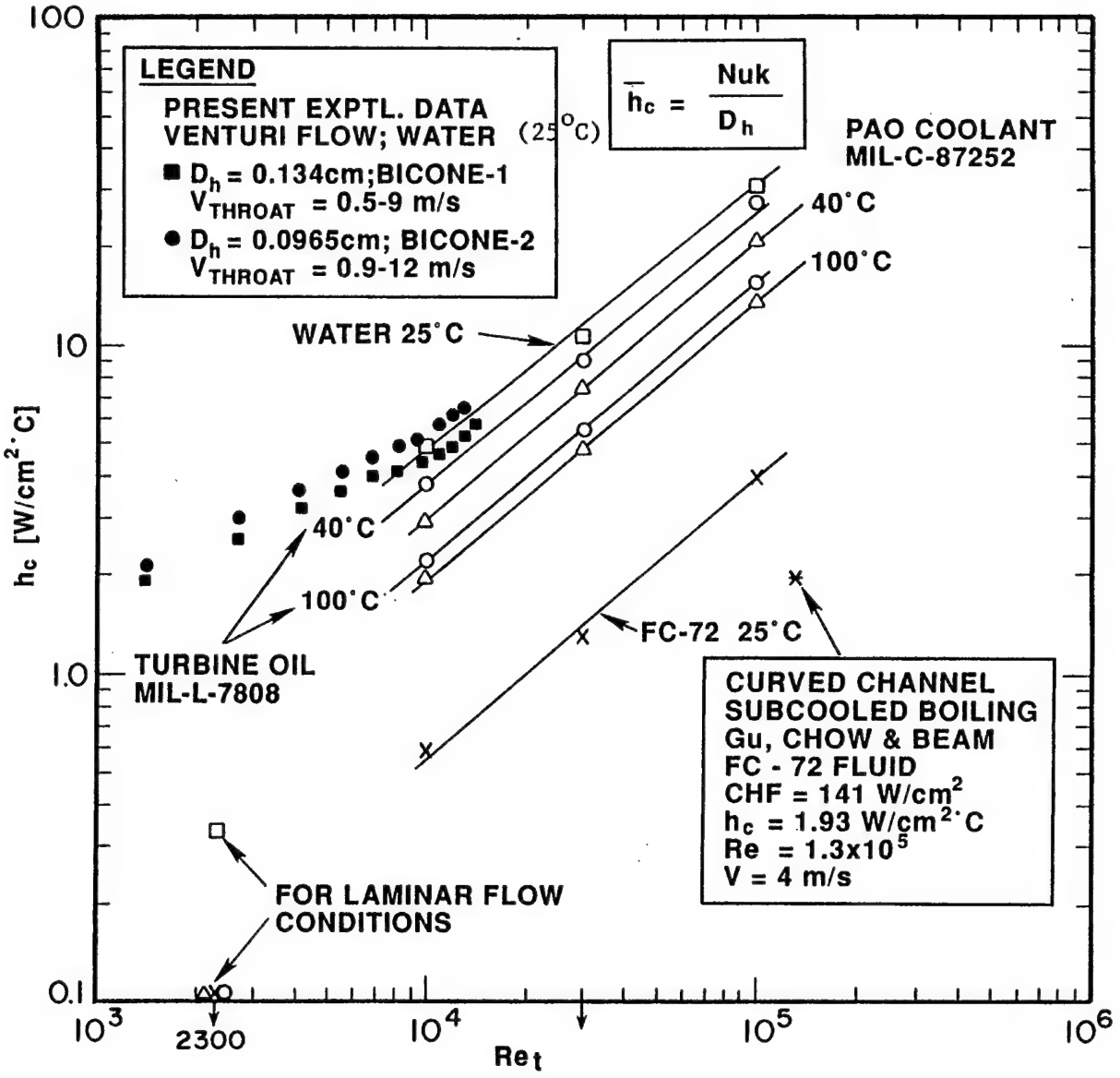

Figure 15. Heat Transfer Coefficient vs. Reynolds Number for Various Fluids.
Experimental Data (D_h = 0.134 and 0.097 cm) and Theory (D_h = 0.1 cm) Compared.

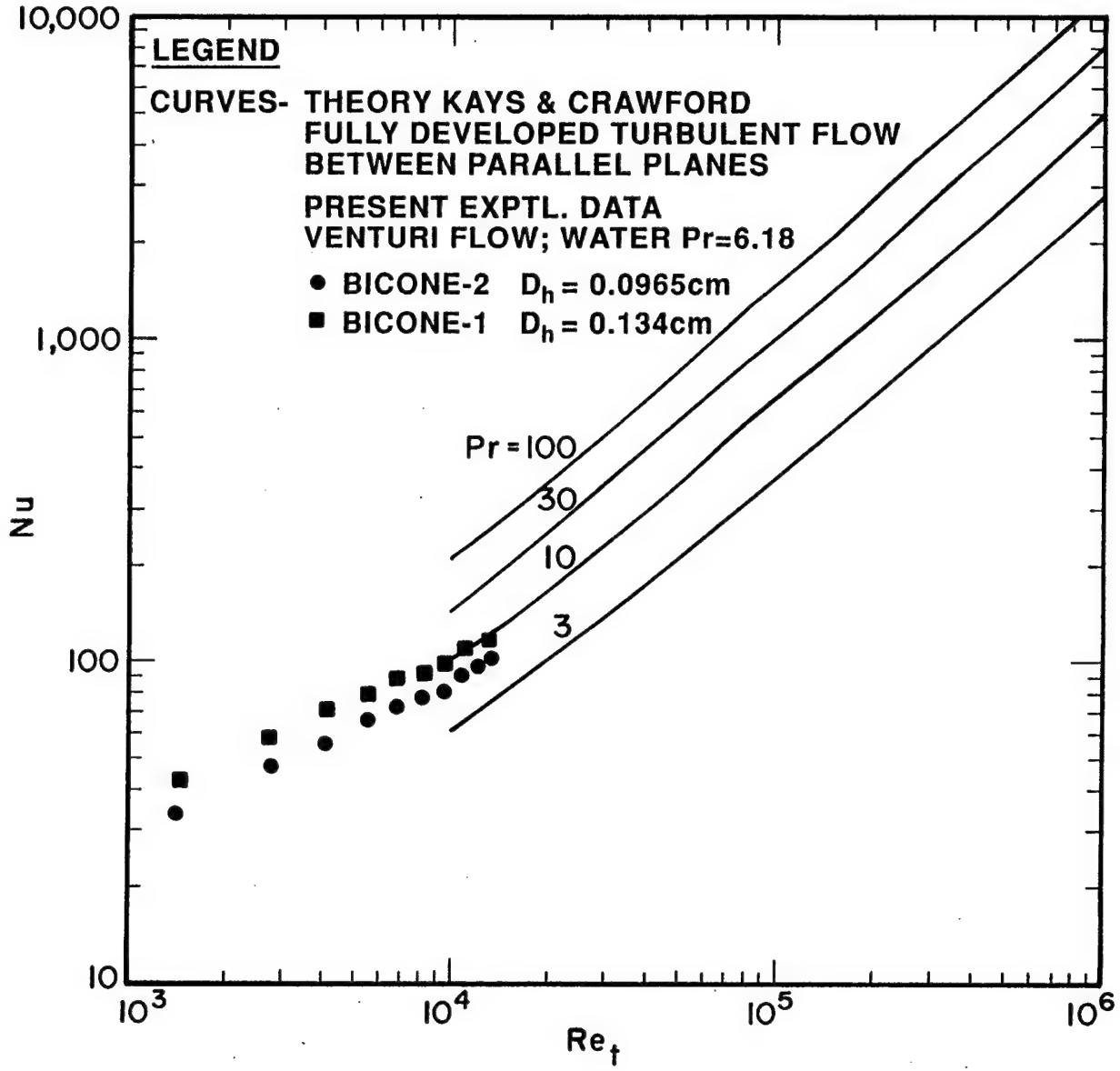

Figure 16. Nusselt Number vs. Reynolds Number for Various Prandtl Number. Comparison of Present Experimental Data with Theory.

For circular flow, the applicable correlation such as in Eq. (19) under-predicts Nu.

$$Nu = 0.023\ Re^{0.8} Pr^{0.4} \quad (19)$$

For example, in the cases of minimum and maximum flow rates of circular flow (Table 6 data), Eq. (19) predicts Nu = 15 and 140 compared to the experimental values of Nu = 351 and 838, respectively. The discrepancy may be attributed to 1) entrance length effects, 2) non-conformity of the present experimental configuration to the standard conventional situation as far as the heat addition is concerned, and 3) difficulty in measuring the fluid-side T_w precisely. A meaningful Nusselt number correction for entrance length effects described in Ref. 8 cannot be applied because of the present unconventional configuration.

However, the present experimental results provide encouraging results to further explore the technique for potential electronic cooling applications.

3.4 SUMMARY

Single phase flow through an annular venturi type geometry was investigated for localized high heat flux cooling applications. In an experimental setup assembled for the present study, tests were conducted with water for both circular tube flow and venturi configurations. The average heat transfer coefficient for the venturi flow was 6.39 W/cm^2°C (for water flow at 25°C and Re = 2.55×10^4 which is about three times higher than that of circular flow. The pressure drop penalty was only marginal - about 37 kPa for a flow rate of 36 lpm. The experimental and theoretical results for $\bar{h}_c$ and Nu corroborated very well in the turbulent flow regime.

4.0 COOLING STUDY USING A HEAT CONCENTRATOR

4.1 COPPER HEAT CONCENTRATOR TEST SECTION

The venturi flow test hardware was made of a circular copper tube (3.33 cm I.D.) with an integral heat flow concentrator as shown in Figure 17. A large 7.5 cm diameter, 3.1 cm long flange was machined and tapered down to a thin disc (0.26 cm) to form the most important heat focusing part for the venturi throat region. Sheathed nichrome heater coil was wound over the helical grooves cut on the flange. The thin disc also enabled radial heat flow rate measurement through calibrated thermocouples installed at precise radial locations. The bicone shaped flow constrictor was placed concentrically in the flow path which created the annular converging-diverging flow called "venturi-flow." Two strain gauge type pressure transducers (Servonic Instruments No. 3031-8705; 0-50 psia) connected to the 0.3 mm diameter pressure taps measured the static absolute pressure of the fluid in two locations at the throat. Both pressure and temperature measurements enabled us to determine if the flow was in the single or two phase regime.

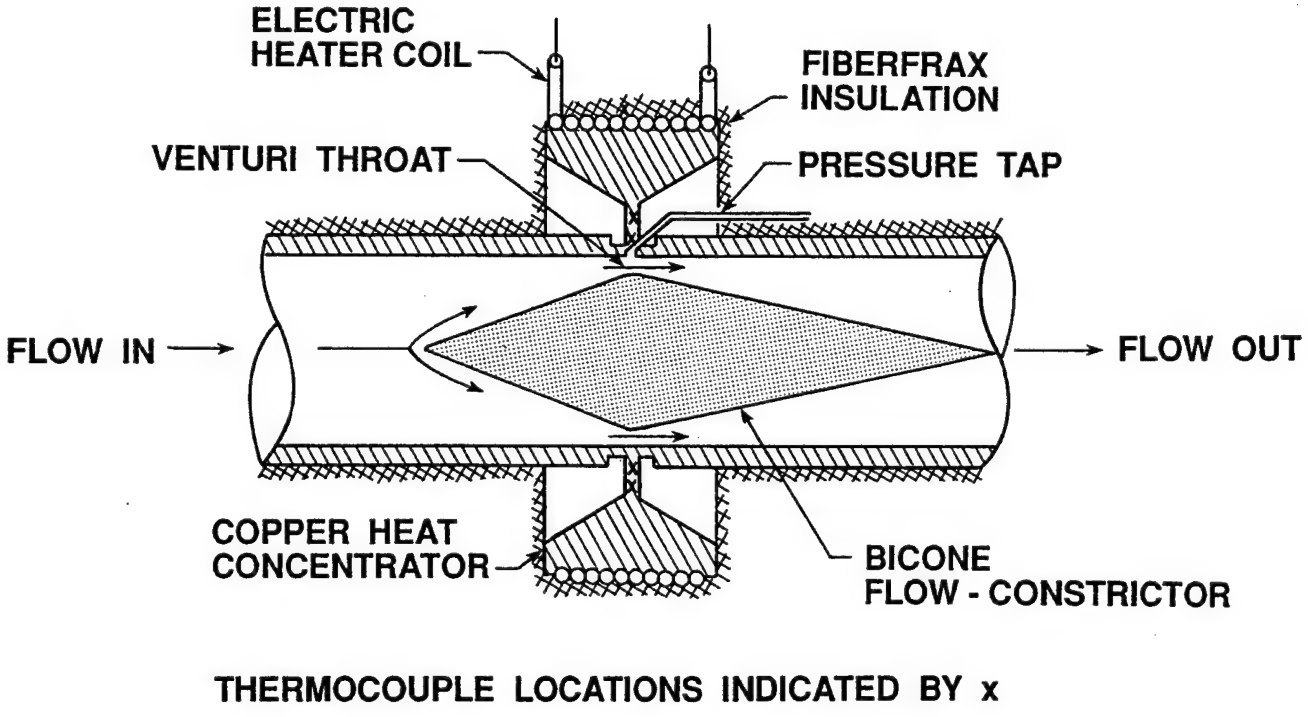

Figure 17. Test Section Heat Concentrator Design.

Radial heat f low measurement was accomplished by precisely measuring the radial temperature profile on the thin disc (0.2642 cm thick). Four redundant pairs of thermocouples were mounted on either side of the disc with the junction aligned at the center of the disc as shown in Figure 18. The radial positions of these sensors from the centerline axis were 2.30 cm and 1. 98 cm and the radial distance between the sensors were precisely measured to be 0.32 cm. Neglecting local heat losses, the radial heat flow rate by conduction can be determined from Eq. (20).

$$Q_{12} = \frac{2\pi k l_t}{\ln(d_1/d_2)} \Delta T_{12} \qquad (20)$$

Substituting the physical dimensions and conductivity of copper (3.8 W/cm°C), Eq. (20) is simplified to

$$Q_{12} = 42.5\ \Delta T_{12} \qquad (21)$$

and ΔT_{12} is the average temperature difference of the four sets of radial temperatures measured. An uncertainty analysis for this measurement is provided in Appendix C.

4.2 PUMP POWER PENALTY

The venturi type f low and the pressure drop created in the present test section shown in Figure 17 are the same as that explained in Sections 2.3.2 and 3.3.1. For the single phase flow, total head loss due to friction in the test section is estimated as the sum of losses in the effuser, throat and diffuser sections. Frictional pressure drops for water at 25°C and 40°C have been calculated for the chosen venturi geometry and flow velocities in the range $10^3 \leq Re \leq 10^5$ and plotted as shown in Figure 12. The maximum pressure drop for a flow rate of 37.9 lpm was 37 kPa. The diffuser section creates maximum loss and this can be reduced by reducing β. The major disadvantage of high frictional loss is the high pumping power requirement. Available flow moving devices such as centrifugal or turbine vane pumps can easily provide the flow rates required in the present design. Positive displacement type, reciprocating pumps or gear pumps could be used if high pressure are required. Within reasonable limits of Re_t ($<10^5$) and V_t (90 m/s), viscous heat dissipation is within 3 W for water flow at 25°C (see Table 5).

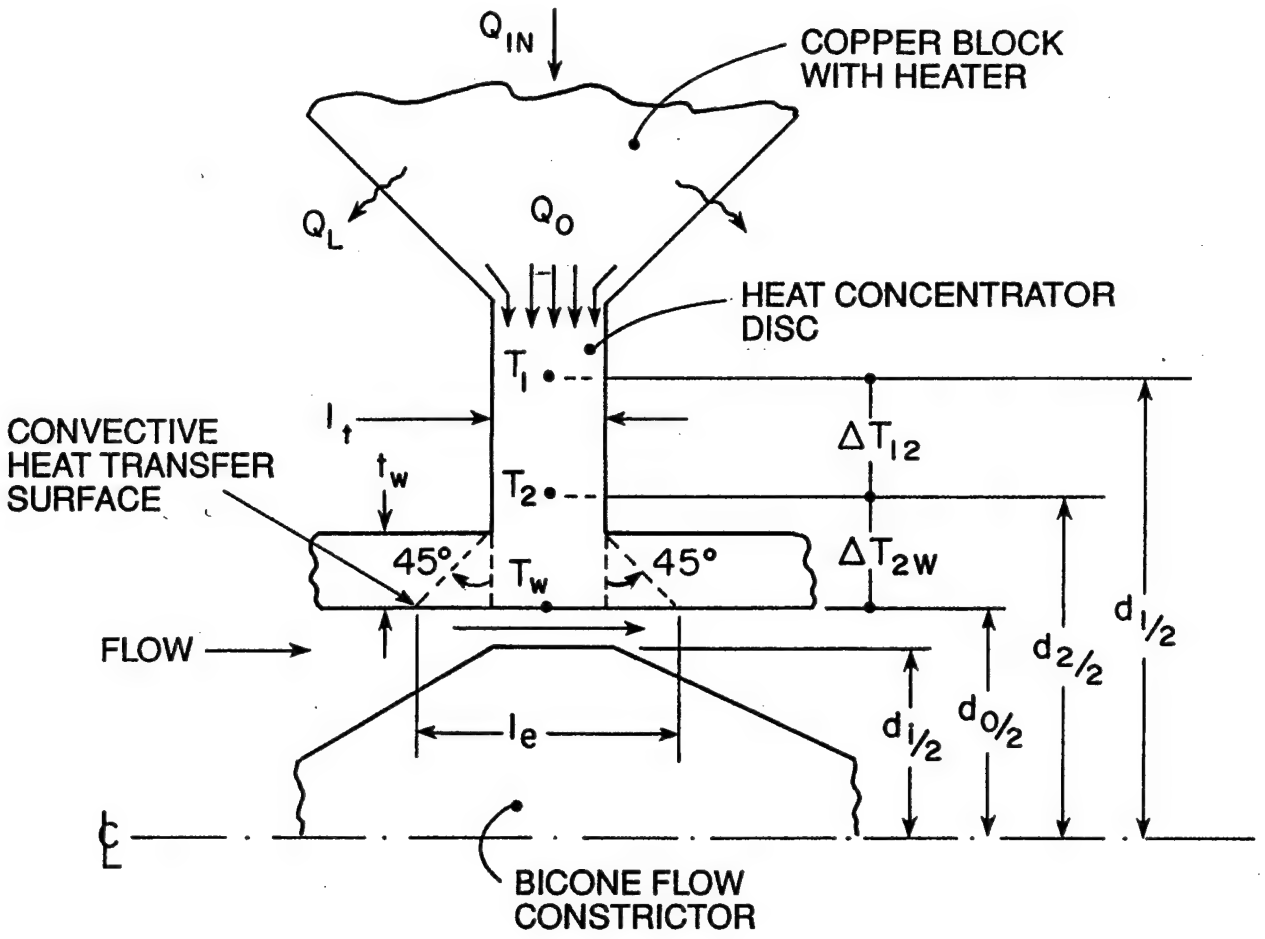

Note: Actual dimensions are provided in drawings in Appendix A.

Figure 18. Radial Heat Flow Measurement Nomenclature and Details at Throat Region.

4.3 TEST SETUP

The experimental setup (seen in Figure 11) was fabricated for conducting the venturi flow cooling experiments. The setup consisted of a copper test section with the heater and venturi arrangement, constant temperature bath, pump, filter, flowmeters, power measuring and data logging instruments. Eight thin gauge copper-constantan calibrated thermocouples were attached on the radial heat focusing disc for measuring the heat flow from the heater to the fluid. The thermocouples were offset in circumferential positions and had four-fold redundancy. Sheathed probe type thermocouples were used to measure the inlet and outlet fluid temperatures. Fiberfrax insulation (75 mm thick) was wrapped around the heater and test section to minimize heat losses.

The test section has stainless steel removable end flange joints with 0-ring seals on either side. The flanges have central hub (connected by machined spokes) to support the bicone on its axis. These specially designed flange-supports with lock screw, rigidly held the bicone in place. A visual inspection of the test section assembly on the bench ensured concentricity of the annular flow area formed between the inner diameter of the test section and the bicone.

4.4 TEST PROCEDURE

All the tests for the present research were done using water as the coolant. Initially, tests were performed for the venturi f low configuration and the same were repeated for circular flow for comparison.

For a selected flow configuration, a range of several test parameters was varied. The resulting changes in steady state temperature profiles were measured along with the heat input, flow rate and coolant temperature. During a typical test run, firstly, the cool bath was set at a constant temperature and the flow rate of the circulation was adjusted to a nominal value of 7.6 lpm. Secondly, heater power was increased in steps of 50 W with 10-20 minutes interval until a safe maximum power input of 1150 W was reached. A protective temperature cutout circuit was incorporated to protect the heater from burning out. The test conditions were

maintained until a steady state was reached. Thirdly, steady state data were recorded for later analysis. Lastly, keeping the maximum power input and coolant temperature the same, flow rate was varied from a maximum of 37.9 lpm to a minimum of 2. 6 lpm in steps of 1. 9 lpm and every time steady state data were recorded.

The above test runs were repeated for coolant flow temperatures of 5°C, 10°C, 20°C and 30°C in order to study the effect of subcooling of the coolant on the heat transfer characteristics. The flow rate range possible with the circulating pump provided a range of Re from 1840 to 2.6790×10^4.

4.5 RESULTS AND DISCUSSIONS

Steady state test results for both venturi and circular flow cases are presented and discussed. Absolute throat pressure, computed fluid-side wall temperature, and heat transfer coefficient variations with Reynolds number are the significant parameters highlighted.

4.5.1 Throat Pressure and Flow Velocity

Absolute throat pressures and flow velocities for venturi and circular flows are plotted in Figure 19. The pressure values plotted are averages of the two pressure transducers located at the top and side of the annular throat. In the case of venturi flow, the difference between those readings for the maximum flow rate was about 5%. The sensor at the top measured lower than that on the side at maximum flow rate whereas they were the same at other flow rates. In the case of circular flow, both readings were the same. There is a significant pressure drop at the throat for venturi flow when Re > 5000 indicating a suction effect which is an expected phenomenon. The drop in saturation temperature for water at the maximum flow rate (37.9 lpm) which corresponds to the minimum throat pressure (72.3 kPa) is 9°C. Also, it is clear from Figure 19 that the venturi throat velocity is 15.87 times higher than that of the circular flow.

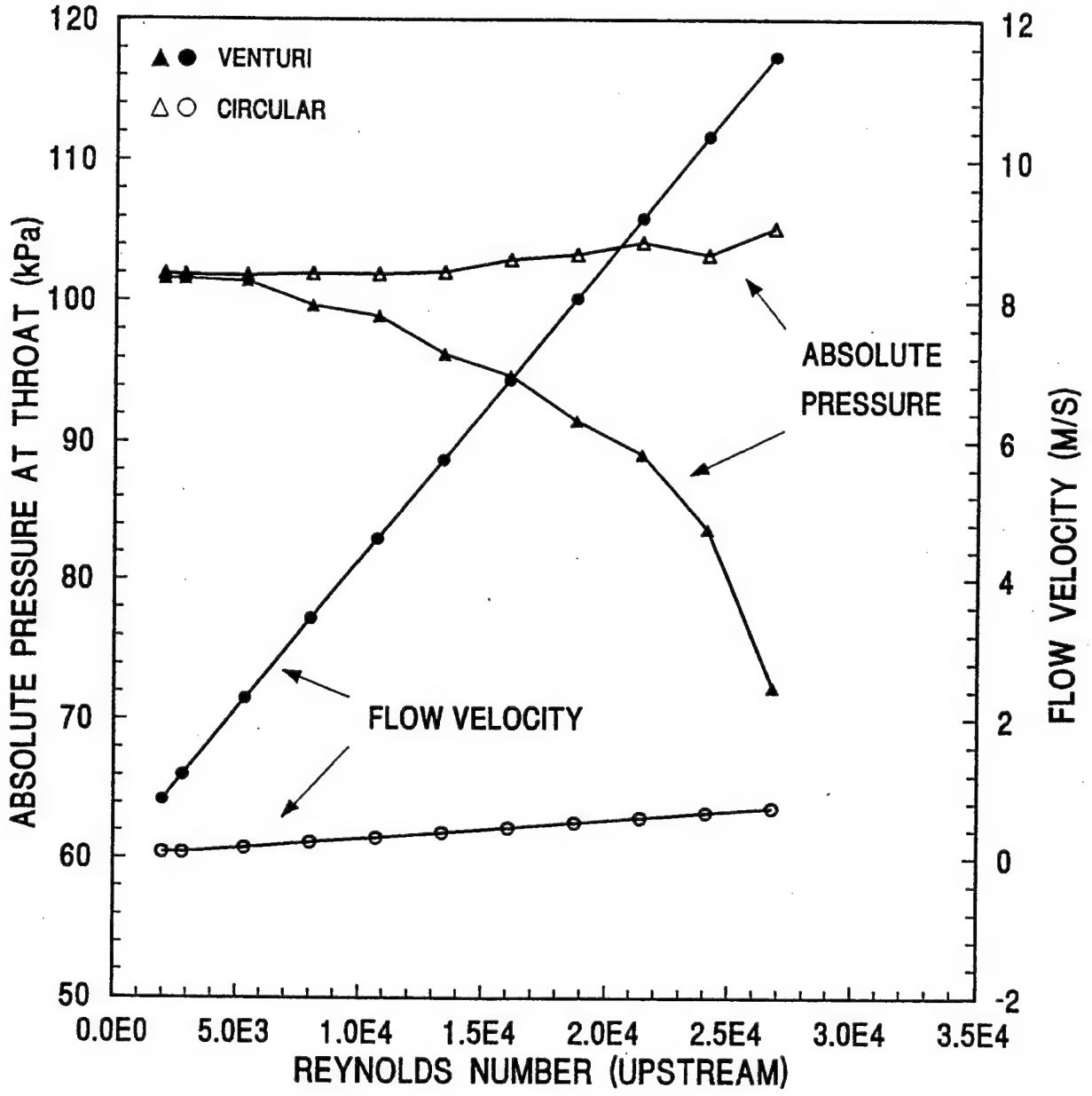

Figure 19. Absolute Throat Pressure and Flow Velocity.

4.5.2 Heat Loss and Calorimetry

Based on the equipment used (magtrol and digital wattmeter), the electrical input power measurement and control accuracy was ±3% of the reported values. The calorimetric measurement (using the water flow rate and temperature rise data) had an estimated uncertainty range of ±12.1% to 30.3% (see Appendix C.2). Because of this high uncertainty, the calorimetric data were considered unreliable. However, the computation of heat flow through the venturi throat based on the heatmeter measurement varied from ±6.5% for 200 W to 1.8% for 900 W (see Appendix C.1). Heat losses to the ambient through the insulation was determined using steady state test data in Eq. (22).

$$Q_L = (Q_{in} - Q_{12})/Q_{in} \qquad (22)$$

Figure 20 shows the heat flow measurement and heat loss data for the maximum flow rate case at 20°C water temperature. Maximum heat loss was about 22%. It can be observed that the calorimetric data are scattered and those of the heatmeter are not.

4.5.3 Effect of Axial Conduction in Determining $\bar{h}_c$

Due to the finite thickness of the wall, the apparent area of heat addition to the fluid is slightly larger than the circumferential disc footprint area of the heat concentrator disc. This is exemplified in Figure 18 showing an assumed 45° spreading angle in the axial direction. The heat addition footprint area is $\pi d_o l_t$ and the area with spreading correction is $\pi d_o l_e$ where $l_e = l_t + 2\, t_w$. In the present setup, the area ratio was 2.2. Hence, the heat flux and heat transfer coefficient results are corrected for conduction spreading by a factor of 2.2. For example, a typical test run (T_f - 20°C) for venturi flow when the input power was the maximum (Q_{in} = 1126 W and Q_{12} = 893 W) the uncorrected versus corrected values of heat fluxes and heat transfer coefficients were 323 vs 147 W/cm^2 and 29.12 vs 13.23 W/cm^2 °C, respectively.

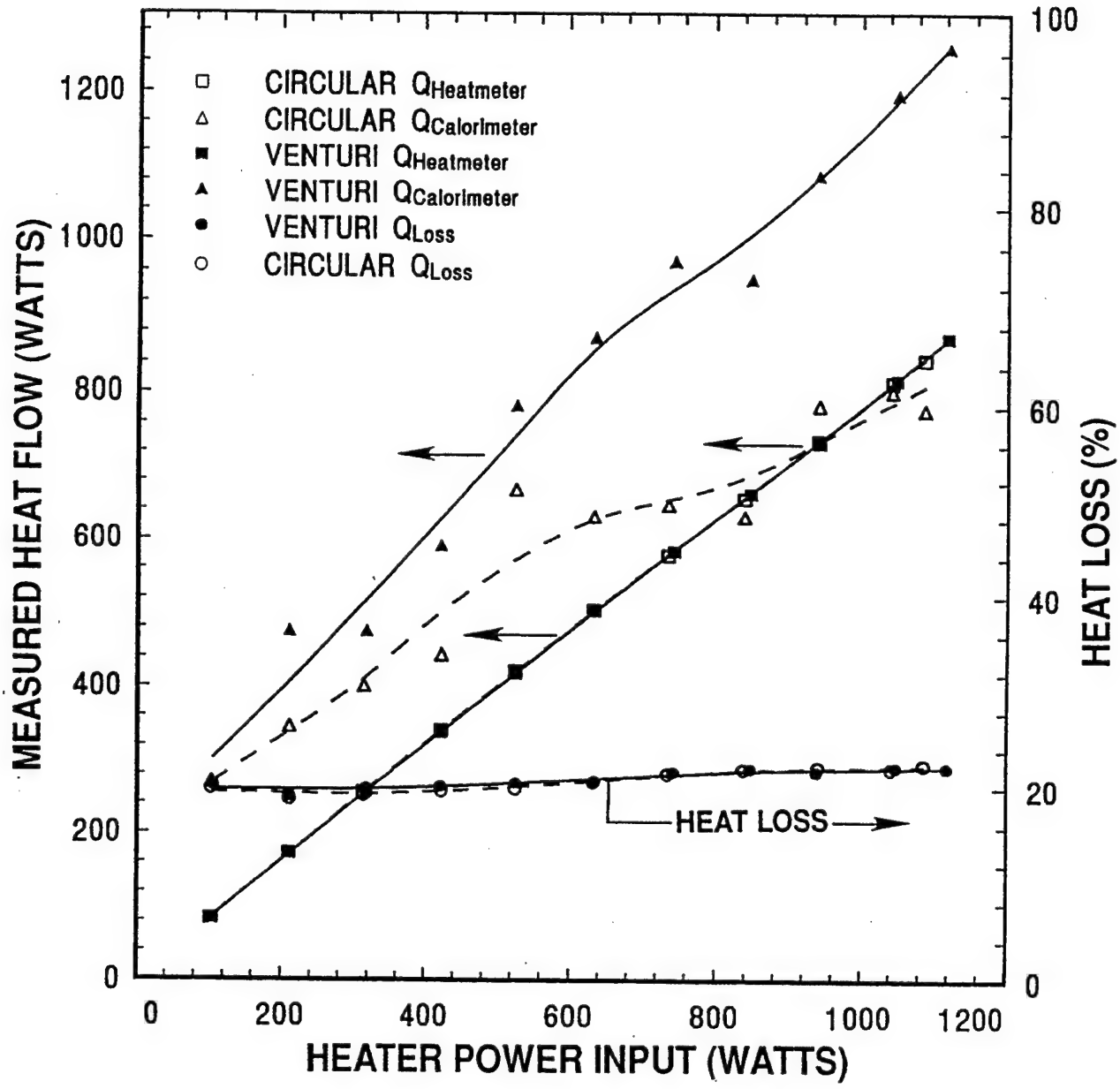

Figure 20. Measured Heat Flow and Heat Loss (Water Flow Rate = 0.631 l/s at 20°C).

Although the 45° spreading assumption is intuitive and its implication on the values of $\bar{h}_c$ is of concern, the major thrust of the present research was to illustrate the four-fold improvement in $\bar{h}_c$ for the venturi flow compared to the corresponding circular flow. An exact value for the effective area of heat transfer can be arrived at by plotting the isotherm of T_w through numerical computation.

4.5.4 Average Wall Temperature

The fluid-side spatially-averaged wall temperature is difficult to measure accurately because attaching a sensor on the inner wall surface would interfere with the flow. Hence, the method of computing it from temperature measurements in the vicinity is used without compromising accuracy. Referring to Figure 18, the radial ΔT_{2w} and $\bar{T}_w$ can be computed from the heat flow Q_{12}, measured earlier by using the radial conduction formulas as in Eqs. (23) and (24).

$$\Delta T_{2w} = Q_{12} \ln(d_2/d_o)/2\pi k l_t \quad \textbf{(23)}$$

$$\bar{T}_w = \bar{T}_2 - \Delta T_{2w} \quad \textbf{(24)}$$

Computed values of $\bar{T}_w$'s are plotted for both flows at various coolant temperatures as function of Re in Figure 21. The wall temperature is the lowest for the case of venturi flow and $T_f = 5°C$. With increase in fluid subcooling, $\bar{T}_w$ dropped more at higher Re than at lower Re. Obviously, circular flow case shows the highest $\bar{T}_w$. In the case of venturi flow, the wall temperature is reduced by one-half that of circular flow. Also, it can be observed that the $\bar{T}_w$'s are low enough ($\bar{T}_w < T_{sat}$) that no boiling occurred at the throat region.

4.5.5 Average Heat Transfer Coefficient

The average wall-to-fluid heat transfer coefficient ($\bar{h}_c$) is determined using the experimental values in Eq. (25).

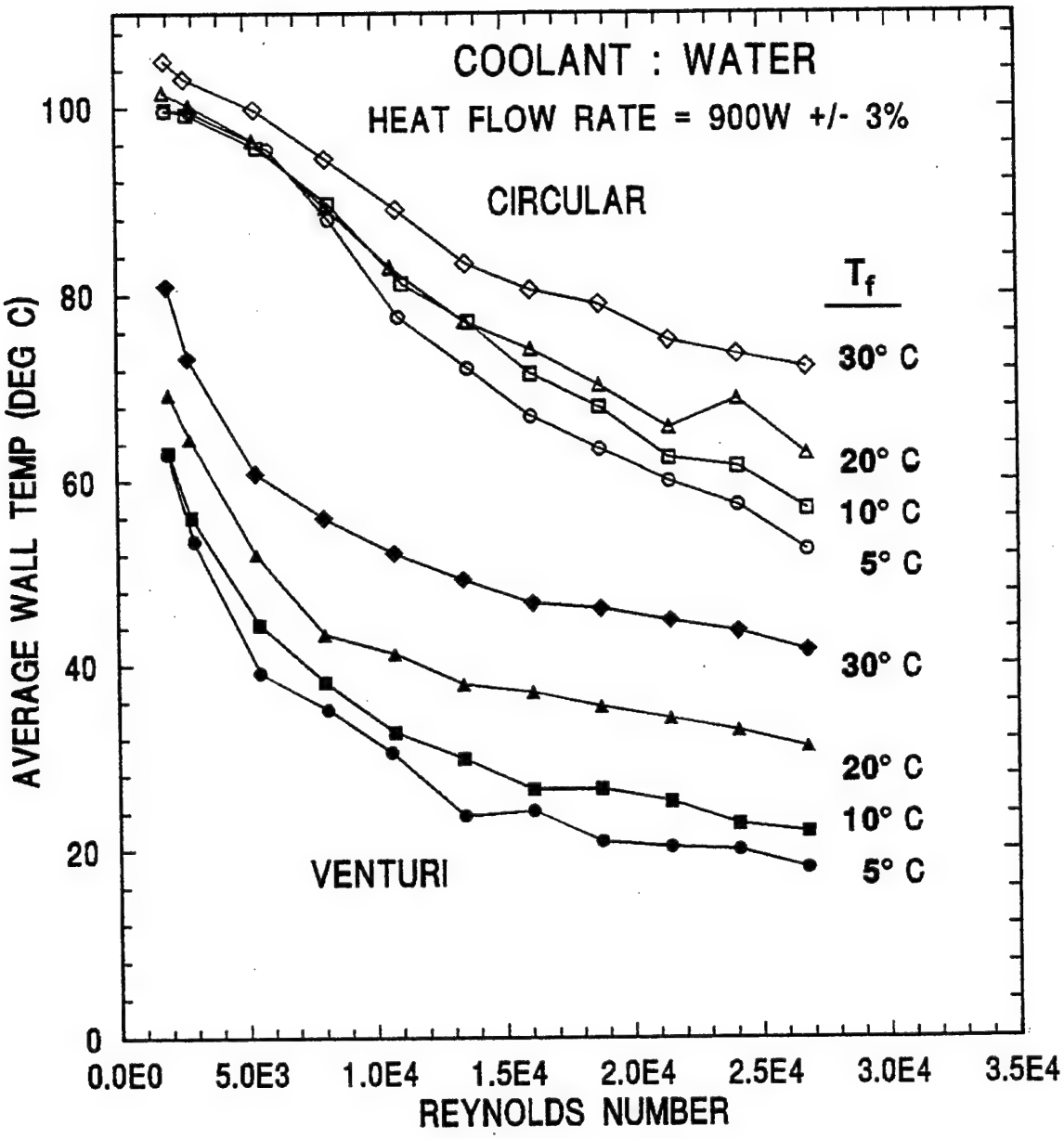

Figure 21. Wall Temperature vs. Re for Circular and Venturi Flows.

$$\bar{h}_c = Q_{12}/A_e\Delta T_{wf} \quad (25)$$

where $\Delta T_{wt} = \bar{T}_w - \bar{T}_f$

$\bar{T}_f = (T_{f,out} + T_{f,in})/2$

$A_o = \pi d_o l_t$ (without correction for conduction spreading)

$A_o = \pi d_o l_e$ (with correction for conduction spreading)

Figure 22 shows the plots for $\bar{h}_c$ with correction for heat conduction spreading as function of Re. In venturi flow, $\bar{h}_c$ increases significantly with Re whereas in circular flow the increase is very small. Effect of fluid subcooling on $\bar{h}_c$ is not significant in both cases. The highest $\bar{h}_c$ measured for the venturi flow at $Re = 2.7\times10^4$ is in the range of 11-13 W/cm^2°C and that for circular flow is 2.5-3 W/cm^2 °C.

4.5.6 Variation of $\bar{T}_w$ and $\bar{h}_c$ with Heat Flow Rate

Results of the tests conducted at constant flow rate and varying power input are presented in Figure 23. The highest flow rate achieved with the pump in the present setup corresponded to $Re = 2.7\times10^4$. Near room temperature ($T_f = 20$°C) was selected for convenience. Wall temperature increased linearly with heat flow rate in both cases. The heat transfer coefficient variation is greater at low heat flow than at higher heat flow in the case of venturi flow whereas for circular flow $\bar{h}_c$ does not vary with heat flow.

4.5.7 Verification of Results with Theory

There are no empirical correlations in the literature exactly matching the present experimental venturi configuration. Hence, it is not possible to verify the results. The nature of localized heat addition with flow velocity variation in venturi flow is a unique model and was never analyzed before.

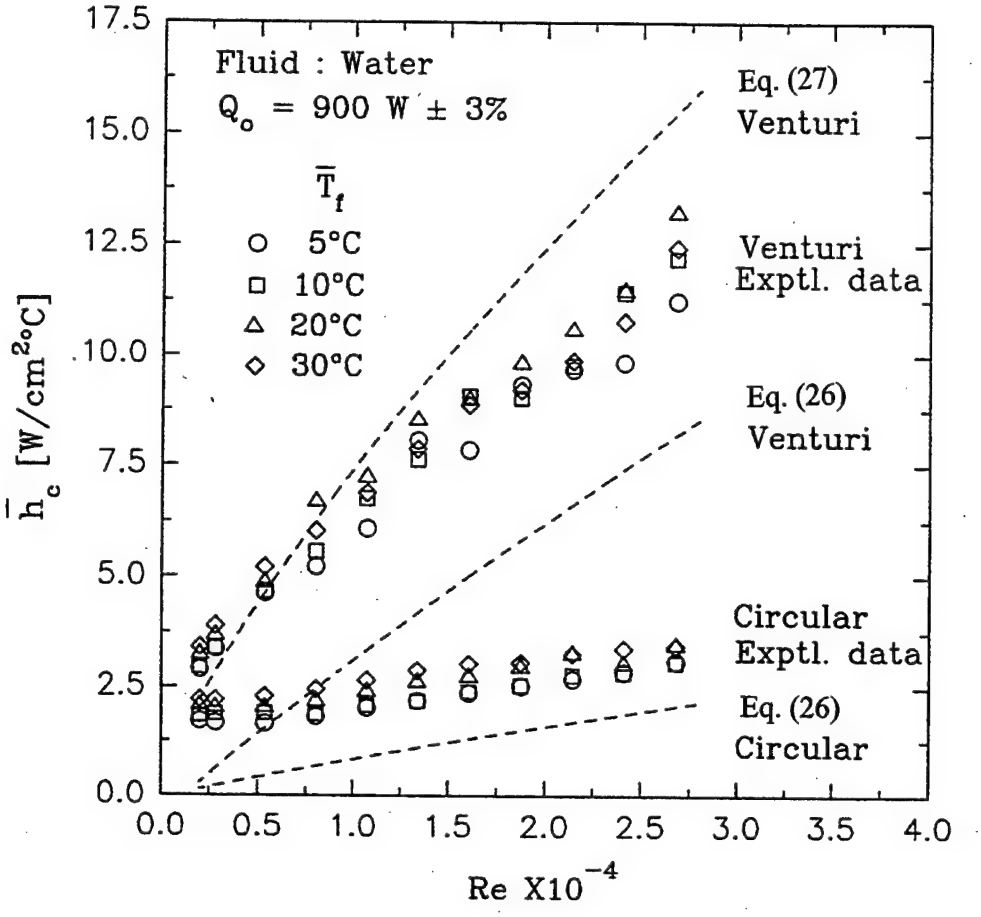

Figure 22. Heat Transfer Coefficient vs Re for Circular and Venturi Flow. Comparison of Experimental Data with Theory.

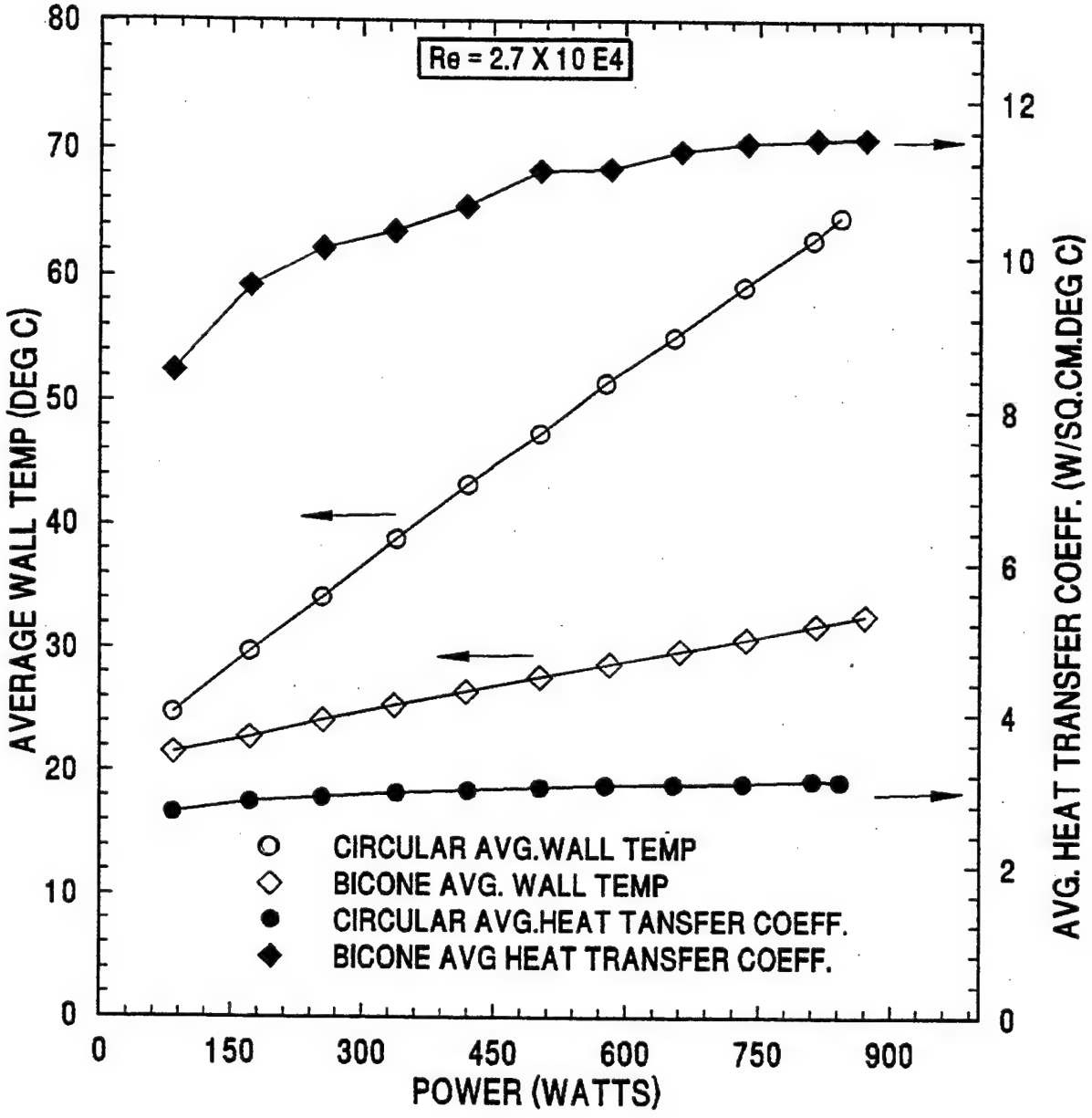

Figure 23. Wall Temperature and Heat Transfer Coefficient Variations with Heat Flow Rate.

However, a rough comparison of the present results was made against the Gnielinski correlation for constant properties fully developed turbulent flow through a smooth circular tube as given in Eq. (26) valid for $1.5<Pr<500$ and $3000<Re<10^6$ [11].

$$N_\infty = 0.012\ (Re^{0.87} - 280)\ Pr^{0.4} \qquad (26)$$

where $\bar{N}u = Nu_\infty[1 + (L/D)^{-2/3}]$ for $100 < L/D < 1000$

$\bar{h}c = \bar{N}uk/d_o$; $L/D = l_t/d_o$ for circular flow (0.08 in the present experiment)

$\bar{h}c = \bar{N}uk/D_h$; $L/D = l_t/D_h$ for venturi flow (2.4 in the present experiment

Results of Eq. (26) computed for the present experimental parameters are plotted in Figure 22. Even though both experimental and correlational results follow similar trends, their actual values deviate by a big margin. A possible explanation for the discrepancy is the validity range of L/D ratio or the definition of an appropriate L/D.

A correlation given by Incropera, et al., for flow over discrete heat sources in a rectangular flow duct is adopted for the present case as given in Eq. (27) [9,12]

$$\bar{N}u = 0.037 Re^{0.75} Pr^{0.35} (l_t/D_h)^{0.85} (k/k_s)^{0.02} \qquad (27)$$

The result of Eq. (27) for the venturi flow only is plotted in Figure 22. The agreement with experiment data is very good in $3000 < Re < 15{,}000$. For circular flow, this correlation predicts very low values and hence is not shown in Figure 22.

4.5.8 Further Study

A computational solution approach to this problem was undertaken under a separate research effort and the related publications are Ref. [13-20]. And also in light of potential applications in the electronic and high flux cooling requirements, the flow, heat transfer and

geometric parameters have to be optimized. Planned further research in this direction was still in progress at the time of writing this report.

4.5.9 Practical Significance/Usefulness

The venturi cooling technique is highly applicable for cooling very high power electronic components where other methods such as direct jet-impingement, immersion and spray cooling cannot be used or difficult to use. Also, this method is ideal for non-boiling type coolants such as turbine oil and poly-alfa-olefin used in aircraft thermal management.

4.6 SUMMARY

The following were the significant results and conclusions of this heat concentrator study:

1) A maximum heat flux of 323 W/cm^2 (147 W/cm^2 with an assumed 45° conduction-spread correction) was achieved with wall temperature ranging from 60-106°C for circular flow and 18-82°C for venturi flow when $5° < T_c < 30°C$ and $1.8\times10^3 < Re < 2.7\times10^4$.
2) The highest average heat transfer coefficient ($\bar{h}_c$) for venturi flow was 13.23 W/cm^2 °C (with correction) for $Re = 2.7\times10^4$ and $T_f = 20°C$. This was about 4 times that of the circular flow.
3) The effect of coolant subcooling on wall temperature was substantial while that on average heat transfer coefficient was minimal in both flow configurations.
4) Absolute pressure measurement at the throat section showed sub-atmospheric pressures which lowered the saturation temperatures. The lowest pressure was 72 kPa and T_{sat} reduction was 9°C.
5) The highest fluid velocity at the throat was 11.5 m/s while the upstream velocity was 0.72 m/s.

6) The venturi flow constriction pressure drop penalty was only marginal - about 37 kPa (for 35.9 lpm flow rate and $T_f = 25\,°C$) which translates to 22 W of pump power.

7) Empirical heat transfer correlations from the literature were used to corroborate the present experimental results with fairly good agreement between them.

5.0 COOLING STUDIES ON MCT IN CONDUCTION MODE OF OPERATION

5.1 DESCRIPTION OF THE MCT TESTED IN CONDUCTION MODE

The MCT technology is still evolving and various packaging configurations exist. The device used in the present study was rated 100 A continuous current at 1.554 Vdc and was a 5-lead JEDEC MO-93 plastic package which is a variation of the TO-218 package. This consisted of a silicon die soldered with 3 mils of solder to 16 mils of copper and encapsulated in 140 mils of plastic using silicon alumina metalization. The hermetic package contained copper-molicopper base with alumina (ceramic) - copper lid. Additional details and description can be found in Temple (1986) [21], Reyes, et al., (1992) [22] and Radun, et al., (1993) [23].

5.2 VENTURI FLOW COOLING CONCEPT FOR MCT COOLING

Flow through a straight circular tube is converted into a tapering annular flow by positioning a specially shaped "bicone constrictor" in the center of the tube directly in the flow path. High power dissipating devices are mounted on the flattened faces directly outside the tube at the throat section. Flow velocity at the throat can be increased beyond an order of magnitude over the upstream velocity. Consequently, Re and Nu are increased for a given high Pr fluid ($5 < Pr < 100$). Boiling could be allowed locally at the throat (depending upon the constraints on the wall temperature and fluid properties) for further enhancing heat transfer. The idea of creating high flow velocity is the key to the success of this method. In addition, the effect is very localized to suit the localized heat source, characteristic to the MCT devices. Both direct and indirect mounting (with respect to the contact with the fluid) are feasible. By suitable design of the taper angles, the liquid pressure drop due to the venturi can be minimized. Viscosity is a major deciding factor in using this type of convective cooling as the pump power and viscous dissipation effects could outweigh the heat transfer enhancement. It has been shown in this context, by experimental and theoretical investigations, that the pump power penalty is only marginal and that the benefit outweighs the problem (see Section 4.2).

5.3 MCT HEAT SINK - CONCEPTUAL IDEAS

In actual applications, clusters of MCTs will have to be mounted as a module to share a common heat sink. Two possible heat sink configurations involving venturi concept are explained here. In Figure 1(a) and (b) a cylindrical geometry with planar external mounting surfaces was illustrated. Figure 24 shows a rectangular duct configuration where both top and bottom panels can be used as heat sinks.

Both geometries offer axisymmetrical flow with multi-stage addition possibilities along the flow direction. Material of construction must be aluminum or copper for good wall-thermal conductivity. Optimized designs of these conceptual ideas can be worked out if MCT module design and heat loads are known.

5.4 EXPERIMENTAL WORK

5.4.1 Setup Design

The present experimental setup consisted of a copper test section with gasket seated end-flanges for easy removal from and assembly to the coolant flow line. A venturi bicone-flow-constrictor made of stainless steel was rigidly held concentrically inside the test section in order to create the high velocity flow at the throat section. Six flat machined faces directly outside the throat section were used for mounting high heat flux heaters or MCTs as in the present experiment. The bicone could be easily removed in order to convert the test section into a circular flow geometry without altering other arrangements.

A schematic of the setup consisting of a constant temperature bath, centrifugal pump, flowmeters, filter, pressure transducers, data logger and heater circuit has been shown in Figure 11. The heater circuit seen in the figure was replaced with the MCT test circuit. A photographic view of the test section showing the MCT is given in Figure 25. The conduction mode test circuit for the MCT was a relatively simple one consisting of a high current, low voltage regulated power supply and a 0.5 mΩ precision shunt resistor for current measurement. This circuit details are shown in Figure 26. The coolant circulation capacity was 0-35 lpm at

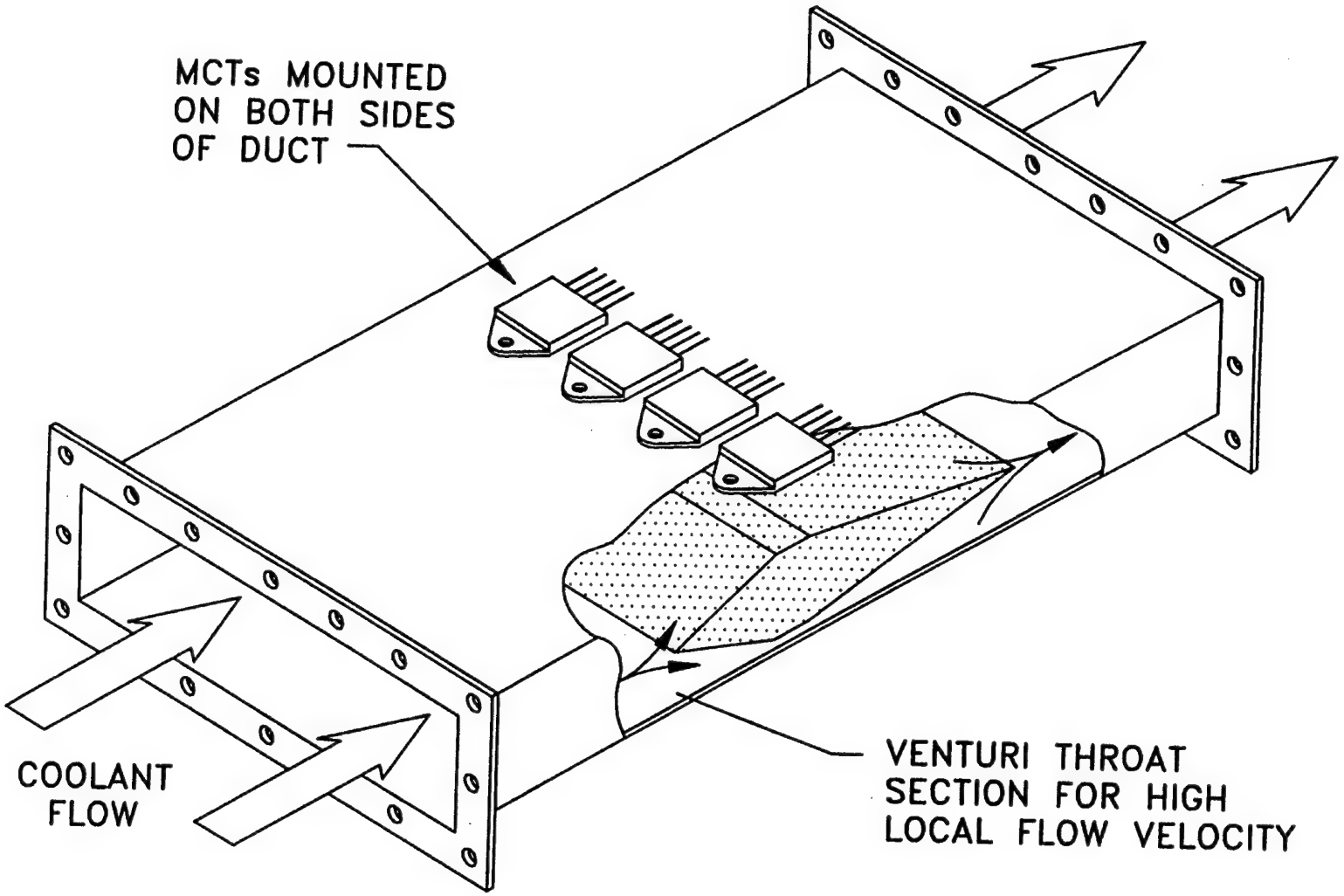

Figure 24. Rectangular Duct Type Flow Venturi Heat Sink Configuration.

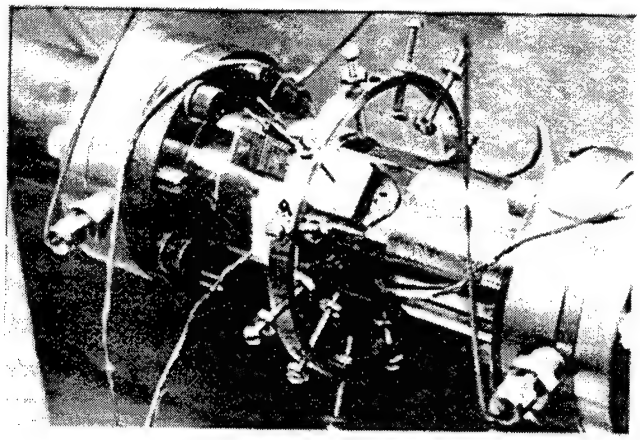

Figure 25. Photograph of the Test Section with MCT.

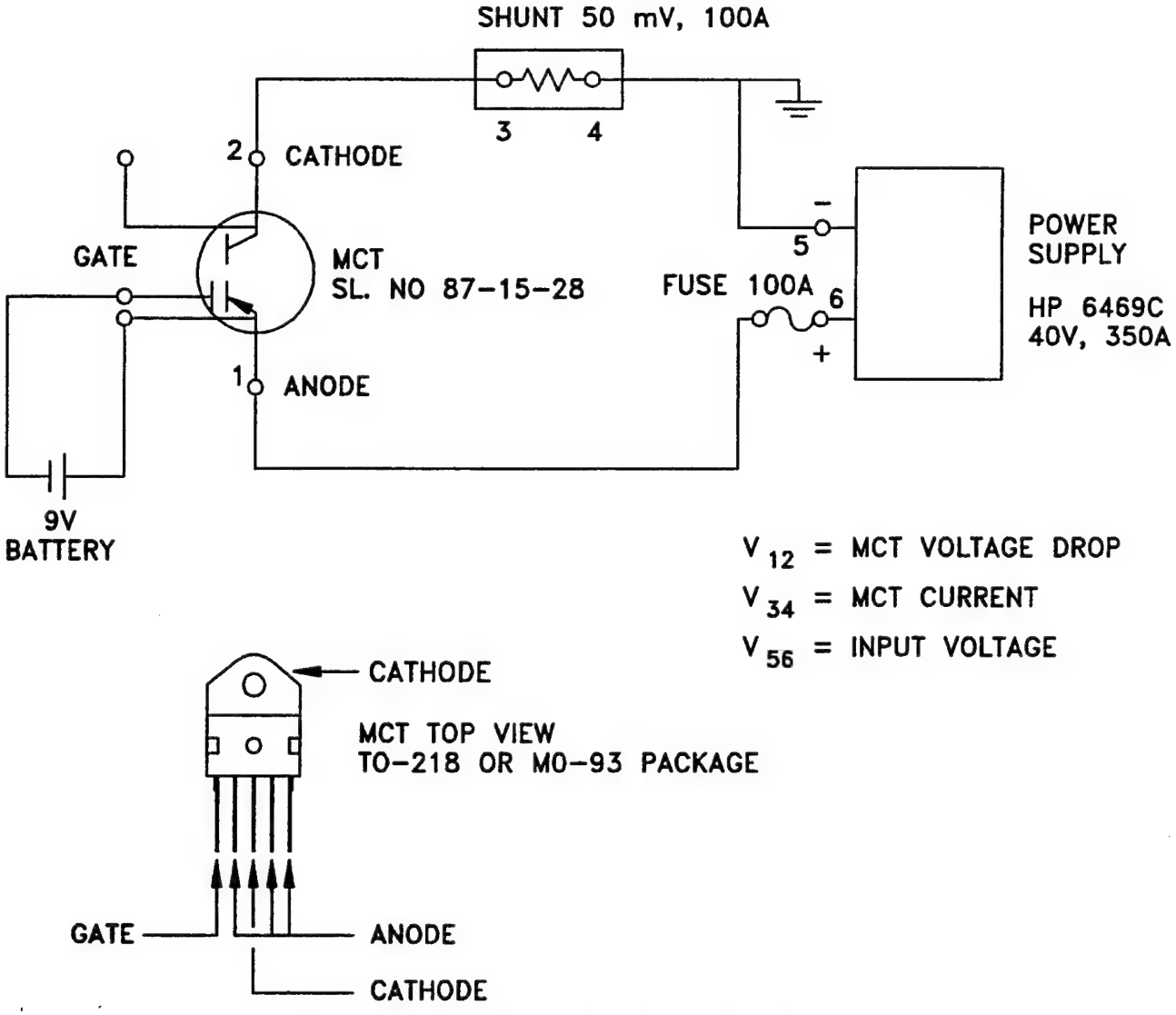

Figure 26. MCT Conduction Mode Test Circuit.

temperatures from 5°C to 30°C through 3.33 cm inner dia. copper pipe. To compare the relative heat transfer performances, three heat sink geometries were tested. Two were based on the venturi test section and the third was a commercially available liquid-cooled aluminum cold plate. The physical dimensions and details are as follows:

Heat Sink Configuration I

Venturi Flow

- Bicone flow constrictor installed
- Hydraulic dia. of annular flow = 0.0965 cm
- Cone angles: upstream = 40°; downstream = 20°
- Upstream flow dia. = 3.33 cm
- Venturi section length = 10.5 cm
- MCT mounted on one of the six flat faces and clamped by a ring clamp
- Due to axisymmetry, one-sixth share of total flow was assumed to be shared by each face

Heat Sink Configuration II

Circular Flow

- Same as configuration I except that the bicone flow constrictor was removed
- Hydraulic dia. = 3.33 cm

Heat Sink Configuration III

Commercial Cold Plate

- Series 180-10 Heat Sink by EG&G Wakefield Engineering (1988) [25]
- Aluminum alloy 6063-T5 plate lined with U-shaped copper tube (3/8" OD, 1/32" wall) 12" long
- MCT mounted at the center of plate directly above the inlet side of the copper tubing
- MCT clamped with a special clamp

5.4.2 MCT and Thermocouple Mounting

The polished metallic surface of the MCT (1.8 cm^2) was mounted on the polished flat surface of the test section with a thin layer of conductive grease applied to both mating surfaces.

The top surface of the MCT was pressed down using a ceramic spacer and a clamp screw. A torque of 20 in.oz. was applied using a torque-screw driver which provided consistent contact pressure for the MCT in all the test configurations.

The foil type thermocouples were used on the top and bottom surfaces of the MCT for temperature sensing. This facilitated the flush-mounting of the MCT. In addition, three other bead-junction thermocouples were mounted on or near the MCT to measure the flange, upstream and downstream wall temperatures. Inlet and outlet coolant temperatures were measured with probe type sensors located on the end-flanges of the test section.

Grounded type cathode connection for the MCT facilitated the test section to be at ground potential even though it was part of the live circuit. Figure 27 illustrates the MCT and thermocouple mounting for the test configurations I and II. Figures 28 and 29 show the views of the commercial heat sink (Configuration III).

5.4.3 Test Procedure

Water circulation rate and temperature were set at the desired values. The MCT gate was triggered open by a 9V battery connected as shown in Figure 26 and the input power to the circuit was raised by increasing the current from zero to a maximum value in steps of 10 A. Steady state values of temperatures, voltages and current were recorded. It took approximately 20 minutes for each setting. A limiting device-temperature of 175 °C (measured at the top surface of the MCT) was imposed to avoid destroying the device. The contact pressure of the MCT was maintained by periodically checking the tightening torque (20 in.oz.) on the clamp screw. Tests were repeated for coolant temperatures of 6.5 °C, 10 °C, 19.5 °C and 23 °C and varying the flow rate from 0.63 lpm to 6.31 lpm at each coolant temperature. The data were recorded in the Fluke datalogger diskette for further analysis and processing.

In a similar manner, tests were repeated for heat sink configurations II and III after suitably modifying the test section.

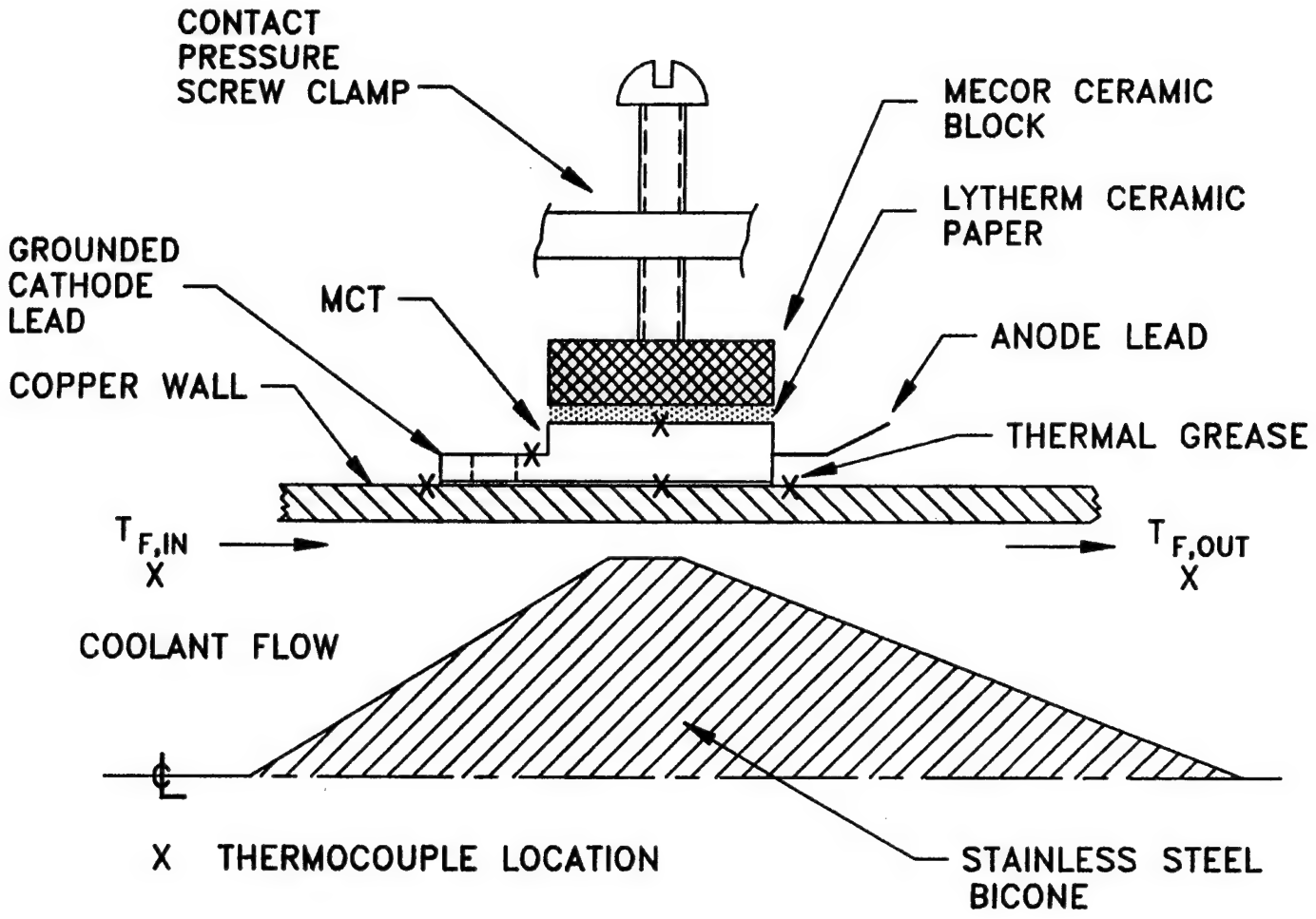

Figure 27. MCT Mounting and Thermocouple Locations (Configurations I and II).

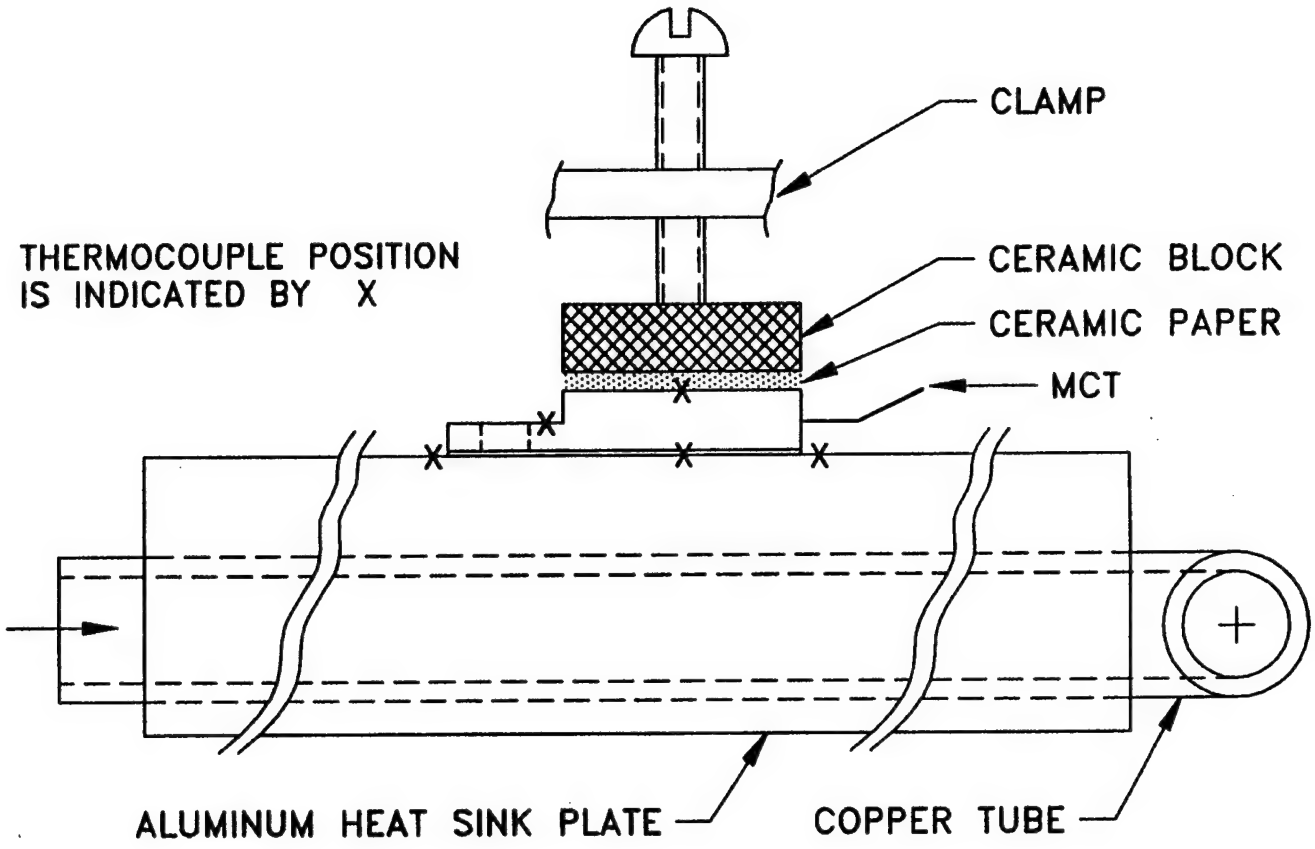

Figure 28. Commercial Liquid-Cooled Cold-Plate Heat Sink Configuration III (Front View).

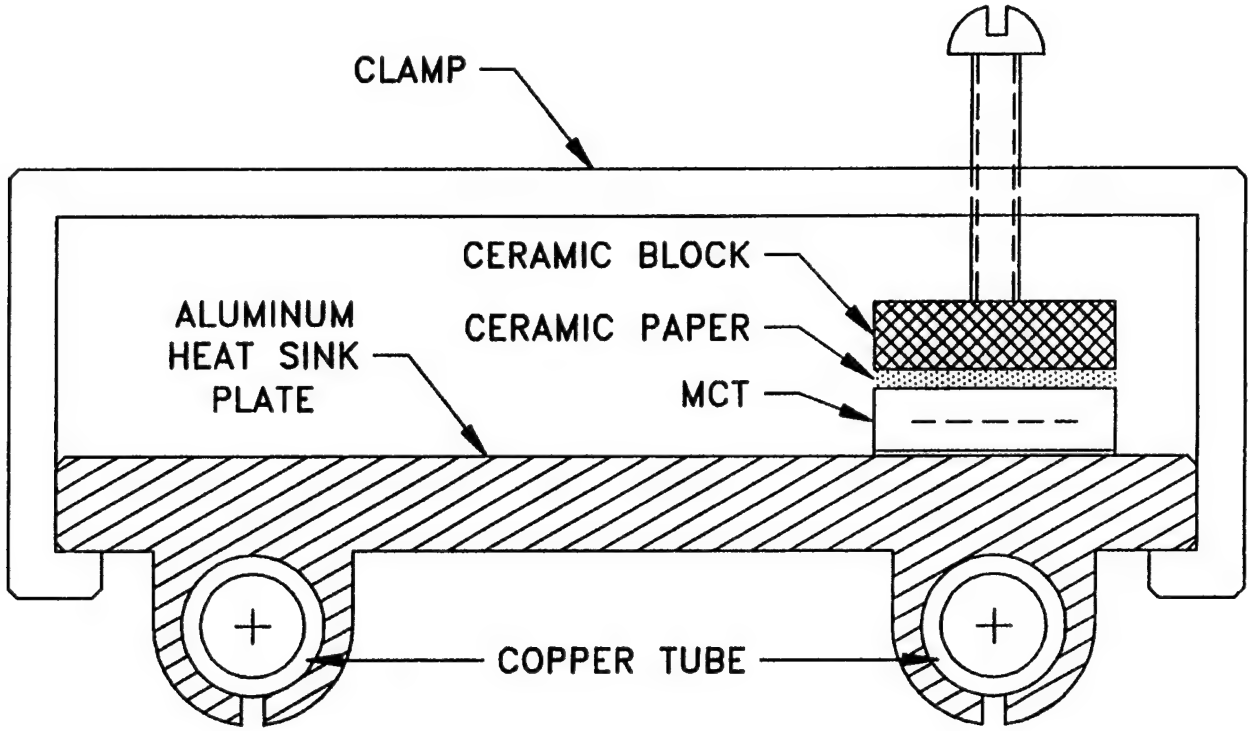

Figure 29. Commercial Liquid-Cooled Cold-Plate Heat Sink Configuration III (End View).

5.5 RESULTS AND DISCUSSION

5.5.1 Temperature Variation

The temperature measurement on the MCT included the top surface, bottom surface and the flange. The device junction temperature could not be measured with this hermetically sealed package. However, the top surface temperature was assumed to be the junction temperature as the top surface was insulated and the temperature drop between the junction and the top surface was neglected. Even though this caused some inaccuracies, thermal resistances could be calculated and compared for various flow configurations.

Figure 30 shows the MCT top, MCT bottom, MCT flange, wall upstream and wall downstream temperature variation with MCT power for venturi flow with coolant at 2.52 lpm and 6.5°C. The top surface temperature was the highest and all temperature variations were linear with power increase. Figure 31 shows the MCT power variation with MCT current for the same test run as that of Figure 30. Similar temperature and power variations were observed for circular flow and commercial heat sink also.

5.5.2 Wall Heat Spreading

Because of the finite wall thickness and high conductivity of the wall material, the heat spreads in the wall to a wider area before dissipating into the fluid. A quantitative estimate of this spreading would be of interest to precisely determine the fluid side wall temperature and heat transfer coefficient. However, it is not simple to calculate because of the conjugate nature of the problem. In addition, the discrete nature of the MCT heat dissipation on the test section makes it more difficult. A separate axisymmetric case of the same system with uniform circular-ring shaped heat-addition problem was numerically solved using the Phoenics computational fluid dynamics code [15,16]. Axial variations of the radial wall-heat flux at the inner wall for a typical set of input parameters for both venturi and circular pipe flows are plotted in Figure 32 The wall thickness and the venturi throat length where heat addition takes place are 3.18 and 2.64 mm, respectively. Heat flux, Re, and coolant inlet temperature are shown in the figure. Axial lengths

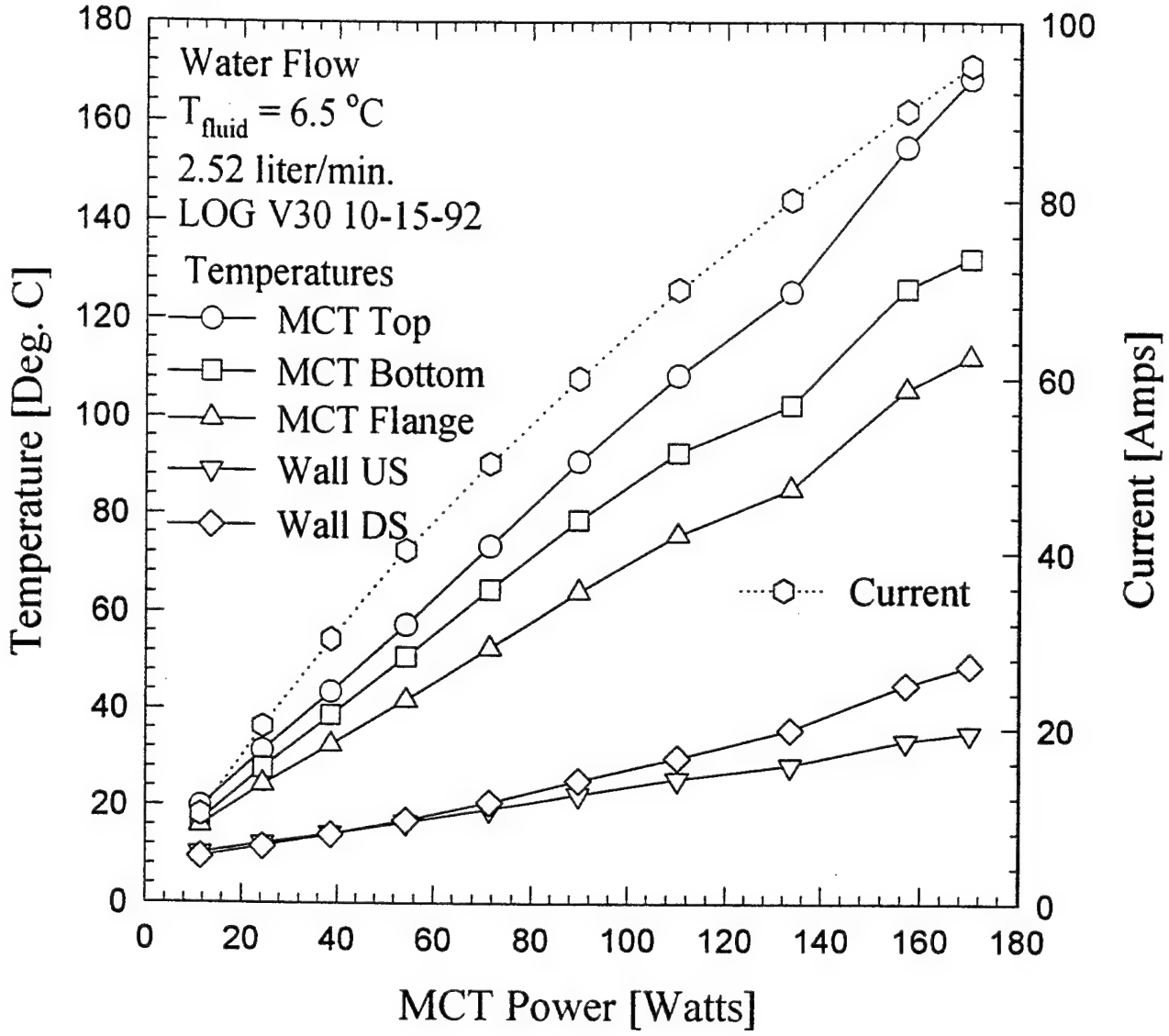

Figure 30. MCT Temperature Profile for Different MCT Power Levels.

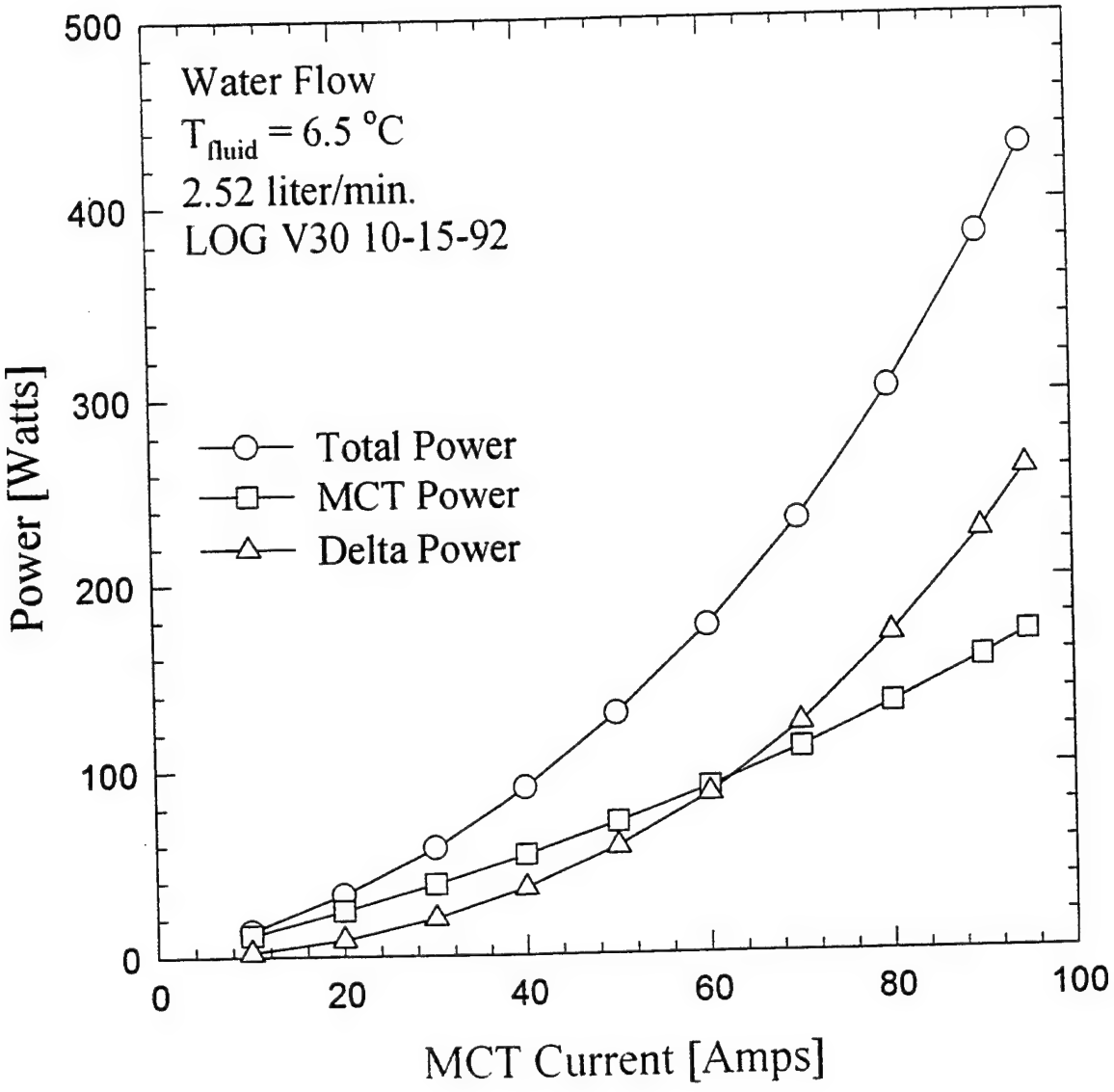

Note: Total Power, (P_1) = Applied Power = (Applied Voltage Across MCT) × MCT Current
MCT Power (P_2) = MCT Voltage Drop × MCT Current
Delta Power = $P_1 - P_2$

Figure 31. MCT Power vs. MCT Current.

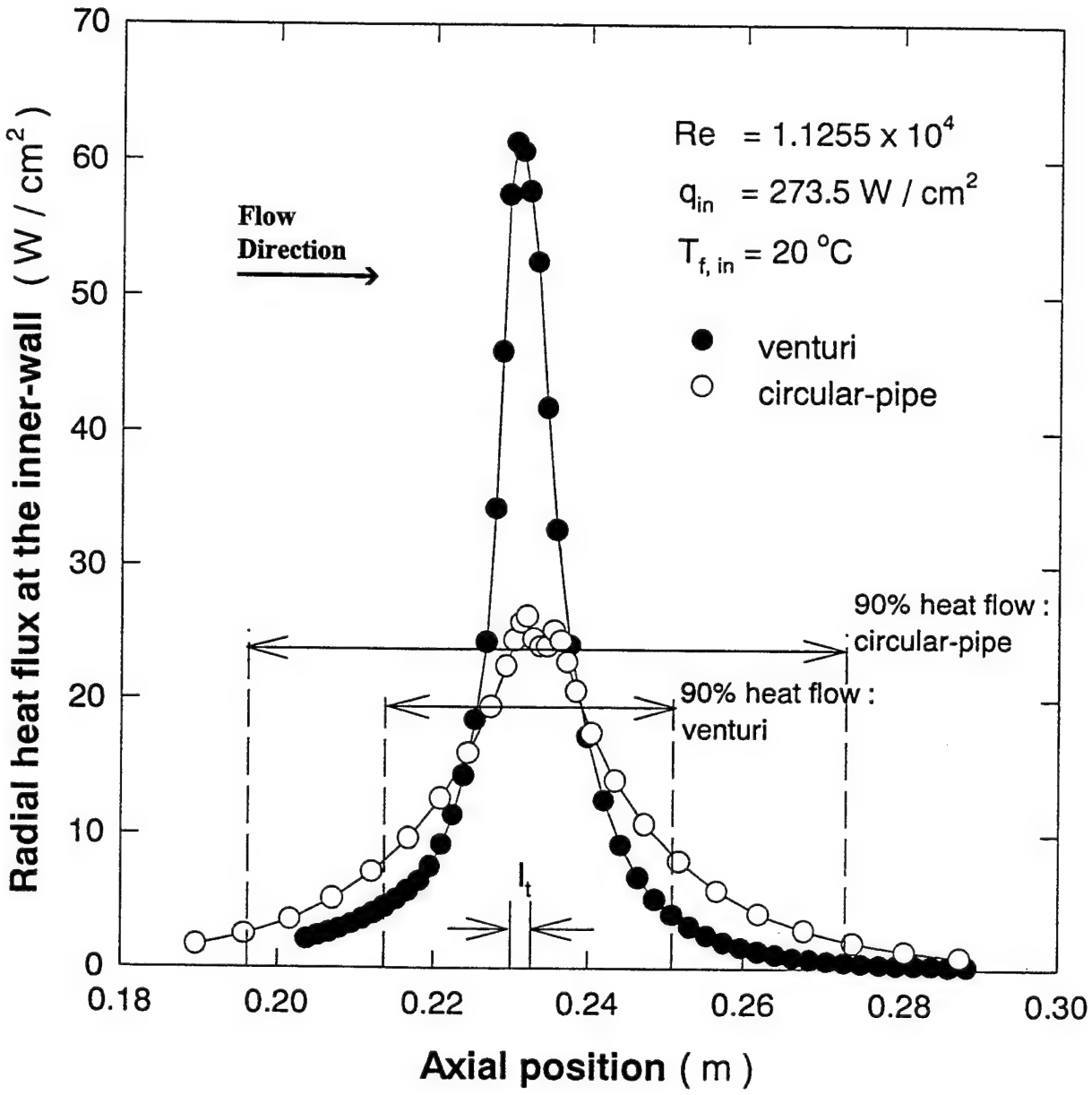

Figure 32. Computational Results Illustrating the Heat Spreading in the Wall at the Throat.

of heat spreading are obtained from the bell-shaped curves (Figure 32) as the effective lengths across which 90% of the radial heat flow to the coolant takes place. Accordingly, it is determined that the heat addition length of 2.64 mm spreads to 40 mm for the venturi flow case and to 80 mm for the pipe flow case, with both cases using copper as the wall material and water as the coolant. A detailed description of this can be found in Ref. [13-18].

5.5.3 Peak Performance Results Summary

The peak performance was judged from the largest MCT current handled in the conduction mode testing for any heat sink tested without exceeding the safe operating temperature for the MCT. Table 7 provides this comparison at coolant temperature of 6.5 °C as a common reference for the three cases. Venturi flow exhibited the largest MCT current of 95 A (continuous) which was very close to the rated value of 100 A. Also, listed in this table are thermal resistances and heat flux values.

5.5.4 Temperature vs. Coolant Flow

At a moderate circuit current of 60 A, the MCT top surface temperatures were compared for all three cases as a function of flow rate. An interesting plot resulted as shown in Figure 33 where the temperature values were the highest for the commercial heat sink and the lowest for venturi flow. The temperature dropped initially and steadied as the flow rate increased for configurations II and III while that for venturi flow exhibited steep drop beyond 4 lpm. This exemplifies the distinct advantage of the venturi cooling concept.

Figure 34 shows the temperature variation and θ_{DF} for all three cases as functions of coolant temperature for a constant flow rate. Venturi flow exhibited better performance at lower T_{Fluid}.

Table 7. MCT Cooling Test Results Summary (Peak Performance Data Compared For Three Cooling Configurations)

Sl. NO.	TEST PARAMETER		VENTURI FLOW	CIRCULAR FLOW	COMMERCIAL HEAT SINK
1.	MCT Current	Amp	95.08	75.02	63.45
2.	MCT Voltage Drop	Vdc	1.789	1.551	1.455
3.	Applied Voltage	Vdc	4.516	3.626	3.253
4.	MCT Power Dissipation	W	170.09	116.33	92.34
5.	Applied Power	W	429.4	272.0	206.4
6.	MCT Temperature:				
	a) Top (Junction)	°C	168.5	161.1	154.9
	b) Bottom (Case)	°C	132.3	138.0	116.0
	c) Flange	°C	112.3	118.1	84.6
7.	Coolant Flow Rate	lpm	2.52	5.05	5.05
8.	Reynolds Number	ND	10,716/5,445	21,432	9,365
9.	Coolant Temperature†	°C	6.5	6.5	6.5
10.	Thermal Resistance:				
	a) Junction-to-case	°C/W	0.213	0.199	0.421
	b) Device-to-fluid	°C/W	0.952	1.329	1.607
11.	Heat Flux:	W/cm^2			
	a) At internal substrate solder ($0.66\ cm^2$)		257.7	176.3	139.9
	b) At the base of MCT ($1.8\ cm^2$)		94.5	64.6	51.3
12.	Test Log No. & Date		V30 10/15/92	C22 10/13/92	W10 10/29/92

Note: †The only independent constant reference parameter for all three cases.

Thermal resistance:

$$\text{i) Junction-to-case, } \theta_{JC} = \frac{T_{Top} - T_{Bottom}}{P_{MCT}} \tag{28}$$

$$\text{ii) Device-to-fluid, } \theta_{DF} = \frac{T_{Top} - T_{Fluid}}{P_{MCT}} \tag{29}$$

Heat flux:

$$\text{i) At internal substrate solder, } q_1 = \frac{P_{MCT}}{A_{Substrate}} \tag{30}$$

$$\text{ii) At the base of MCT, } q_2 = \frac{P_{MCT}}{A_{Base}} \tag{31}$$

where T is measured MCT temperature and P is MCT power which is the product of measured circuit current and forward voltage drop. The substrate and base area of the MO-93 package was $0.66\ cm^2$ and $1.8\ cm^2$, respectively.

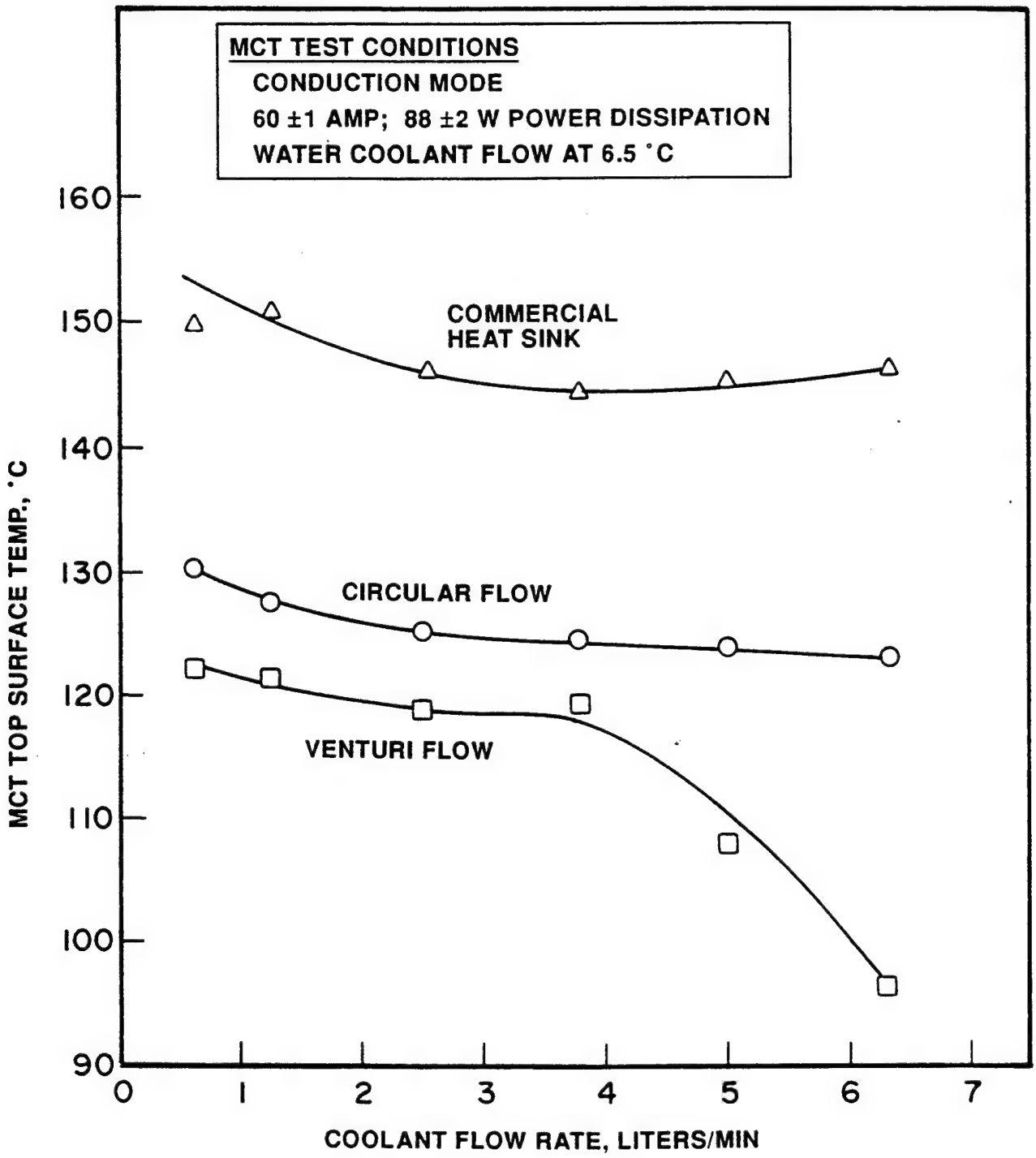

Figure 33. MCT Top-Surface Temperature vs. Coolant Flow Rate.

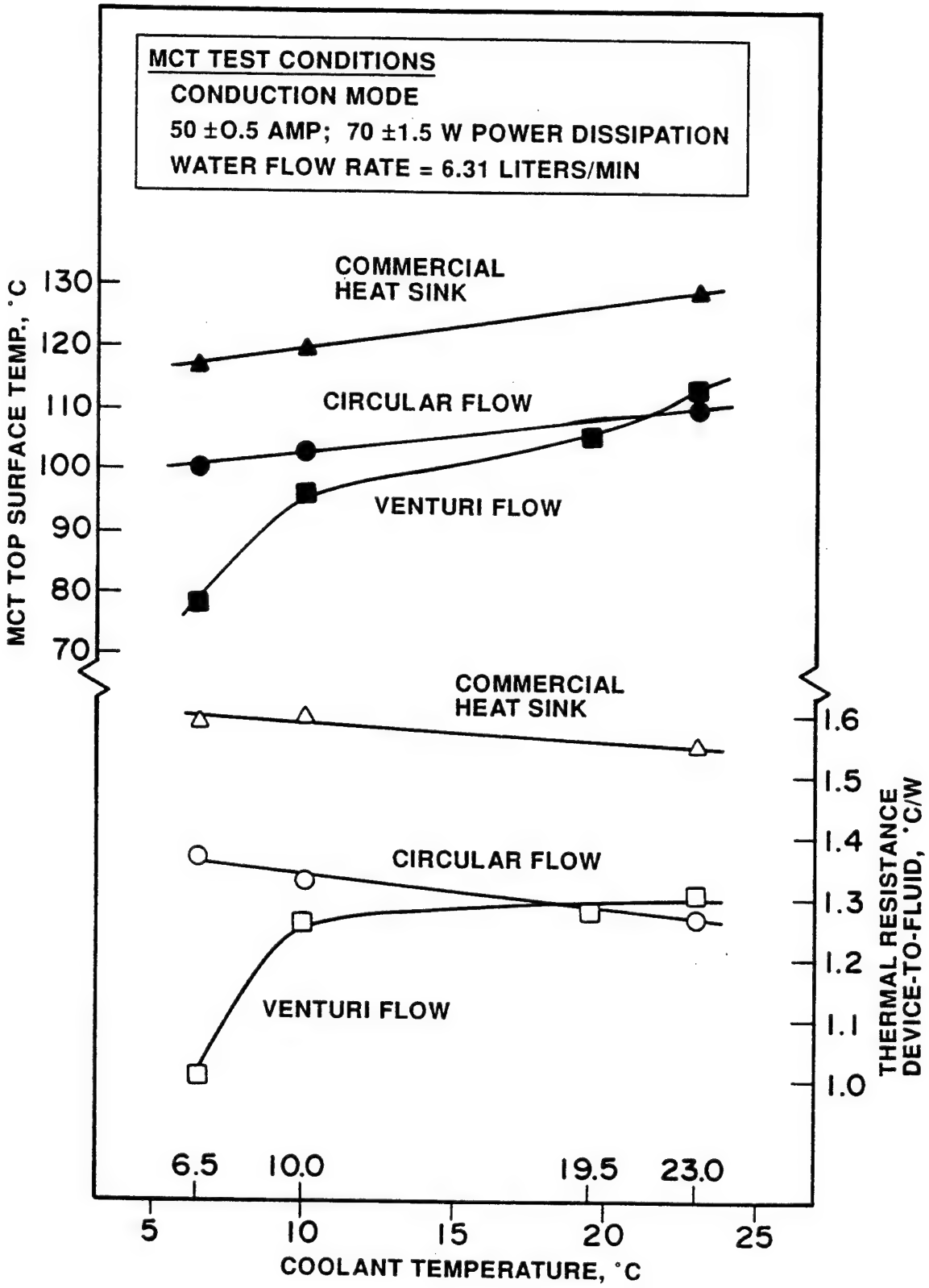

Figure 34. MCT Top-Surface Temperature and Thermal Resistance (θ_{DF}) vs. Coolant Temperature.

5.5.5 Thermal Resistances vs. MCT Power

θ_{JC} and θ_{DF} were plotted as functions of MCT power for all three cases at $T_{Fluid} = 6.5\,°C$ and flow rate of 2.52 lpm as seen in Figure 35. θ_{DF} values were larger than θ_{JC} for all cases as θ_{DF} includes the external thermal resistances such as contact resistance, wall conduction, and wall-to-fluid resistance. θ_{JC} includes only the internal MCT substrate bonding resistances and body (casing) resistance. In the case of the commercial heat sink test, θ_{JC} was higher than that for the other two configurations. The reasons may be attributed to higher MCT operating temperature and non-uniform cooling of the MCT bottom by the commercial heat sink. Also, with high operating temperature, the substrate bonds could weaken and exhibit high thermal resistance. This discrepancy was not observed for circular and venturi flows wherein θ_{JC} values were more or less equal.

The θ_{DF} values of the MCT in Figure 35 clearly demonstrate again that venturi flow is superior than the other cases. The decrease in θ_{DF} up to MCT power of 70 W could be explained by the facts that the internal MCT substrate bonding and packaging materials expand with heating and their thermal conductivities vary with temperature.

5.6 SUMMARY

Single phase liquid cooling of MCT device using an annular venturi type flow was successfully demonstrated. This cooling method has been proven very effective for localized high heat flux applications. A comparison of performance results between commercial liquid-cooled cold-plate, circular flow and venturi flow heat sinks showed superior performance by the venturi flow.

Coolant flow-rate increase and coolant temperature decrease produced sharp drop in device temperature and device-to-fluid thermal resistance respectively for the venturi flow and not seen for circular flows. Venturi flow cooling technique is suitable for any localized high heat flux applications such as the MCT cooling. Use of other coolants and geometry-optimization is possible. The liquid pressure drop penalty due to venturi constriction is only marginal.

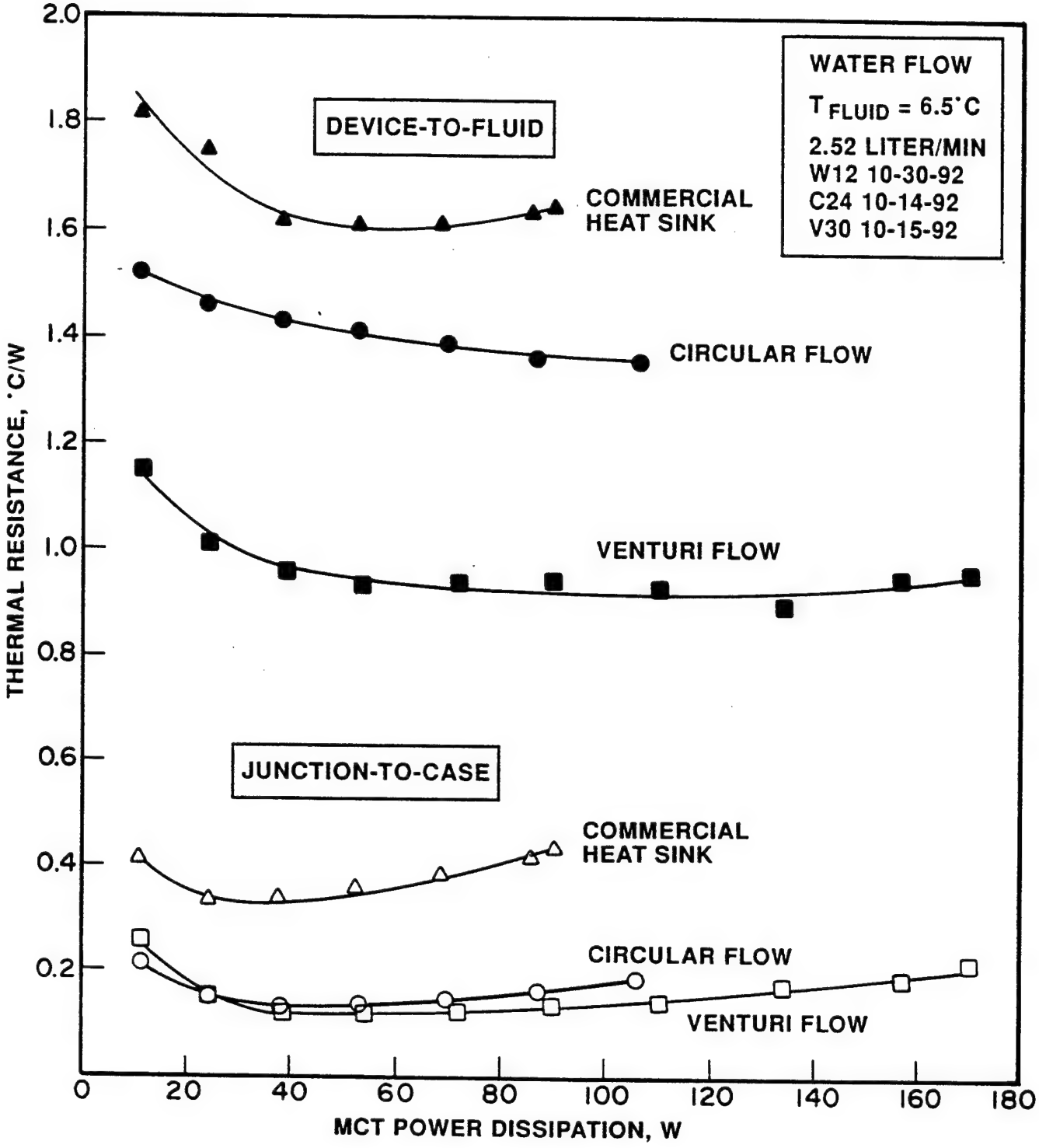

Figure 35. Thermal Resistances vs. Power Dissipation.

6.0 COOLING STUDIES ON MCT AND IGBT IN SWITCHED MODE OF OPERATION

6.1 DESCRIPTION OF THE DEVICES USED IN SWITCHED MODE

It should be noted that the batch of MCT devices used here were different from those described in Section 5.1 and the ratings were somewhat different as per manufacturer's information.

MCT [26]: This device is meant for switching currents on and off by negative and positive pulsed control of an insulated MOS gate. It is used in motor control, inverters, line switches and other switching applications. This 5-lead TO-218 package consists of silicon die soldered with 3 mils of solder to 16 mils of copper and encapsulated in 140 mils of plastic using silicon alumina metalization. The hermetic package contains moli-copper base with alumina-copper lid. This device has a continuous rating of 75 A at 90°C and maximum power dissipation of 208 W. Prior tests show that the forward drop for this device is 2.03 V at 100 A, with a turn-off time of 1.6 μs using a 14 μH load. The junction-to-case thermal resistance (R_{JC}) is 0.6°C/W. Figure 36 shows the typical cell cross-section of the MCT.

IGBT [27]: The IGBT is meant for similar applications as that of the MCT. This 3-pin TO-247 package consisted of a 20 mil silicon die soldered with 3-5 mil solder to 80 mil nickel-plated copper and encapsulated in a 200 mil plastic package. This device has a continuous current rating of 30 A and a maximum power dissipation of 200 W. The junction-to-case thermal resistance (R_{JC}) is 0.625°C/W. A typical cross-section of this IGBT is shown in Figure 37. Table 8 provides the ratings of the devices.

6.2 COOLING SYSTEM DESCRIPTION

Venturi cooling: Forced convection cooling of the devices without direct contact to the coolant was used. A simple pipe flow was converted into a converging-diverging flow by a specially designed venturi test section described earlier. The high-heat-dissipating devices were mounted directly above the throat section of the flow where the flow velocity could be increased beyond an order of magnitude over the incoming fluid velocity.

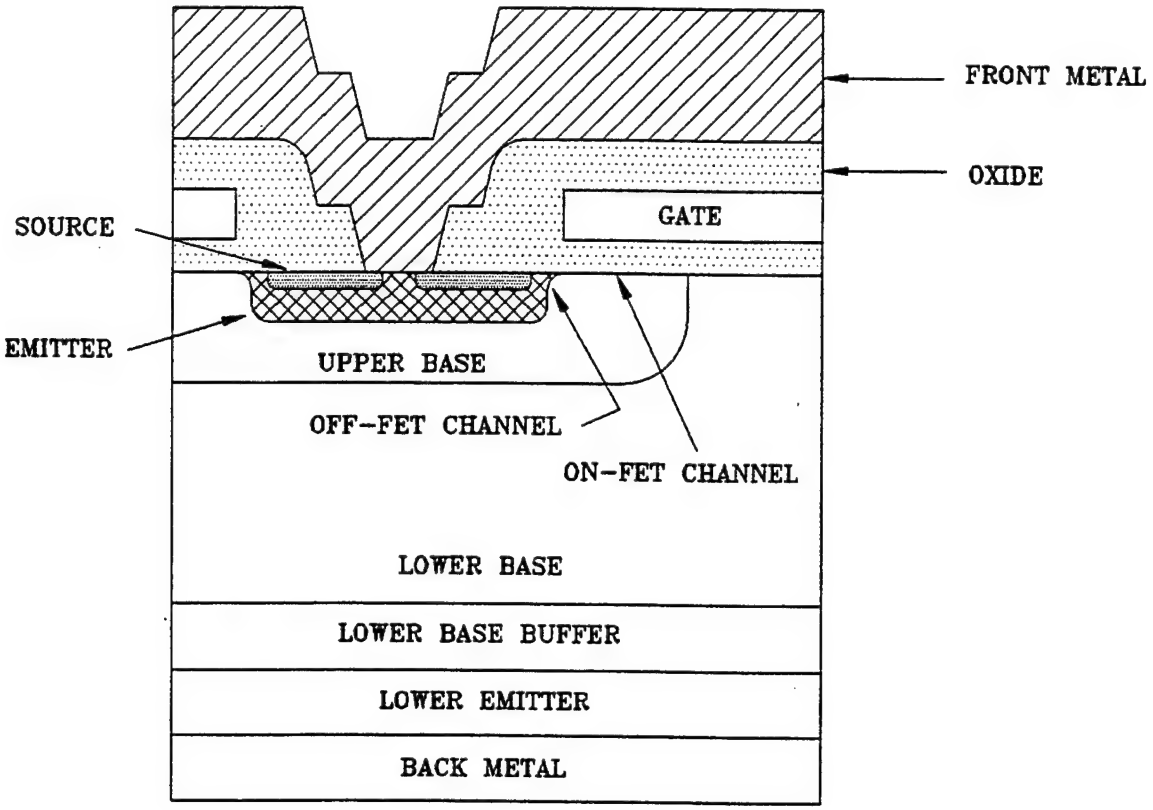

Figure 36. Typical Cell Cross-section of the MCT.

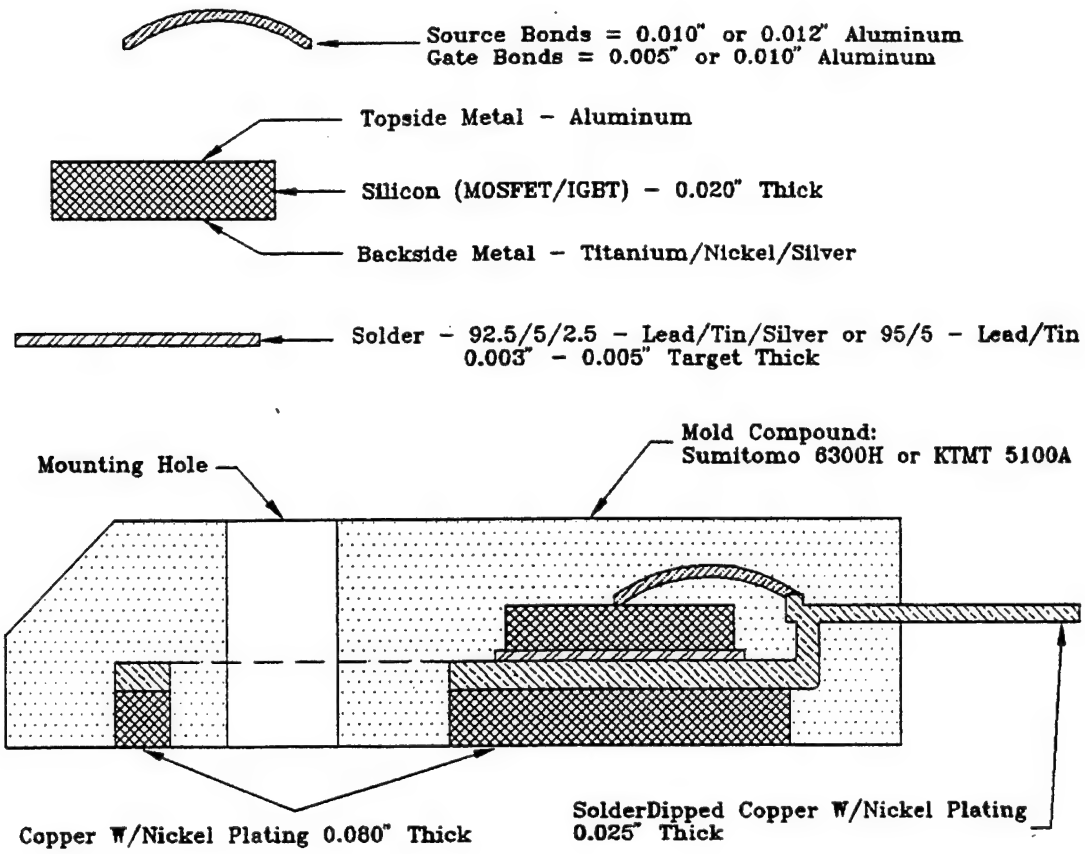

Figure 37. Typical Cross-section of the IGBT in TO-247 Package.

Table 8. Quick Reference Data of Manufacturers' Ratings on MCT and IGBT Devices (All ratings at case temperature of 25 °C unless otherwise specified)

SL No.	Parameter/Feature		MCT	IGBT
1.	Package		MCTV75P60E1 TO-218 5 leads P-Type	APT45GF60BN TO-247 3 leads N-Channel
2.	Voltage	V	-600 (peak off-state)	600 (collector-emitter break down)
3.	Continuous Current†	A	85 @25°C 75 @90°C (cathode)	45 @25°C 30 @90°C (collector)
4.	On-State Voltage	V	1.4	2.5 (collector-emitter)
5.	Max. Power Dissipation	W	208	200
6.	Operating and Storage Junction Temp. Range	°C	-55 to 150	-55 to 150
7.	Junction-to-Case Thermal Resistance	°C/W	0.6	0.625
8.	Junction-to-Ambient Thermal Resistance	°C/W	--	40
9.	Max. Load temp. for Soldering (Under standard setting)	°C	260	300
10.	Mounting Torque Using 6-32 or 3mm machine screw	in-lbs	Not Specified	10
11.	Footprint Area for Mounting	cm^2	2.62	3.35

Note: Data extracted from Ref. [26] and [27].

See Figure 38 for illustrations of MCT and IGBT devices.

†The standards of specifying the continuous current ratings of devices may vary between manufacturers according to the electronic experts familiar with this work.

MCT & IGBT DESCRIPTION

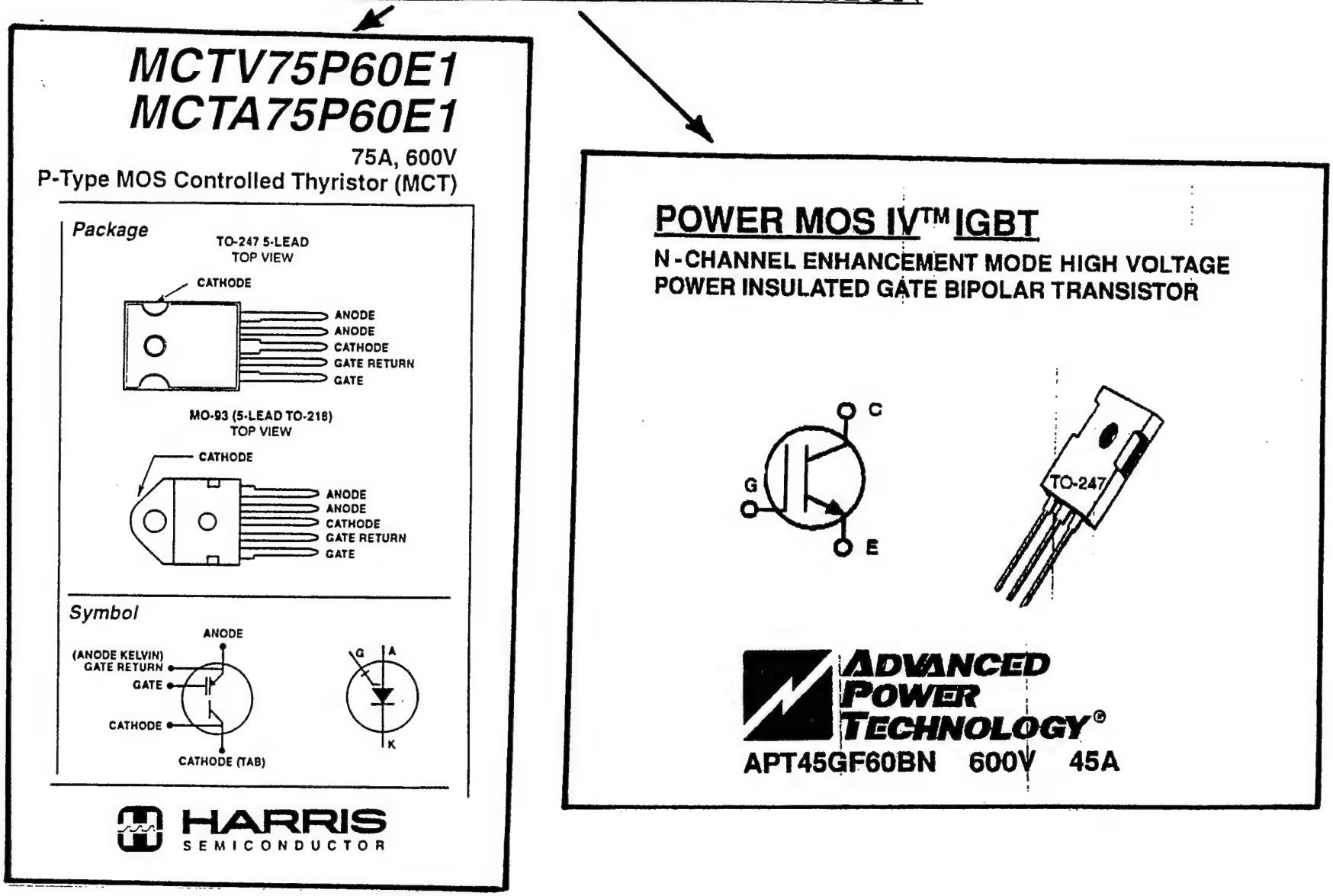

Figure 38. Manufacturer's Illustrations of MCT and IGBT.

6.3 EXTERNAL THERMAL RESISTANCES OF THE DEVICE-MOUNTING

The physical mounting configurations were kept identical for the two devices under test. The bases of the devices were electrically isolated by a thin layer of Kapton film or diamond wafer from the metallic wall of the heat sink. This film or wafer added extra thermal resistance to the cooling circuit with consequent temperature difference (ΔT) between the device and the fluid. The stack of thermal resistances (R_1 to R_5) associated with the mounting of the device to the heat sink is illustrated in Figure 39. The installation of temperature sensors at appropriate locations, enabled measurement of ΔTs and computation of thermal resistances. These experimental values of resistances can be verified with the design data of various items in the stack adding to R_{DF}.

The total resistance defined as device-to-fluid thermal resistance, R_{DF} is obtained by adding all the resistances in series. In terms of temperatures, it is given by

$$R_{DF} = R_1 + 2R_2 + R_3 + R_4 + R_5 = \frac{T_{TOP} - T_{FLUID}}{P_{DEVICE}} \qquad (32)$$

As the top surface of the device is insulated thermally and the convection and radiation losses from the sides are minimal, T_{TOP} can be assumed to be equal to $T_{JUNCTION}$ and the approximate value of the junction-to-case resistance R_{JC} can be obtained from

$$R_{JC} = \frac{T_{TOP} - T_{BOTTOM}}{P_{DEVICE}} \qquad (33)$$

This is possible only if T_{BOTTOM} is measured experimentally. The individual resistances were determined using R = L/kA for conduction and R = 1/hA for convection where L = thickness of the individual layer considered (such as the grease, Kapton film, diamond wafer, heat sink wall, etc.), k = thermal conductivity, A = base area of the device, and h = convective heat transfer coefficient of the venturi flow. The R-values thus calculated based on the conductivity value from the suppliers' data sheet are listed in Table 9. It is clear from the table that the introduction

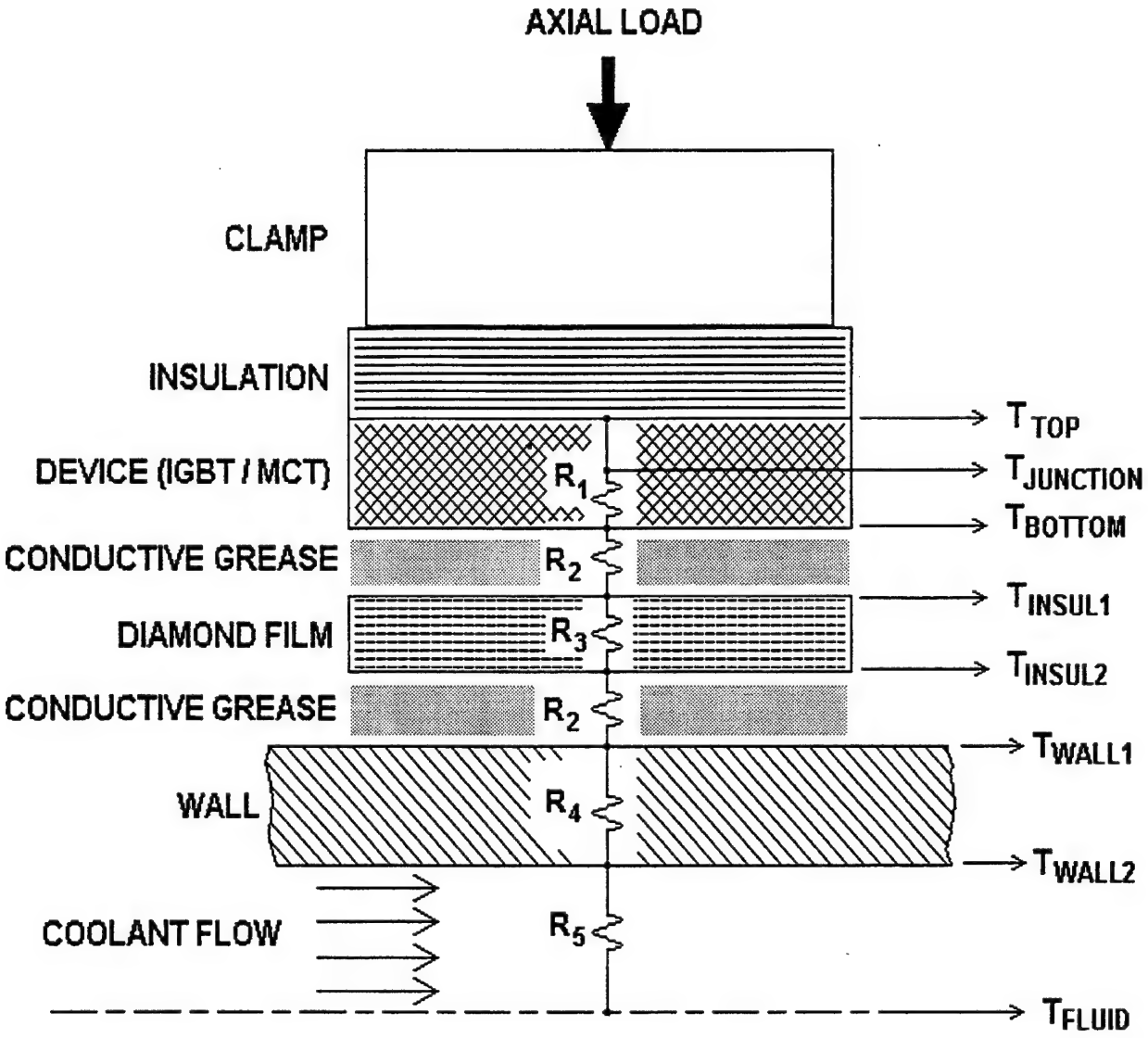

Figure 39. Thermal Resistance Associated with Mounting a Device to the Heat Sink.

Table 9. Estimates of Thermal Resistance Values for Device Mounting

SL No.	ITEMS	Thermal Resistance, °C/W: MCT Mounting A = 2.62 cm^2	Thermal Resistance, °C/W: IGBT Mounting A = 3.35 cm^2
1.	Device: R_1 (Vendor Data)	0.6000	0.6250
2.	Thermal Grease: R_2 L = 0.0127 mm; k = 0.735 W/m °C	0.0659	0.0515
3. (a)	Kapton® Film: R_3 L = 2 layer × 0.01 mm per layer; k = 0.12 W/m °C	Not used	0.4975
(b)	CVD Diamond Wafer: R_3 L = 12 mil = 0.3048 mm k = 1000 W/m °C	0.0012	0.0009
4.	Copper Heat Sink Wall: R_4 L = 3.18 mm; k = 380 W/m °C	0.0319	0.0249
5.	Convection Heat Transfer: R_5 h = 1 to 6 W/cm^2 °C	0.0636 to 0.3817	0.0497 to 0.2985
6.	Total Resistance: R_{DF} with 3(a)	0.761 to 1.079 ($R_1+R_2+R_4+R_5$)	1.300 to 1.549 ($R_1+2R_2+R_3+R_4+R_5$)
	with 3(b)	0.763 to 1.081 ($R_1+2R_2+R_3+R_4+R_5$)	0.804 to 1.052 ($R_1+2R_2+R_3+R_4+R_5$)

® Registered Trademark of DuPont Electronics, USA [28]

of Kapton insulation contributes to more than 50% of the resistance increase. Consequently, the device with Kapton insulation will run at much higher temperatures than that with diamond wafer for the same power dissipation.

6.4 INSULATION MATERIAL CHOICES

Other electrical insulating materials with better thermal conductivity values than Kapton and less expensive than the diamond may be used. These include, Beryllia (242), Alumina (29) and Mica (0.59) where the values in parenthesis are conductivities in W/m°C. Availability, cost, handling, surface finish, compliance, etc., would have serious influence on the choice of these materials.

6.5 EXPERIMENTAL WORK

6.5.1 Setup

The present experimental setup consisted of a copper test section with gasket-sealed end-flanges for easy removal-from and assembly-to the coolant flow line. A venturi bicone-flow-constrictor made of stainless steel was rigidly held concentrically inside the test section in order to create the high velocity flow at the throat section. One of six flat-machined faces directly outside the throat section was used for mounting the devices. As before, the setup consisted of a constant temperature bath, centrifugal pump, flowmeters, filter, pressure transducers, data logger and test circuit. The switched mode test circuit for the MCT or IGBT consisted of a high-voltage high-current d.c. power supply, resistive load bank (250 A, 270 V), current transformer, function generator, driver circuit, digital storage oscilloscope, and RCD (resistor-capacitor-diode) snubber circuit. The electrical test circuit details are illustrated in Figure 40 and Figure 41. The difference between the MCT and IGBT test circuits was very subtle and pertaining to the pin connections (the anode and cathode pin connections of the MCT become collector and emitter pins respectively in the IGBT circuit). The coolant used was water and the circulation capacity was 0-35 lpm at temperatures from 5°C to 35°C through the 3.33 cm diameter copper pipe.

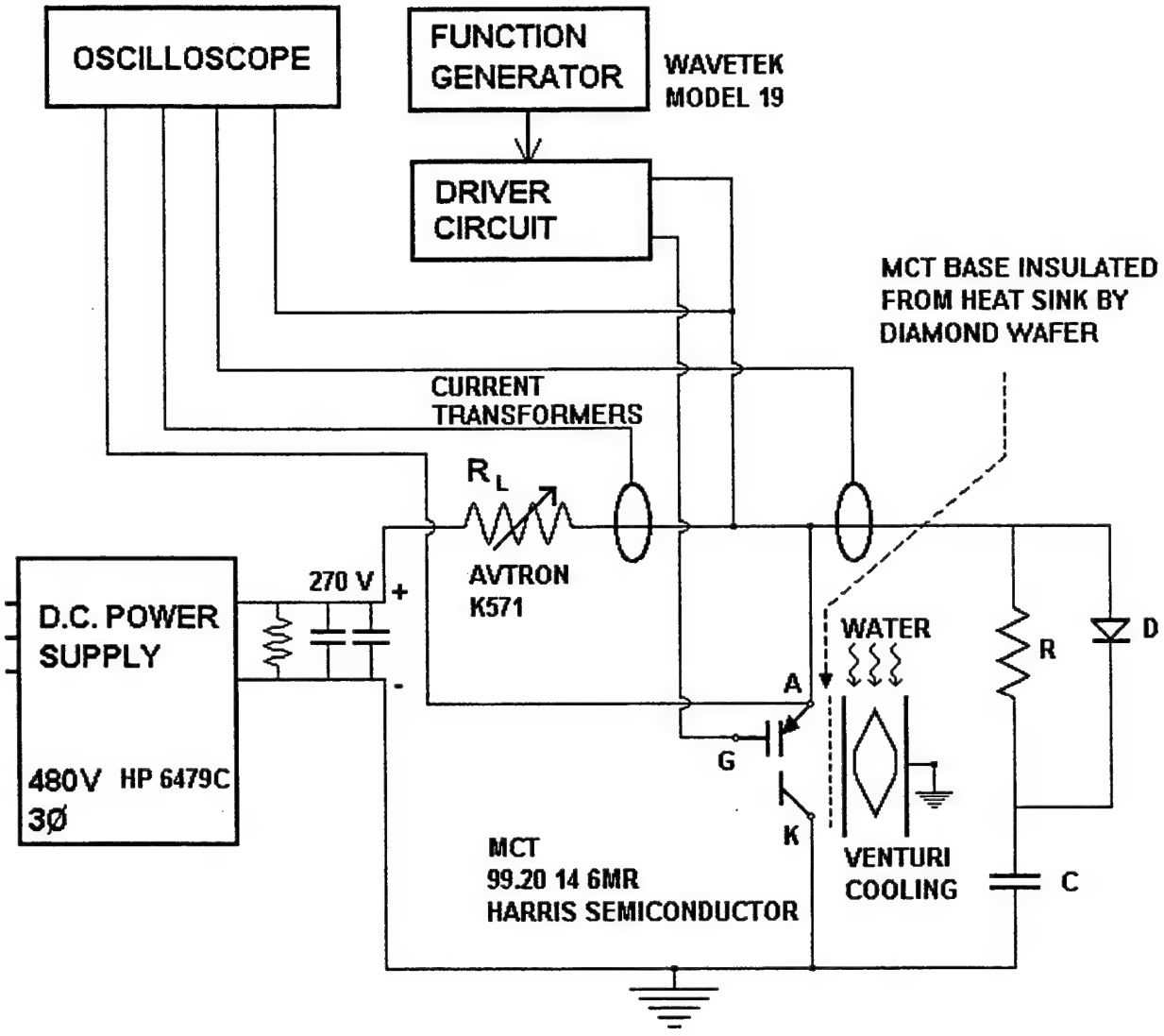

Figure 40. Electrical Test Circuit for MCT.

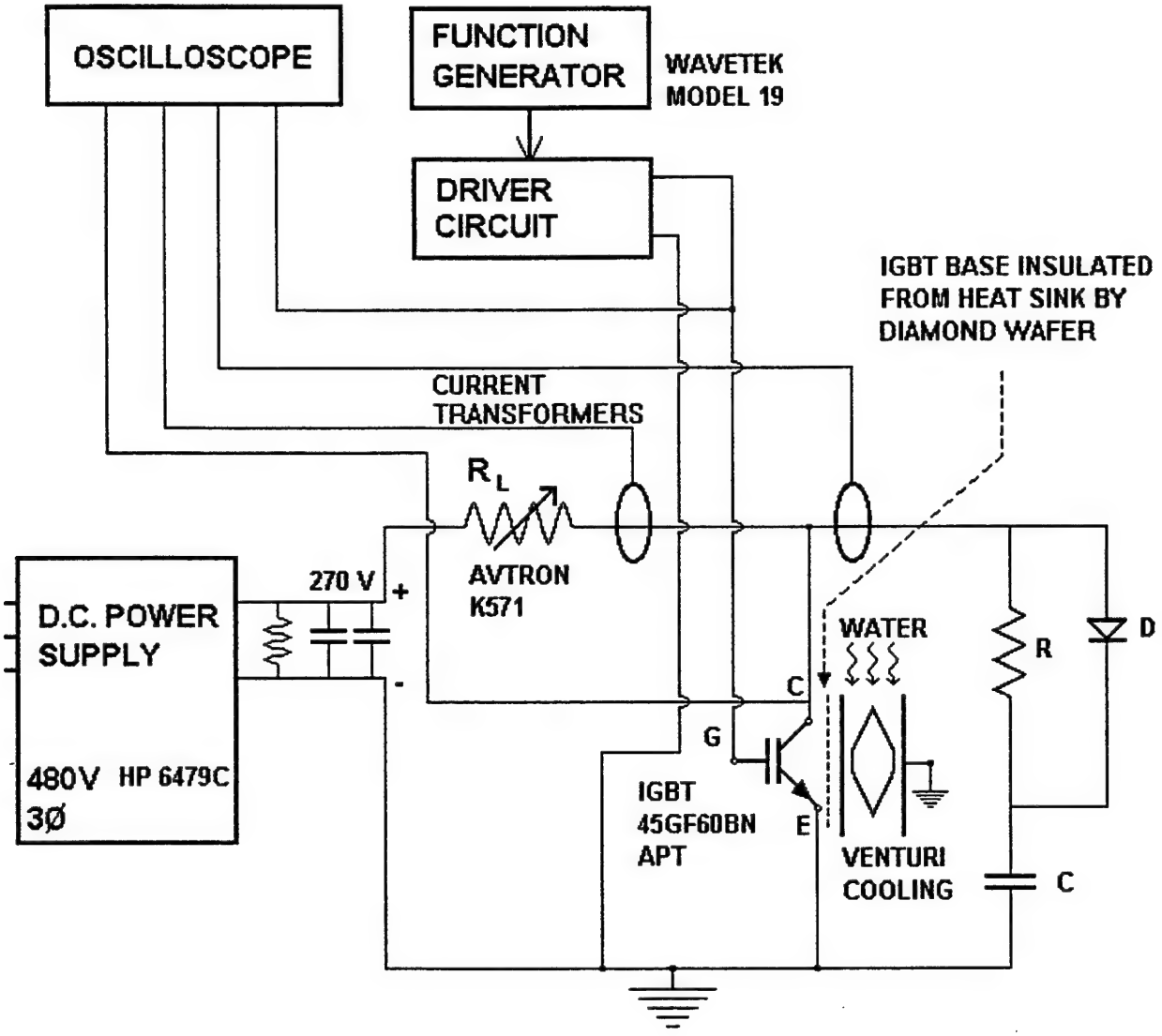

Figure 41. Electrical Test Circuit for IGBT.

6.5.2 Device, Load-cell, and Thermocouple Mounting

The polished metallic surface of the MCT or IGBT was placed on the insulation layer (Kapton or diamond) which in turn was mounted on the polished flat outer-surface of the test section with a thin layer of thermal grease on each of the contact surfaces. The top surface of the device was pressed down using a ceramic spacer and a clamp screw. A load-cell capable of measuring the clamping-load on the device was placed directly on the opposite face of the test section. Figure 42 shows these details. By varying the tightening-torque on the ¼-20 clamp screw, the axial load on the device could be set at any desired value. Foil type thermocouples were used to facilitate flush-mounting on the flat surfaces of the devices. Beaded-junction or probe type thermocouples were used in other sections. Figure 42 also illustrates the mounting of the device (MCT) and thermocouple locations.

6.5.3 Test Procedure

Water circulation rate and temperature were set at the desired level. The function generator was set for the required frequency and the current load was pre-selected in the load bank. While the oscilloscope was used for registering the voltage and current waveforms, power was slowly raised and held at a constant level for nearly 20 minutes. The supply voltage to the device was constant at 270Vdc for all average current (0-35 A) and frequency (1-10 kHz) settings. Steady state data recording included all temperatures, flow rate, voltage and current waveforms. An alarm limit of 150°C was set for the device temperature. The measurement accuracy for temperature was within ±0.5°C in the range 0-200°C. The electrical power measuring accuracy was within ±1% in the range of 0-30 lpm.

6.5.4 Problems Encountered

Several technical problems were encountered during the tests and are recorded here for use as a guideline to serve as warnings for the future. The major problem was overheating of the snubber circuit components (the resistor and the capacitor). Special air cooling arrangements

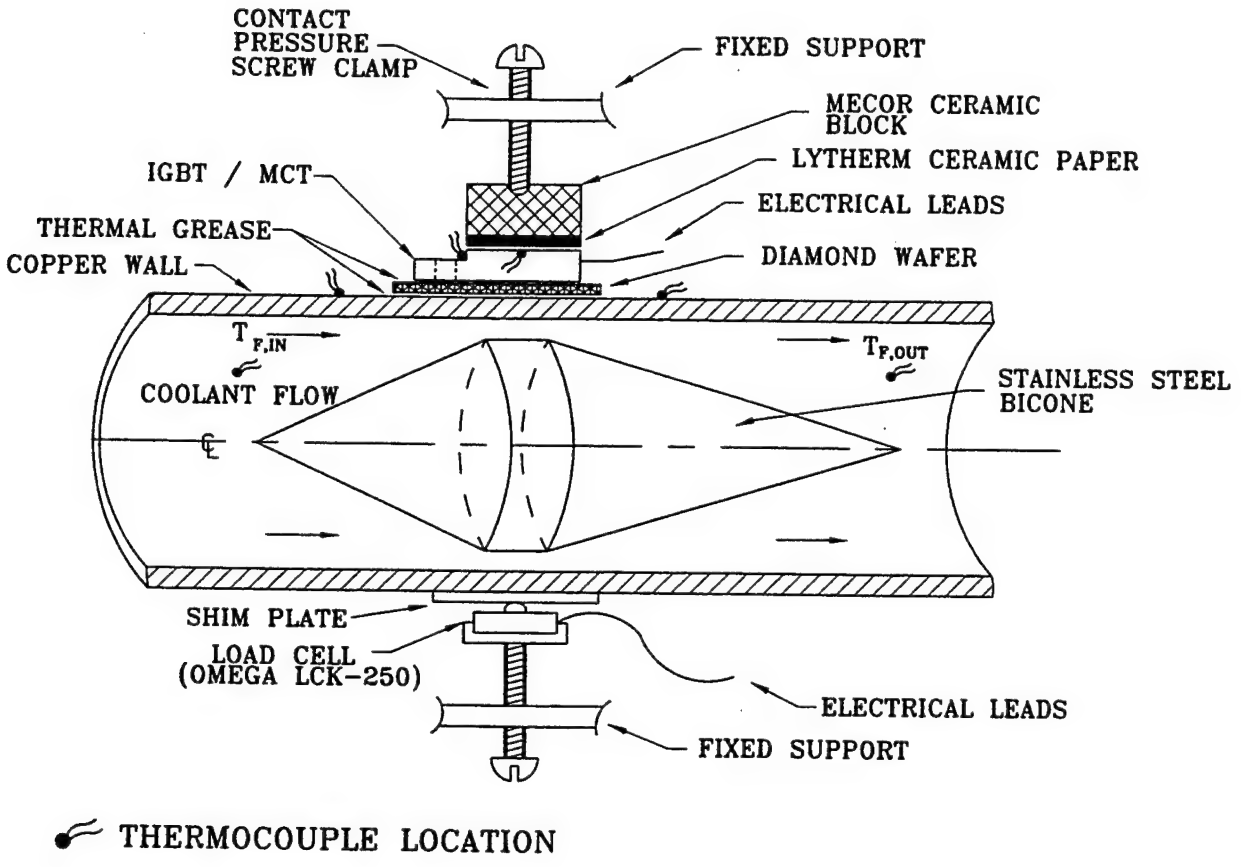

Figure 42. A Cross-sectional View of the Test-Section Showing the Device, Load Cell and Thermocouples.

were made and their respective temperatures were monitored in order to maintain them within safe operating ranges (under 175°C). The following list in Table 10 provides the details of the failures and corrective measures :

Table 10. IGBT Test Circuit Failures and Corrective Measures

Sl. No.	Test Date	Failure	Corrective Measure
1.	6/16/95	Insulation around the cable connected to the emitter pin on IGBT melted at 30A load.	Replaced with heavier insulation and thick conductor cable.
2.	6/21/95	IGBT device showed erratic performance as a result of the above failure.	Replaced with a new device.
3.	6/23/95	IGBT driver circuit malfunctioned.	Replaced with a new driver module.
4.	6/28/95	Capacitor in snubber circuit melted at 15A. IGBT also failed.	Replaced with 4 capacitor module in series-parallel combination and air cooling applied. New IGBT installed.
5.	7/27/95 a.m.	Power supply died at 30A. Fuse was blown in wall breaker box.	New fuse installed.
6.	7/27/95 p.m.	Device failed at 30A repeat test; leads arced and melted. Voltage feedback/surge damaged driver circuit module also.	New device and new driver module installed.

6.6 RESULTS AND DISCUSSIONS

6.6.1 Switching Characteristics

The circuits for the switching tests of both MCT and IGBT were identical. The wiring of the circuit was not optimal due to instrumentation requirement. Hence, the circuit was not set up for minimum inductance, which resulted in a voltage spike across the device. An RCD snubber was added to limit this spike. At 70 A peak current and 270 V source voltage, the voltage waveform showed a 560 V spike, resulting in high switching loss. The typical waveforms of switching with 50% duty cycle are shown in Figure 43 and Figure 44. During the device

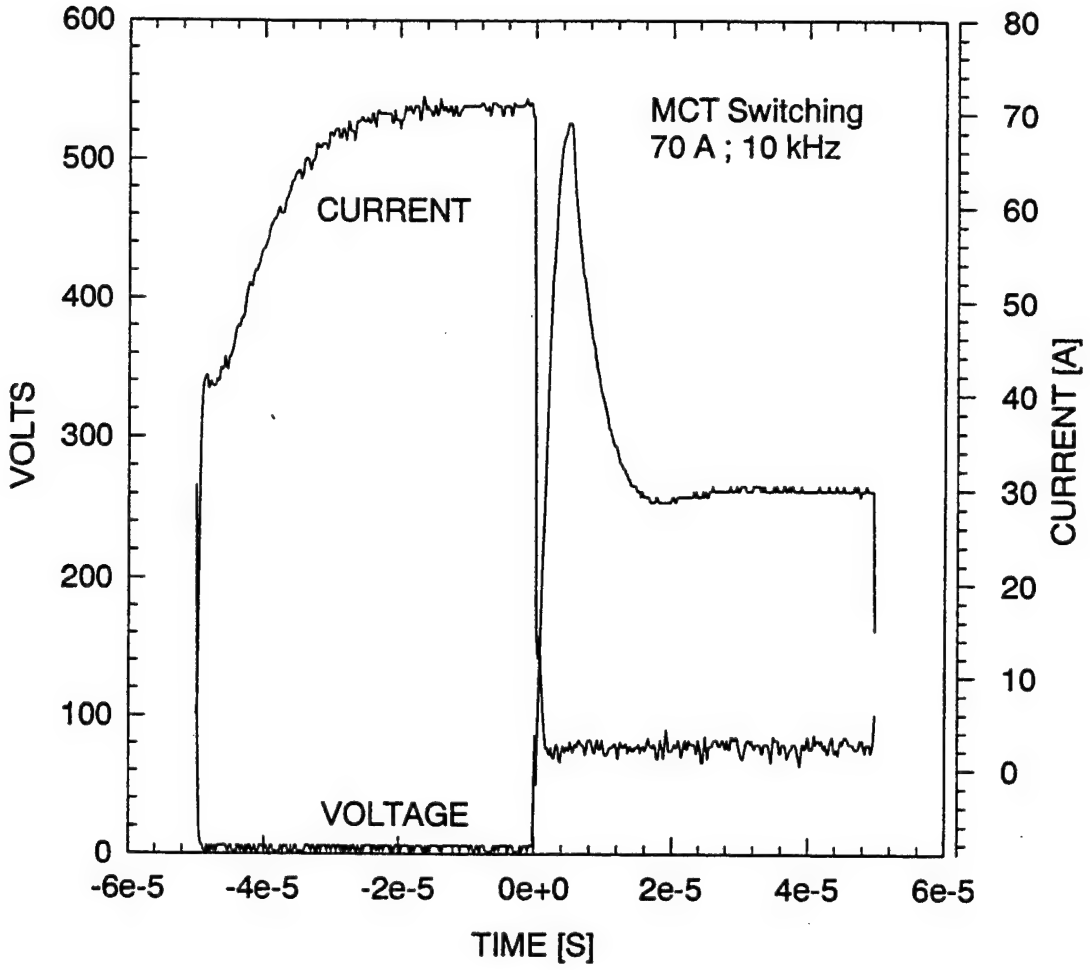

Figure 43. Voltage and Current Waveforms at Turn-off (MCT: 70 A; 10 kHz).

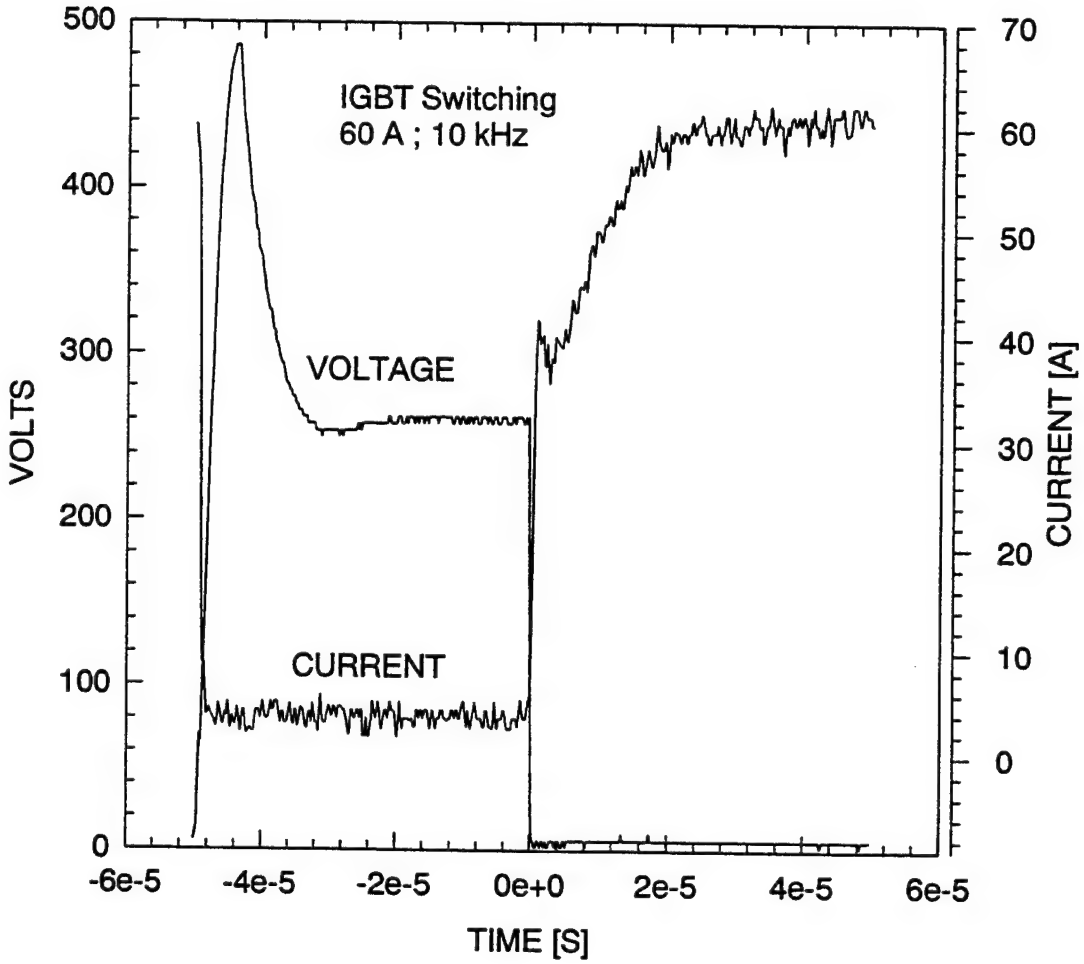

Figure 44. Voltage and Current Waveforms at Turn-off (IGBT: 60 A; 10 kHz).

turn-off, the current pulsed in the negative direction due to snubber capacitor discharging through the resistor load. This current does not pass through the device, even though it appears so because of the location of the current transformer. Continuous operation and long wire length also made the switching waveform deviate from ideal characteristics. The switching frequency was limited to 10 kHz as a safe-guard against unexpected failure. Higher frequencies might have been possible but with unpredictable results.

6.6.2 Temperature Variation

By repeated tests at various flow rates up to 37.8 lpm, it was found out that the device temperature (T_{TOP}) was not sensitive to flow rates above 3.78 lpm. Hence, this minimum flow rate was used for all tests. Figure 45 shows the measured temperature profiles of the devices (with diamond wafer and thermal grease at a clamp-load of 30±2 lbs) as functions of average device current at the highest switching frequency (10 kHz) tested. The IGBT top temperatures were higher than those of the MCT due to higher heat dissipation also illustrated in the figure. However, the flange temperatures showed a different trend due to the minor variations in physical details of the devices. It is interesting to note that the devices operated at considerably lower temperatures (20-86°C) compared to their maximum safe operating temperature of 175°C.

6.6.3 Peak Performance Results

A summary of the highest performance numbers obtained in the present tests for the devices is provided in Table 11. The results are compared on the common reference of coolant temperature (19.5°C) and flow rate (3.78 lpm). The measured R_{DF} values fall within the estimated ones given in Table 9.

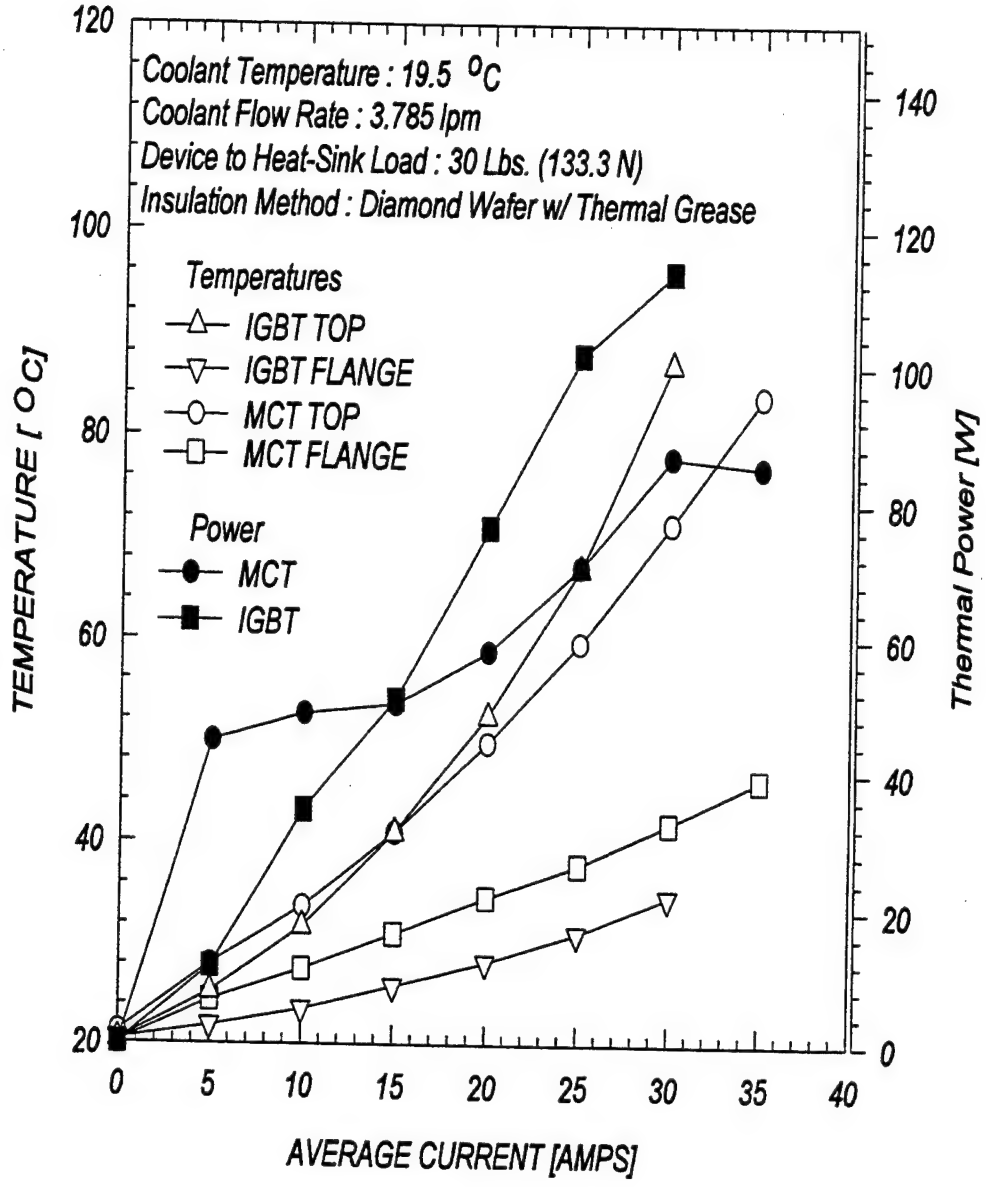

Figure 45. Device Temperatures and Thermal Power vs. Average Current at 10 kHz.

Table 11. Switched Mode Test Results of the Devices - Experimental Data at Peak Performance (Diamond wafer insulation with thermal grease; contact-load=133.4 N (30 lbs))

Item No.	PARAMETER		MCT	IGBT
1.	Current:			
	a) Continuous Average	A	35	30
	b) Peak	A	70	60
2.	Frequency	kHz	10	10
3.	Voltage	V	-270	270
4.	Power Dissipation:			
	a) Electrical Measurement		167.1	163.4
		W	85.4	113.8
	b) Thermal Measurement	W		
	c) Lost to Ambient and		81.7	49.6
	Unaccounted	W		
5.	Device temperature:			
	a) Top (junction)		83.8	86.9
		°C	46.0	34.7
	b) Flange	°C		
6.	Thermal Resistance:			
	R_{DF} (measured)	°C/W	0.753	0.592
	R_{DF} (estimated)	°C/W	0.8-1.1	0.8-1.5
7.	Heat Flux:			
	Based on Footprint Area	cm^2	2.62	3.35
	Heat Flux	W/cm^2	32.6	33.9
8.	Coolant Flow Rate (Total Flow)	lpm		
			3.78	3.78
9.	Coolant Temperature	°C	19.5	19.5

6.6.4 Power Dissipation

The total power dissipated as heat by the device is the result of switching and conduction losses. This was obtained by both electrical and thermal measurements. The electrical measurement enabled the computation of the conductive and switching losses from the product of the voltage and current waveforms integrated over one turn-on/turn-off cycle. The thermal measurement provided the calorimetric data of coolant heat-removal from the device which did not account for all the heat dissipated by the device. The heat losses through the leads and exposed surfaces of the device were not accounted for in this study. Power dissipation versus average current for the MCT and IGBT are plotted in Figure 46 and Figure 47, respectively for 10 kHz tests. The curves for electrical power include the switching and conduction losses and exclude the snubber-circuit power. The difference between the electrical and thermal data is attributed to i) unaccounted heat losses from the device, ii) digitizing error in computing the power from the waveforms and iii) inaccuracies in measuring the flow and temperature data.

6.6.5 Thermal Resistance

The resistance R_{DF} calculated using Eq. (1) with the experimental data is plotted in Figure 48. It is interesting to note that the measured R_{DF} values for the devices are much smaller compared to the estimated data (Table 9). Experimental values for R_{JC} could not be computed because, the temperature of the bottom face of the device was not measured due to practical difficulties.

6.7 SUMMARY

Two commercial high power switching devices (MCT and IGBT) were tested in conjunction with the venturi-cooling heat-sink in order to evaluate their hard-switching mode characteristics along with their thermal behaviors. Both devices functioned successfully up to 10 kHz and their operating temperatures were under 100°C, very much below their safe operating

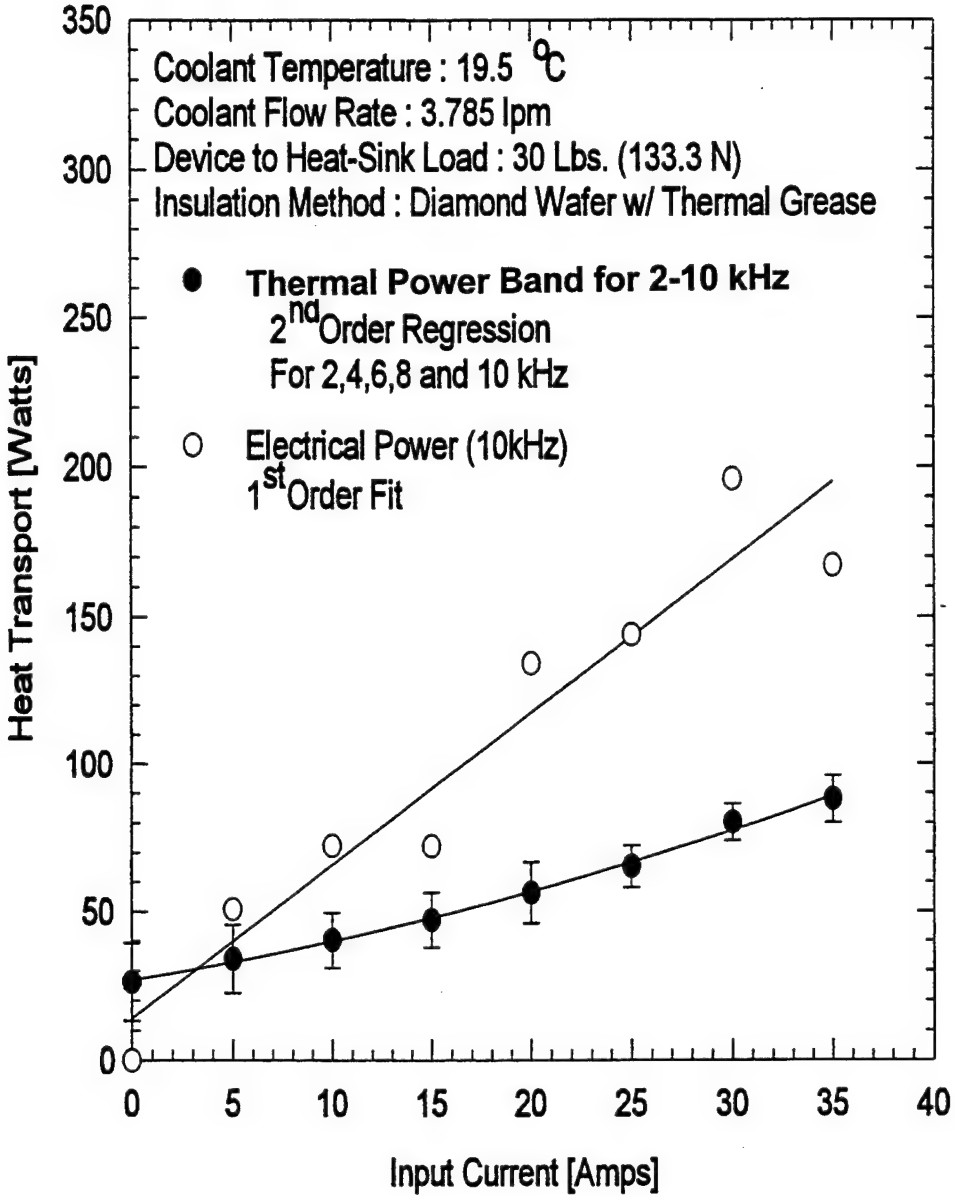

Figure 46. Power Dissipation (Electrical and Thermal) of MCT vs. Average Current at 10 kHz.

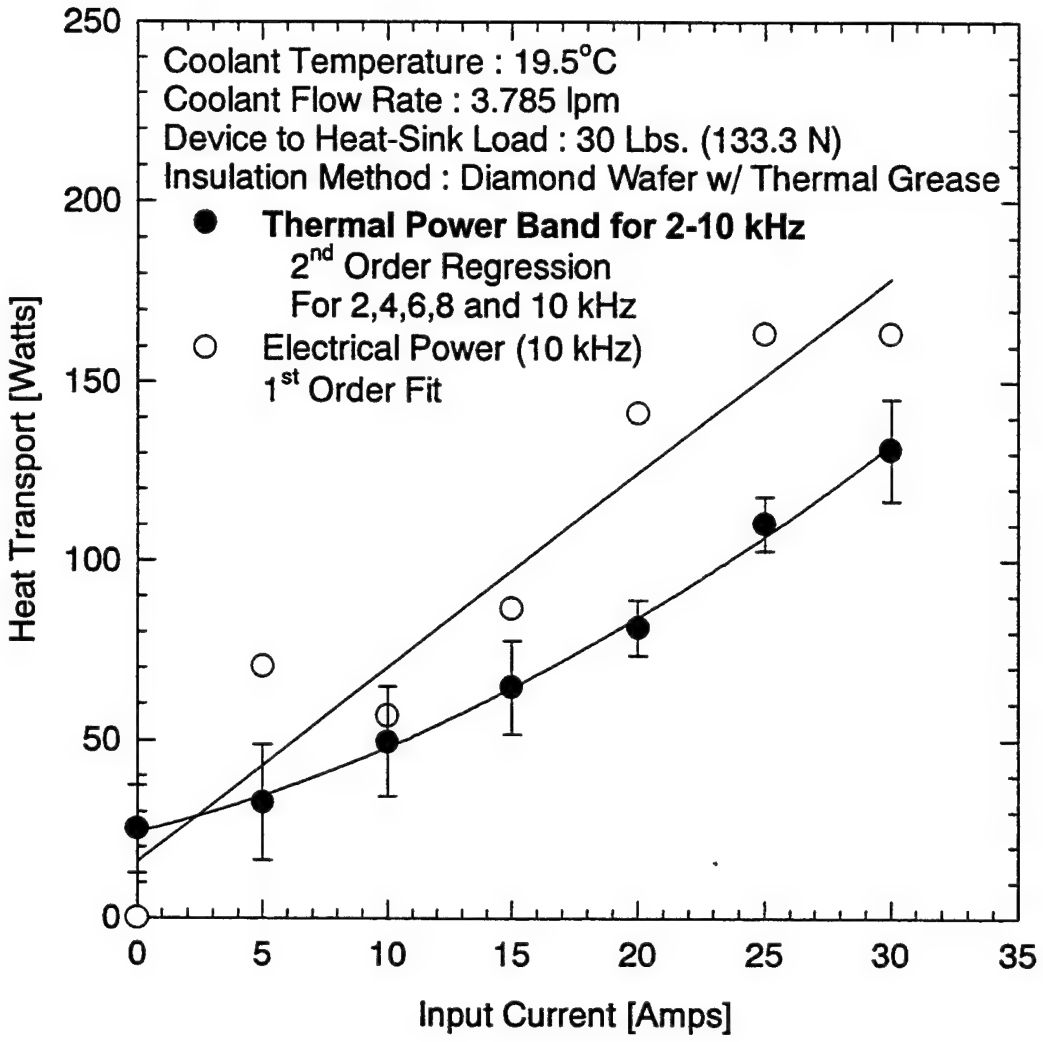

Figure 47. Power Dissipation (Electrical and Thermal of IGBT vs. Average Current at 10 kHz.

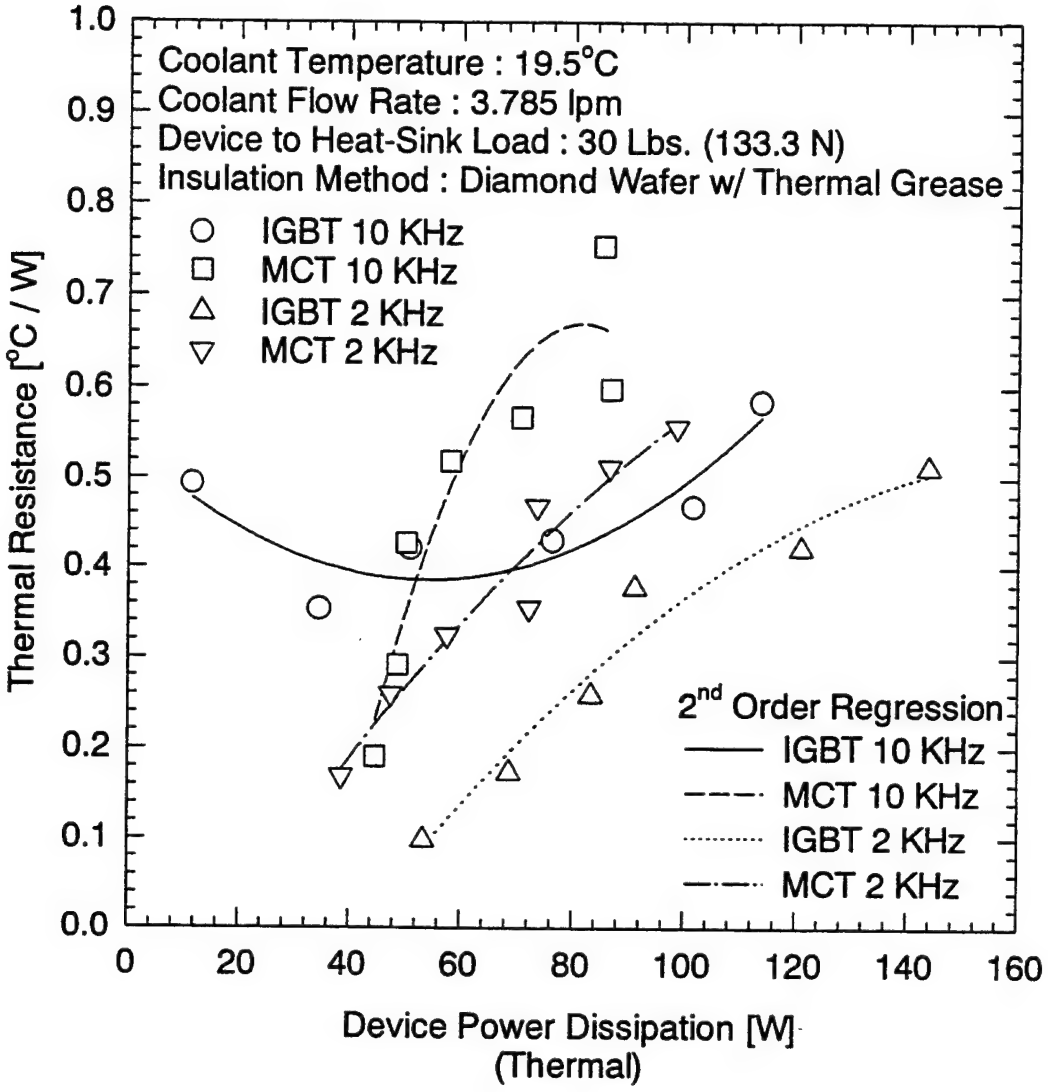

Figure 48. Measured R_{DF} as a Function of Thermal Power Dissipation.

limit of 150°C. There are no published performance data of these devices with other cooling methods comparable to the present results. The electrical power losses and thermal dissipations were measured and compared. The effect of mechanical contact-pressure on the device-temperature with and without thermal grease was studied thoroughly. An increase in the contact-load from 30 to 160 lbs. reduced the temperature from 135° to 105°C in the case of dry contact. For greased contacts, the temperature response is invariant to contact loads. The coolant flow rate and switching frequency did not influence the device temperatures as much as the device current did. It is again confirmed that, for localized heat removal applications, venturi cooling is very well-suited. A high thermal-conductive material such as the diamond wafer, instead of the Kapton film is recommended for electrically insulating the device from the heat-sink.

7.0 INFLUENCE OF EXTERNAL THERMAL RESISTANCES ON COOLING OF POWER DEVICES

7.1 TEST SETUP AND TEST PROCEDURE

The experimental setup and procedure used for this study were the same as those described under Section 6.0.

7.2 RESULTS AND DISCUSSIONS

7.2.1 Effect of Contact-Pressure

The effects of insulation material, thermal-contact-grease and contact-load were also investigated. Figure 49 shows the device temperature variation due to the contact-load for IGBT 30 A/10 kHz tests with diamond insulation with and without thermal grease. It is interesting to observe that without the grease (dry-contact), the device runs much hotter even with high contact pressure. The temperature is almost constant for any contact-load in the case of wet-contact. Figure 50 illustrates a similar behavior as explained above for the Kapton insulation also except that the major difference being the maximum current level reached is only 20 A. The comparison of results with dry and wet contacts clearly emphasizes the need for filling the interstitial gaps between the contact surfaces for improving heat transfer.

7.2.2 Thermal Resistance/Conductance Factors

The resistance value, R_{DF}, calculated using Eq. (32) with the experimental data is a measure of the overall thermal efficiency of the heat sink system. Figure 51 presents the results of the present system for the case of diamond isolator with and without thermal grease as a function of the contact-pressure. Figure 52 presents similar data for the case of Kapton isolator. As expected, R_{DF} decreases with the increase of contact-pressure in both cases. The application of grease to the interfaces has significant impact in reducing the thermal resistance. Another

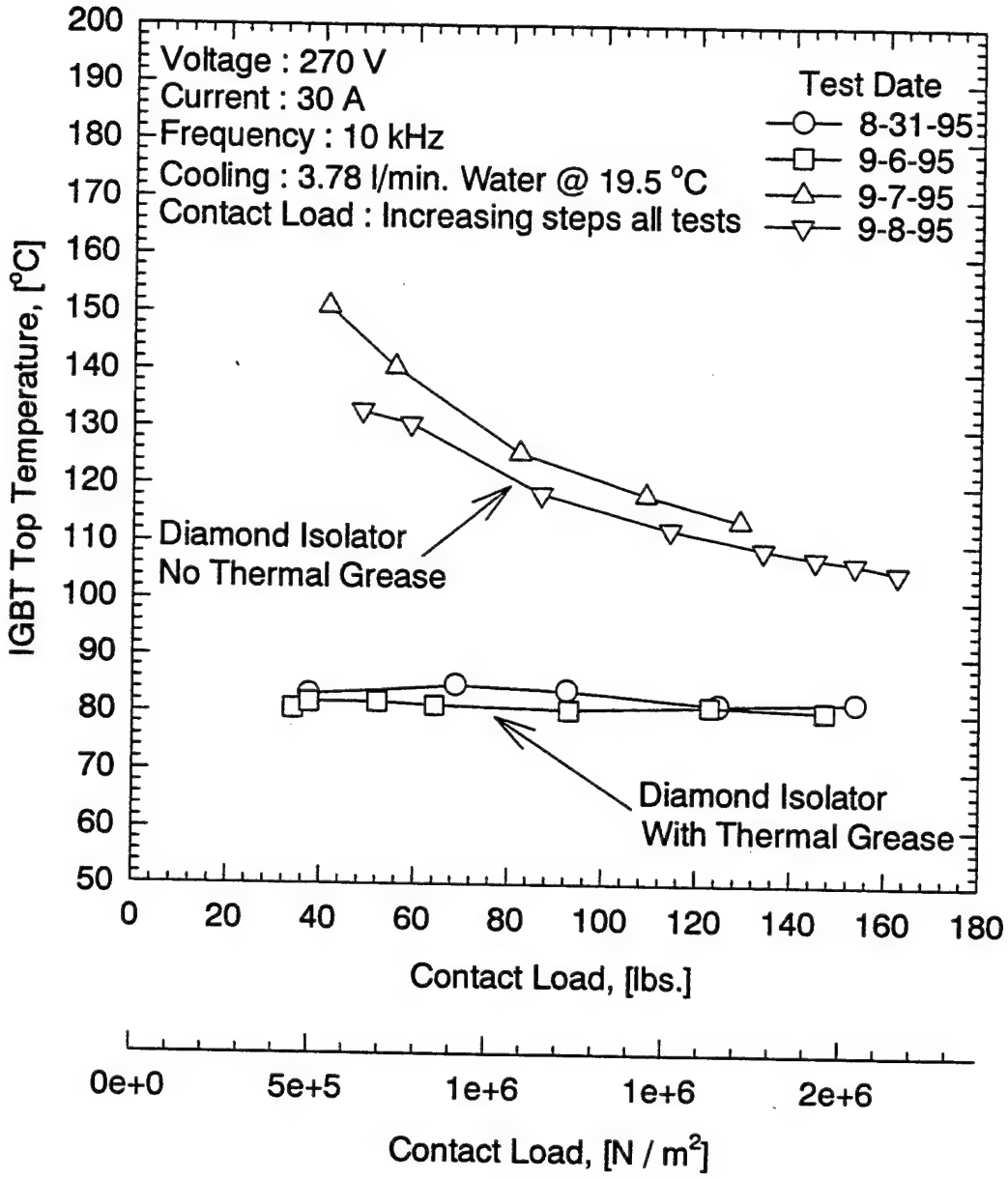

Figure 49. IGBT Top Temperature vs. Contact Load. (Diamond; with and without Grease; 30 A/10 kHz.)

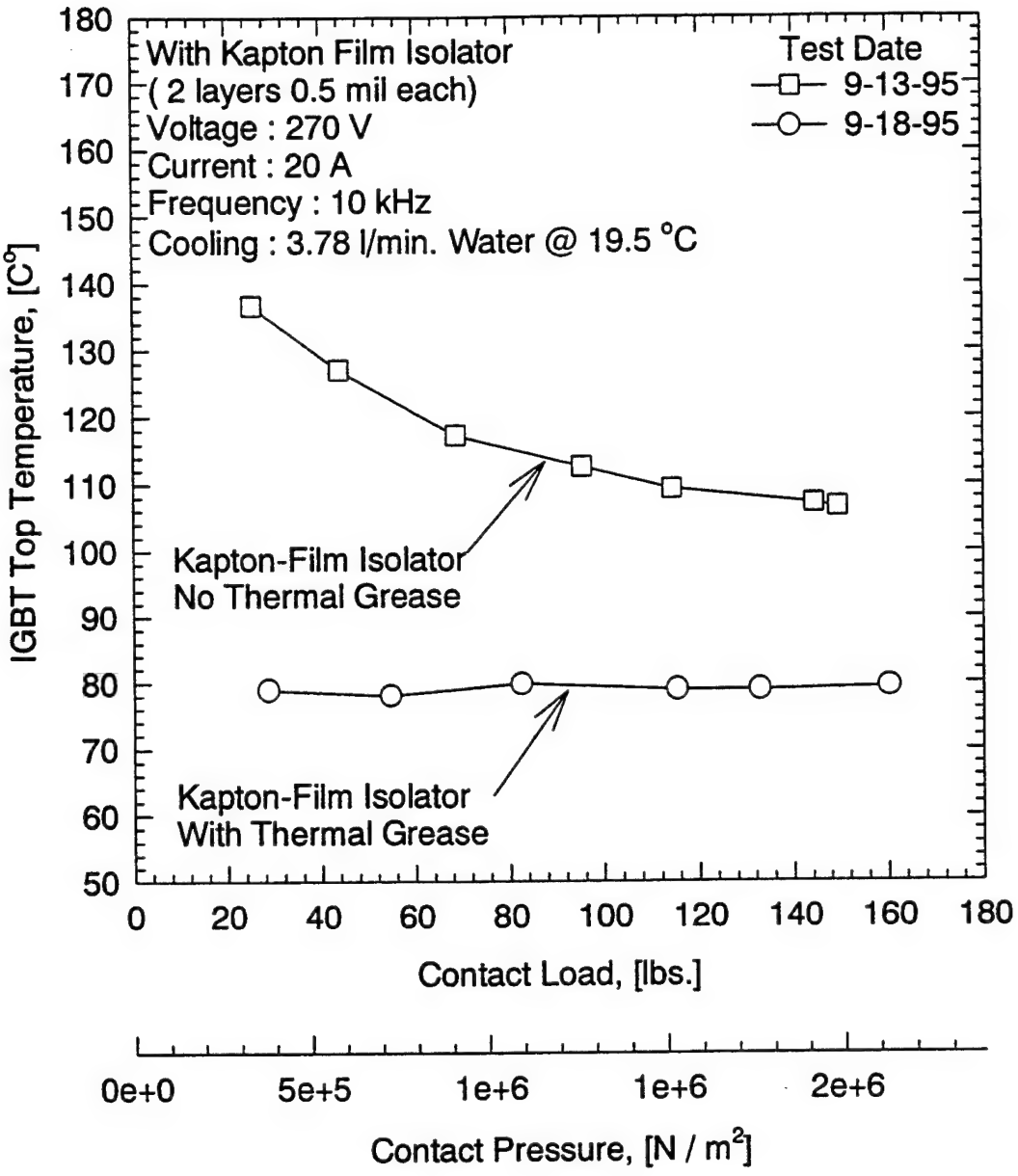

Figure 50. IGBT Top Temperature vs. Contact Load. (Kapton; with and without Grease; 20 A/10 kHz.)

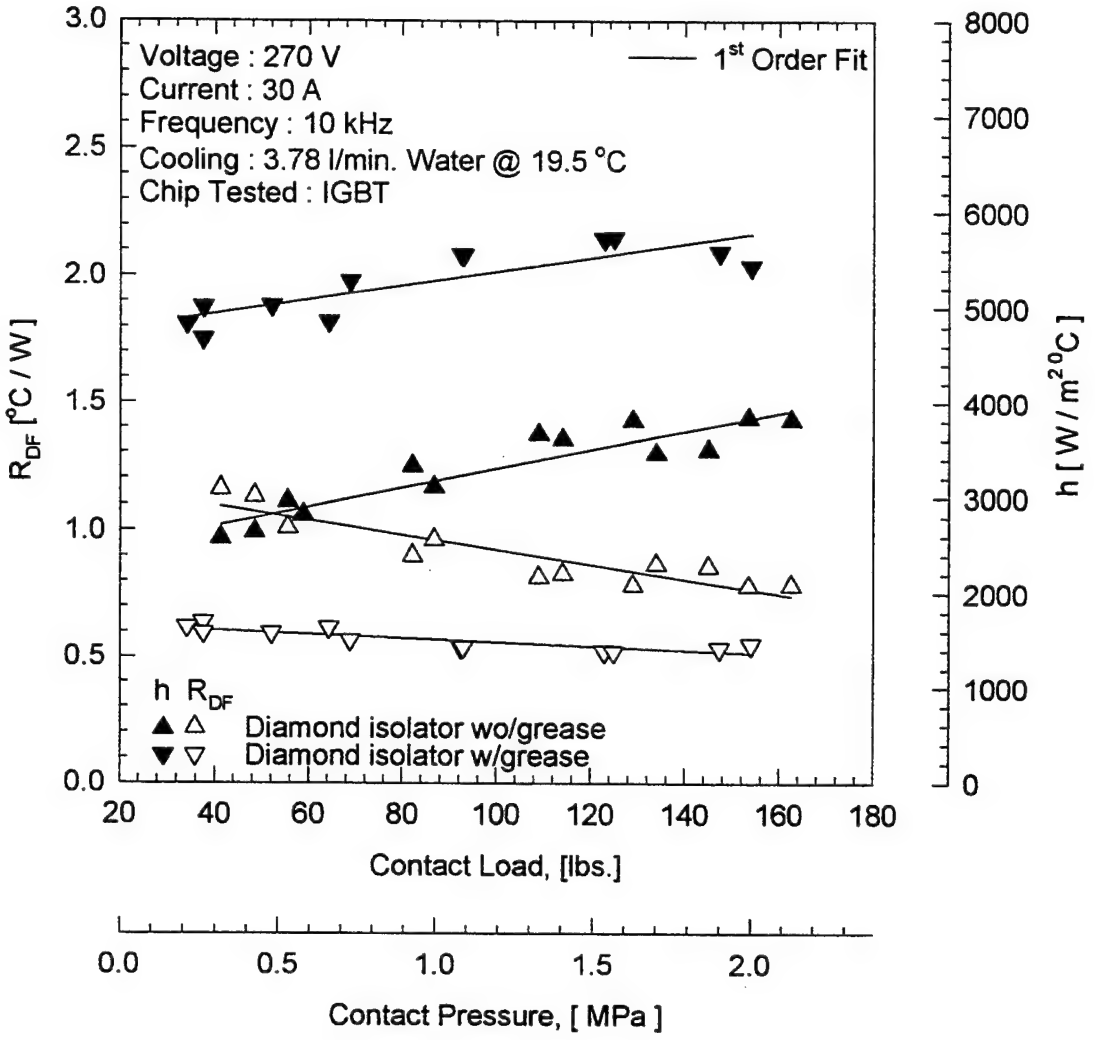

Figure 51. Thermal Resistance and Conductance Factors as Functions of Contact-Pressure. (IGBT; Diamond Isolator with and without Grease; 30 A/10 kHz)

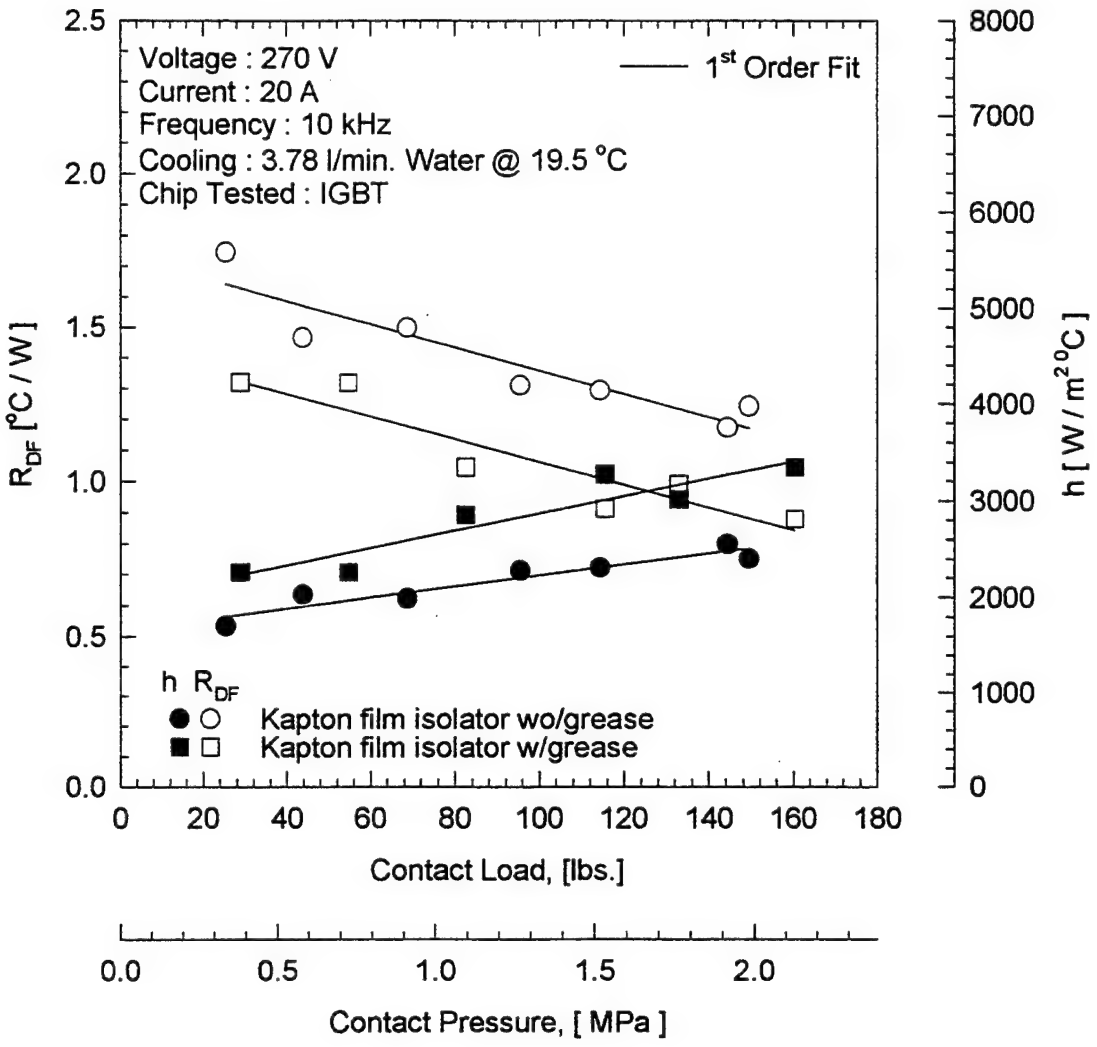

Figure 52. Thermal Resistance and Conductance Factors as Functions of Contact-Pressure. (IGBT; Kapton Isolator with and without Grease; 20 A/10 kHz)

important thermal parameter, called the overall conductance factor (K), can be calculated using Eq. (34) where A=mounting footprint area of the device.

$$h = K = \frac{1}{AR_{DF}} \tag{34}$$

This factor is similar and interchangeable to the convective heat transfer coefficient and is often used in the electronic packaging and thermal management literature for comparing the performances of cooling systems [15,16]. Figures 51 and 52 also present the values of h or K for the cases of diamond and Kapton isolators, respectively. The values of h or K for the present heat sink varied from 1700 to 5700 W/m2°C as seen from these figures and this result matches with the typical heat transfer coefficient of 4500 $W/m^2°C$ for water forced-convection.

The R_{DF} values are also plotted as functions of the device operating temperatures for both devices as shown in Figure 53. The results corresponding to 2 kHz and 8 kHz were chosen as representative data to illustrate the dependence of resistance on frequency. The resistance increased sharply with increase in device temperature for both devices indicating that the devices need efficient cooling systems when operating at temperatures higher than near-room temperature. The effect of increase in operating frequency is apparent from the figure. At higher frequencies, the devices dissipated higher switching losses and consequent higher operating temperatures.

7.3 PRACTICAL CONSIDERATIONS

The shape and size of the venturi flow heat sink can be designed to suit any application and used with any available fluid. Instead of the tubular designs shown in Figures 1 and 32, a rectangular duct type multi-stage venturi configuration given in Figure 54 may be considered wherein both top and bottom panels could be used as heat sinks. Both geometries offer axisym-metrical flow with the flexibility to add multi-stage venturi-sections for cooling large numbers of power devices. The material of construction could be aluminum or copper for good wall conduction. Stainless steel will also work except that the wall conduction-spreading would be minimal. The annular-throat flow area of the venturi and the bicone-restrictor cone angles could be optimized for desired velocity amplification and fluid pressure recovery. The fluid pumping-power required for this cooling system is very marginal compared to the cooling capabilities.

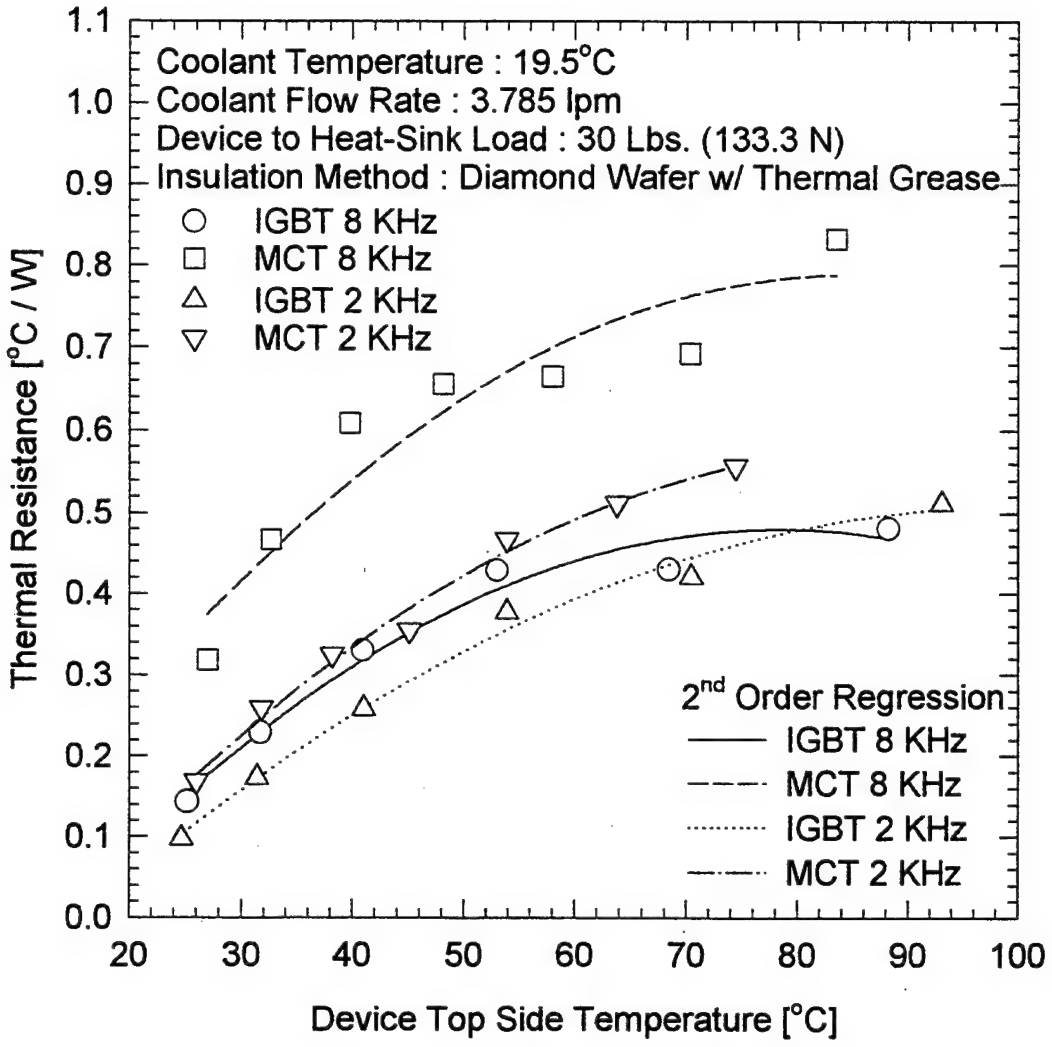

Figure 53. Measured R_{DF} as a Function of the Device Top Temperature at Various Frequencies.

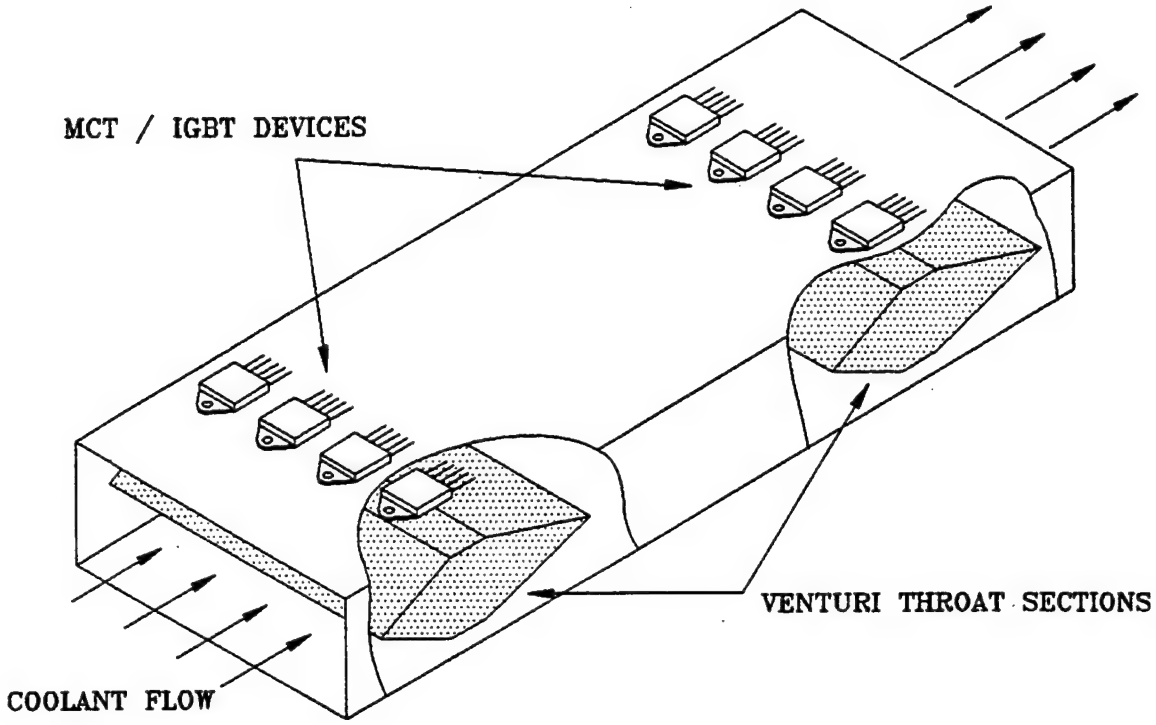

Figure 54. Rectangular Duct Type Multi-Stage Venturi Flow Heat Sink.

7.4 SUMMARY

Two commercial high-power switching devices (MCT and IGBT) were tested in conjunction with the venturi-cooling heat-sink in order to evaluate their hard-switching mode characteristics along with their thermal behaviors. Both devices functioned successfully up to 10 kHz and their operating temperatures were under 100°C, very much below their safe operating limit of 150°C. There are no published performance data of these devices with other cooling methods comparable to the present results. The electrical power losses and thermal dissipations were measured and compared. The effect of mechanical contact-pressure on the device-temperature with and without thermal grease was studied thoroughly. An increase in the contact-pressure from 0.5 to 2.2 MPa reduced the temperature from 135° to 105°C in the case of dry contact. For greased contacts, the temperature response is invariant to contact-pressures. The measured and estimated thermal resistance values are in good agreement. A high thermal-conductive material such as the diamond wafer, instead of the Kapton film, is recommended for electrically insulating the device from the heat-sink.

8.0 CONCLUSIONS AND RECOMMENDATIONS

8.1 CONCLUSIONS

1) A novel cooling concept called "venturi flow cooling" has been developed for applications wherein very high localized heat loads have to be cooled. Parametric analysis show that heat transfer coefficients up to 3.0 W/cm^2 °C and fluxes up to 200 W/cm^2 based on the assumption of 45° conduction spreading can be achieved by this method of cooling when using PAO fluid of 40°C, Re = 10^4, flow rate of 86 liters/min. and wall-to-fluid $\Delta T = 85$°C.

2) An experimental setup for demonstrating this new concept was constructed successfully and tests were performed using water as the coolant and ceramic strip heaters for simulating the heat load. It was demonstrated that the venturi configuration produced a local average heat transfer coefficient of 6.39 W/cm^2 °C (for water flow at 25°C and Re = 2.55×10^4) which was about three times that of a pipe (circular) flow.

The venturi throat velocity amplifications attainable with the test apparatus were 12.6 and 17.5 times that of the upstream fluid velocity using two bicones of slightly different dimensions.

3) The test section with nichrome heater and heat concentrator design was able to perform at a maximum heat flux of 323 W/cm^2 (without allowing for conduction spread in the wall). Much higher heat transfer coefficient (13.23 W/cm^2 °C) was achieved in this design compared to the ceramic strip heater design.

A few existing heat transfer correlations for turbulent flow through pipes were used for comparing the present experimental results. The agreement between the theory and experiment was fairly good. A perfect match cannot happen as the correlations are not exactly applicable to our present geometry.

The effect of wall conduction spreading on the heat transfer coefficient was realized and a separate numerical modeling effort (outside the scope of this task) using PHOENICS commercial code was initiated and results were presented that show extensive spreading.

4) The venturi flow cooling concept was successfully employed for testing an actual power electric device (MCT) at 95 A close to its maximum rated current of 100 A in conduction mode for the first time. Earlier laboratory tests by others using air cooling or water cooling did not yield results even close to 20% of the present study.

Comparison of MCT performances using three different cooling arrangements under identical conditions of flow and heat dissipation proved that venturi cooling was superior to pipe flow and commercial cold plate cooling arrangements.

5) Extended performance tests using venturi cooling on MCT and IGBT devices in switched-modes of electrical performance were successfully conducted up to 10 kHz with the devices operating under 100°C which is about 50 degrees below their safe operating limit.

There are no published performance data of these devices with other cooling methods comparable to these present results.

6) A load cell was used to measure the contact pressure of the device mounting on the heat sink. An increase in contact pressure from 0.5 to 2.2 MPa reduced the temperature of the device from 135°C to 105°C. A CVD diamond wafer was employed as an electrical insulator and thermal spreader under the electrically-hot base of the device.

7) Venturi cooling concept can be effectively used for high localized heat load applications where single phase fluid flow is available and is proved to be superior to air cooling or pipe flow arrangements.

8.2 RECOMMENDATIONS

The following suggestions are made for further extension of this study:

1) The venturi system design may be optimized in terms of the geometry, heat load, flow parameters and system hardware configurations unique to the electronic packaging requirements.

2) A test section with rectangular-duct type configuration may be fabricated and tested for multiple devices mounted in a row.

3) The arrangement of several venturi-throat sections in series with a large number of power devices may be attractive for industrial type packaging. The heat transfer modeling of such a system may be challenging.

4) The most common fluid used for Air Force aircraft thermal management applications, namely PAO, was never used in the present study. This fluid may be experimentally evaluated in the venturi flow concept.

5) Also, the velocity amplification idea can be extended to air-flow cooling applications as well.

6) In the case of the heat concentrator version of the venturi study (Section 4.0), phase change (liquid to vapor) possibility at the throat section appeared probable at temperatures close to the saturation level. This may be further explored numerically as well as experimentally.

7) The calorimetric measurements in the case of MCT and IGBT testing were very difficult due to the complications of the electrical circuits for snubber and gate-driver. Also, the frequent failures of the gate driver limited the tests to only 10 kHz. These may be improved and the level of switching frequency may be increased significantly in the future.

8) In realizing the importance of electronic packaging, it may be advisable to plan any cooling scheme along with the device manufacturer at the device design stage itself.

9) In addition to the venturi flow concept, other methods such as jet-impingement, spray, immersion, etc., may be explored as dictated by the application under consideration.

9.0 REFERENCES

1. A.D. Kraus and A. Bar-Cohen, "Thermal Analysis and Control of Electronic Equipment," Hemisphere Publishing Corp., New York, 1983.
2. Mackowski, Michael, "Requirements for High Flux Cooling of Future Avionics Systems", SAE Aerospace Technology Conference and Exposition, 24 September 1991, Long Beach, CA.
3. Gu, C.B.; Chow, L.C.; and Beam, J.E., "Flow Boiling in a Curved Channel", Heat Transfer in High Energy/High Heat Flux Applications, ASME HTD, Vol. 119, Proc. of Winter Annual Meeting, 1989.
4. Iversen, Arthur H., Thermal Management of High Flux Electronic Components in Space and Aircraft Systems, Final report by Coriolis Corp., AF Report WRDC-TR-90-2122, SBIR Phase I, 1991.
5. Wadsworth, D.C.; and Mudawar, I., "Enhancement of Single-Phases Heat Transfer and CHF from an Ultra-High-Flux Simulated Microelectronic Heat Source to a Rectangular Impinging Jet of Dielectric Liquid", Advances in Electronic Packaging ASME 1992, Vol. 1, pp. 143-151, ASME, New York, NY.
6. Ponnappan, R.; Reyes, A.S.; and Beam, J.E., "Venturi Flow Cooling Concept for High Heat Flux Applications", Ibid. pp. 225-234.
7. Ponnappan, R.; and Beam, J.E., "A Novel Electronic Cooling Concept", SAE Paper No. 929478, Proc. 27th IECEC Vol. 2, pp. 411-416, Aug. 1992.
8. W.M. Kays, and M.E. Crawford, 1980 Convective Heat and Mass Transfer, 2nd Edition, McGraw-Hill Book Co., New York.
9. G.P. Peterson and A. Ortega, "Thermal Control of Electronic Equipment and Devices," in Advances in Heat Transfer, Vol. 20, Academic Press, 1990, pp.181-314.
10. Roy, D.N., Applied Fluid Mechanics, Ellis Horwood Limited, John Wiley & Sons, New York, 1988.
11. Shah, R.K. and Johnson, R.S., Correlations for fully developed turbulent flow through circular and noncircular channels, Proc. Sixth National Heat and Mass Transfer Conf., Madras, India, December 29-31, 1981, D-75 - D-93.
12. Incropera, F.P., Kerby, J.S., Moffatt, D.F., and Ramadhyani, S., Convection Heat Transfer from Discrete Heat Sources in a Rectangular Channel, Int. J. Heat Mass Transfer, Vol. 29, No. 7, pp. 1051-1058, 1986.

13. V. Shanmugasundaram, R. Ponnappan, J.E. Beam and J.E. Leland, "Venturi-flow cooling system : comparison of numerical and experimental results," Paper No. 942177, Aerotech '94, Los Angeles, CA, Oct. 3-6, 1994.

14. V. Shanmugasundaram, R. Ponnappan and J.E. Leland, "A parametric study of the conjugate heat transfer problem in an axisymmetric venturi-type cooling system," SAE Paper No. 951439, Aerospace Atlantic Conference and Exposition, Dayton, OH, May 23-25, 1995.

15. V. Shanmugasundaram, R. Ponnappan, J.E. Leland and J.E. Beam, "Conjugate heat transfer in a venturi-type cooling system : numerical and experimental studies," AIAA Paper N0. 95-2114, 30th AIAA Thermophysics Conference, San Diego, CA, June 19-22, 1995; also, submitted for publication in the Journal of Thermophysics and Heat Transfer.

16. V. Shanmugasundaram, R. Ponnappan, J.E. Leland and J.E. Beam, "Analysis of conjugate heat transfer in a venturi-based cooling system for high heat-flux sources," Paper No. 95-161, 30th Intersociety Energy Conversion Engineering Conference, Orlando, Fl., July 31-August 4, 1995.

17. V. Shanmugasundaram, "A numerical investigation of conjugate heat transfer in a venturi-flow cooling system," Paper presented at the 30th National Heat Transfer Conference, Portland, Oregon, August 5-9, 1995.

18. V. Shanmugasundaram, "A numerical study of conjugate heat transfer in a 2D venturi-type cooling system," Paper presented at the 6th International Symposium on Computational Fluid Dynamics, Lake Tahoe, NA, September 4-8, 1995.

19. V. Shanmugasundaram, R. Ponnappan, J.E. Leland and J.E. Beam, "Effect of geometry on the conjugate heat transfer in a venturi-based cooling system," AIAA Paper 96-0362, 34th AIAA Aerospace Sciences Meeting & Exhibit, Reno, NV, Jan. 15-18, 1996.

20. V. Shanmugasundaram, J.E. Leland and R. Ponnappan, "A numerical study of conjugate heat transfer from a discrete heat source," AIAA Paper 96-1909, 31st AIAA Thermophysics Conference, New Orleans, LA, June 17-20, 1996.

21. Temple, V.A.K., "Mos-Controlled T hyristors - A New Class of Devices", IEEE Trans Electron Devices, Vol. ED-33 No. 10 pp. 1609-1618, Oct. 1986.

22. Reyes, A.S.; Nguyen, B.T.; Weimer, J.A.; Beam, J.E.; and Chow, L.C., "Operation Characteristics of a MOS Controlled Thyristor (MCT) Using a Liquid Cooling Approach". SAE Paper No. 929477, Proc. 27th IECEC, Vol. 2, pp. 2.405-2.410, Aug. 1992.

23. Radun, Arthur; and Richter, Eike, "A Detailed Power Inverter Design for a 250 kW Switched Reluctance Aircraft Engine Starter/Generator". SAE Paper No. 931388, 1993 SAE Aerospace Atlantic Conf. and Exposition April 20-23, 1993.

24. Ponnappan, R.; Leland, J.E.; Chang, W.S.; and Beam, J.E., "Results of a Single Phase Venturi Flow". Proc. 6th International Symposium on Transport Phenomena in Thermal Engineering, Seoul, Korea, May 9-13, 1993.

25. EG&G Wakefield Engineering. Innovative Thermal Management Solutions - Components for Liquid-Cooled Systems. Active Cooling Products Catalog 1988, Wakefield, MA.

26. MOS Controlled Thyristor - User's Guide and File No. 3374, Harris Semiconductor (DB307), Melbourne, FL 32902.

27. Power MOS IV IGBT - Technology Brochure Advanced Power Technology, Bend, OR 97702.

28. DuPont Electronics, Kapton Film General Specifications Bulletin GS-92-6, 8 pages, Wilmington, DE, 1992.

RELATED BIBLIOGRAPHIC REFERENCES

B1. W. Aung (Ed) Cooling Technology for Electronic Equipment, Hemisphere Publishing Corp., New York, 1988.

B2. D.S. Steinberg, Cooling Techniques for Electronic Equipment 2nd Edition, John Wiley & Sons Inc., New York, 1991.

B3. Advances in Electronic Packaging 1992, ASME EEP-Vol. 1-1 Proc. 1992, ASME/JSME Conf. on Electronic Packaging, W.T. Chen (Editor).

B4. C. Soule, "Yesterday's Cooling Won't Work on Tomorrow's Electronics", PCIM - Power Conversion & Intelligent Motion, Nov 1994, pp 34-36.

B5. V.W. Antonetti, S. Oktay, and R.E. Simons, "Heat Transfer in Electronic Packages," Ch. 4 in Microelectronic Packaging Handbook, Ed. R.R. Tummala, E.J. Rymaszewski, and A.G. Klopfenstein. Van Nostrand Reinhold, New York, 1989, pp. 167-224.

APPENDIX A

VENTURI TEST SECTION DRAWINGS

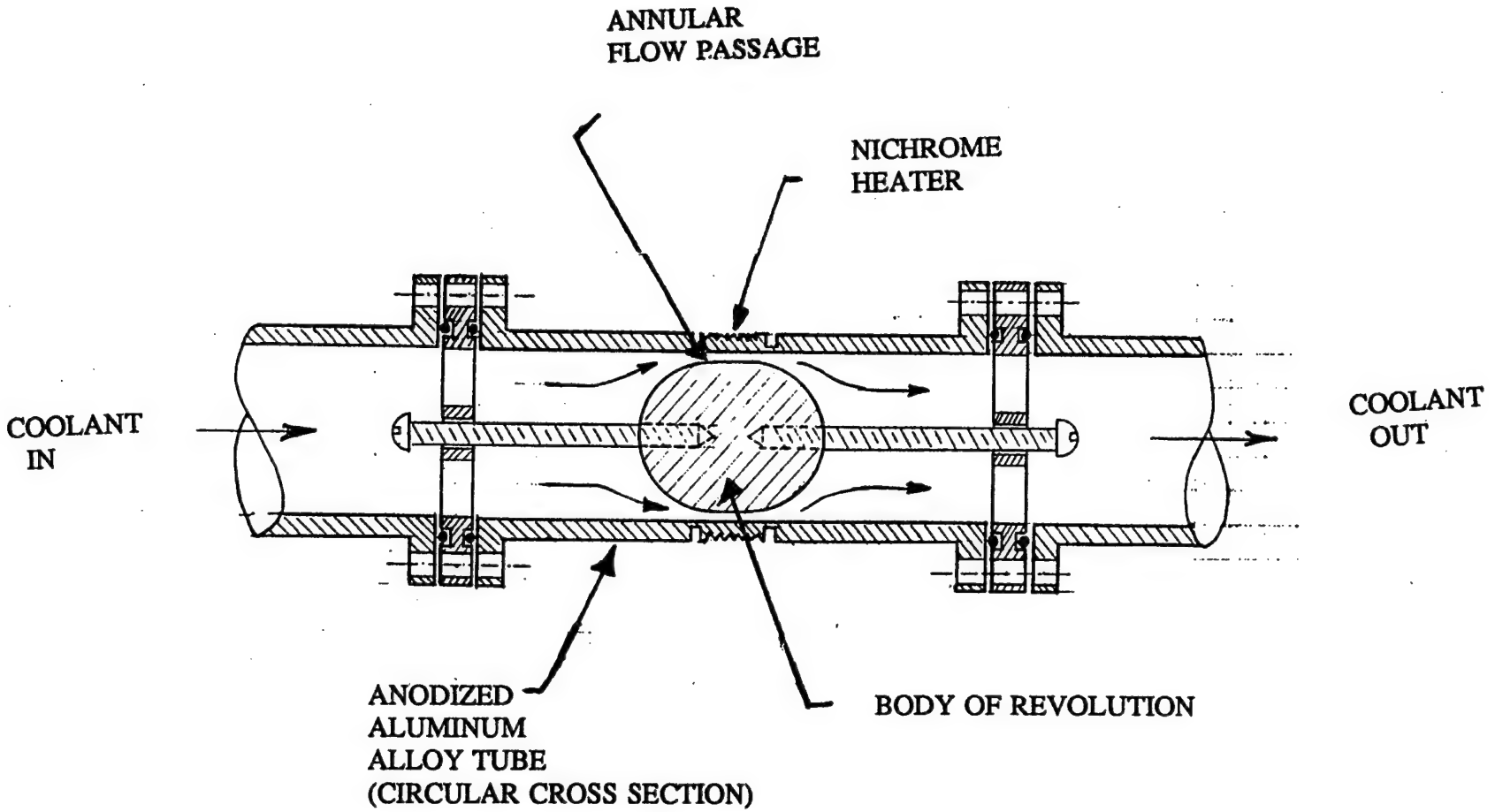
ANNULAR
FLOW PASSAGE
NICHROME
HEATER
COOLANT
IN
COOLANT
OUT
ANODIZED
ALUMINUM
ALLOY TUBE
(CIRCULAR CROSS SECTION)
BODY OF REVOLUTION

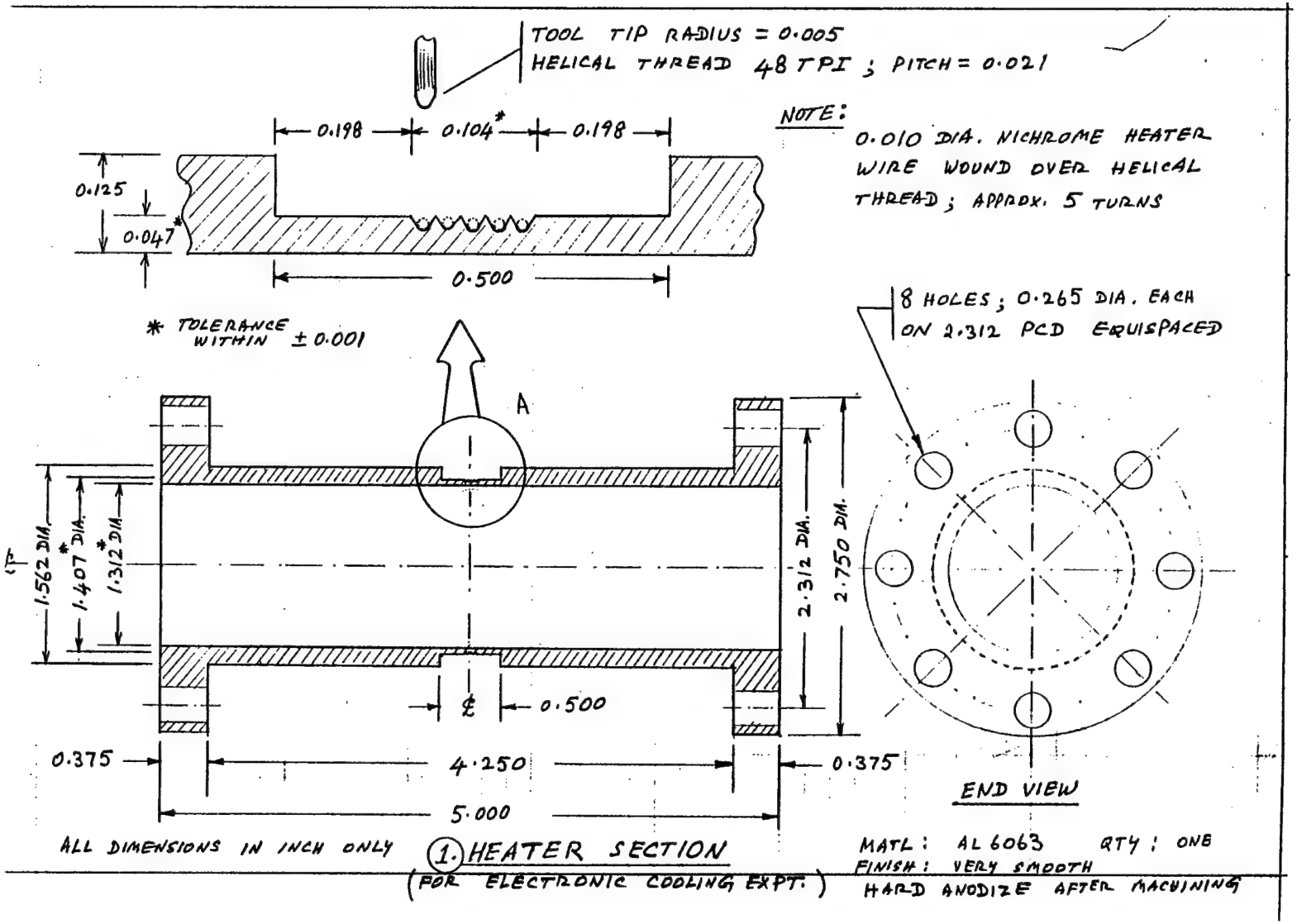
TOOL TIP RADIUS = 0.005
HELICAL THREAD 48 TPI ; PITCH = 0.021
NOTE:
0.010 DIA. NICHROME HEATER WIRE WOUND OVER HELICAL THREAD ; APPROX. 5 TURNS
0.198
0.104*
0.198
0.125
0.047*
0.500
* TOLERANCE WITHIN ± 0.001
8 HOLES ; 0.265 DIA. EACH ON 2.312 PCD EQUISPACED
A
1.562 DIA.
1.407* DIA.
1.312* DIA.
2.312 DIA.
2.750 DIA.
℄
0.500
0.375
4.250
0.375
5.000
END VIEW
ALL DIMENSIONS IN INCH ONLY
1. HEATER SECTION
(FOR ELECTRONIC COOLING EXPT.)
MATL : AL 6063 QTY : ONE
FINISH : VERY SMOOTH
HARD ANODIZE AFTER MACHINING

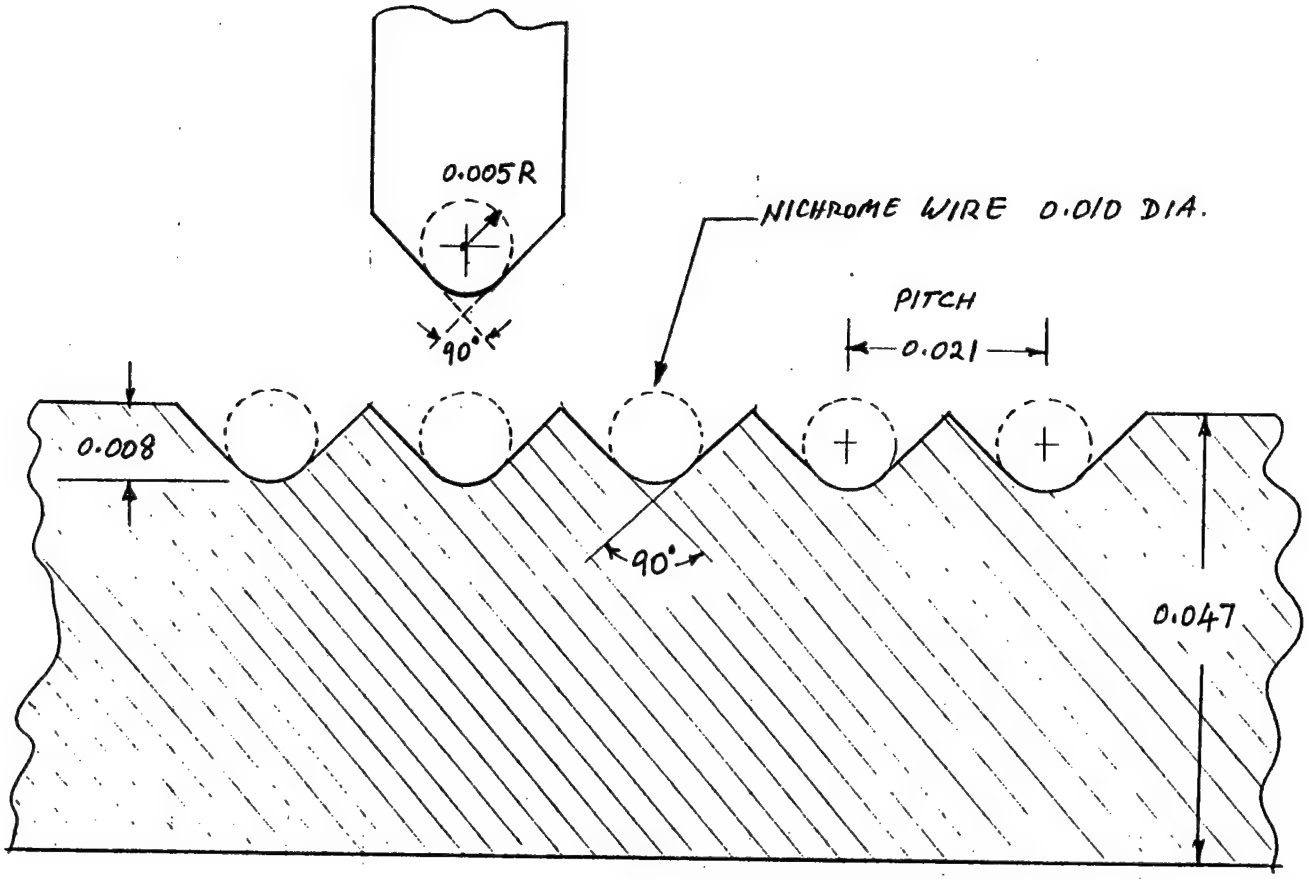

SCALE 50 : 1

DETAIL - A

NOTES

(A) DRILL AND TAP FOR #6-32 THREAD ON 1 OF 2 PIECES

(B) DRILL TROUGH HOLE DIA. 0.137 ON 1 OF 2 PIECES

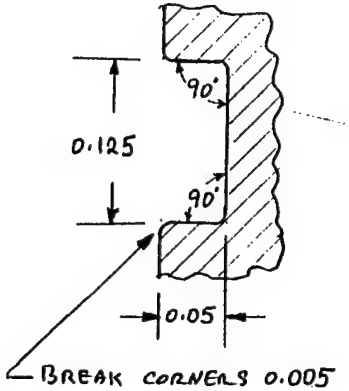

DETAIL OF GROOVES FOR O-RINGS

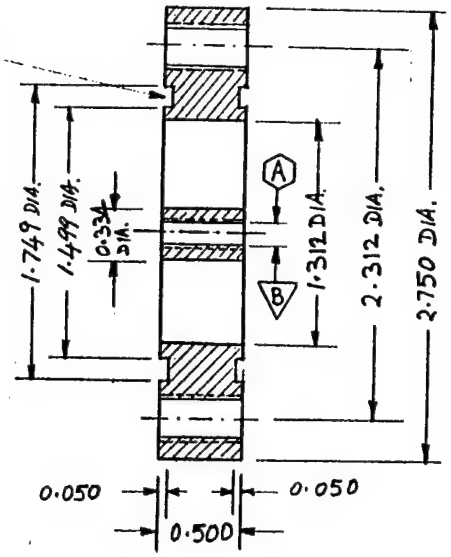

SECTION-BB

DRILL AND TAP 1/4-28 THREAD 8 HOLES EQUISPACED ON 2.312 PCD TO MATE WITH PART (1)

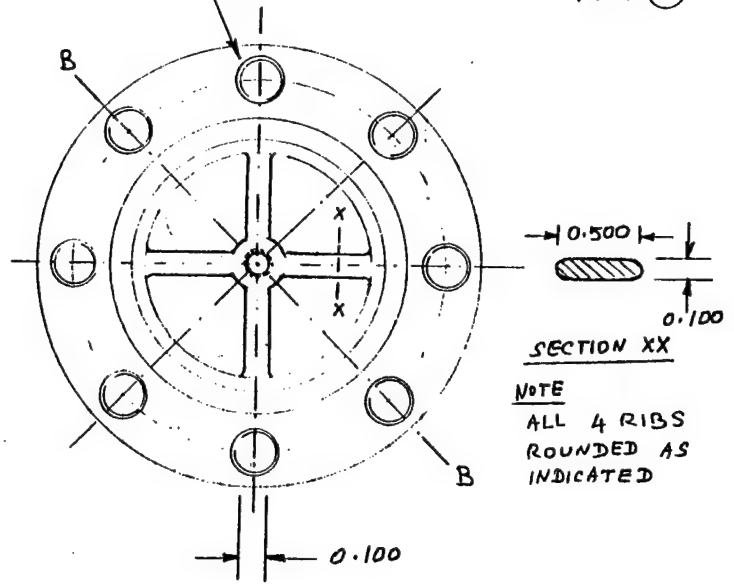

SECTION XX

NOTE
ALL 4 RIBS ROUNDED AS INDICATED

END VIEW

(2) O-RING FLANGE

MATL : SS304 QTY : 1 WITH (A) 1 WITH (B)

FINISH : VERY SMOOTH

O-RING TO FIT PART (2)

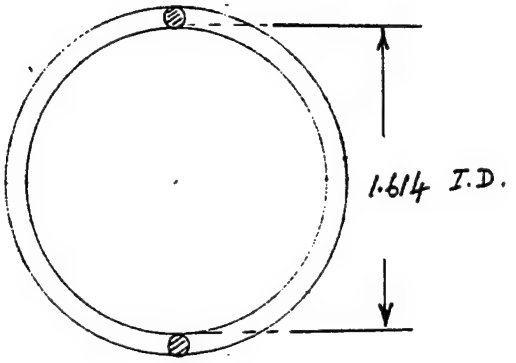

WIDTH OF O-RING W = 0.070

O-RING No. 030

MATL : NITRILE (BUNA N)
B46-70 HARDNESS 70°A
-37 TO 125°C

NATIONAL O-RINGS (MFR)

QTY : 4

(3), O-RING

(A) DRILL AND TAP FOR #6-32 THREAD TO MATCH PART (2)

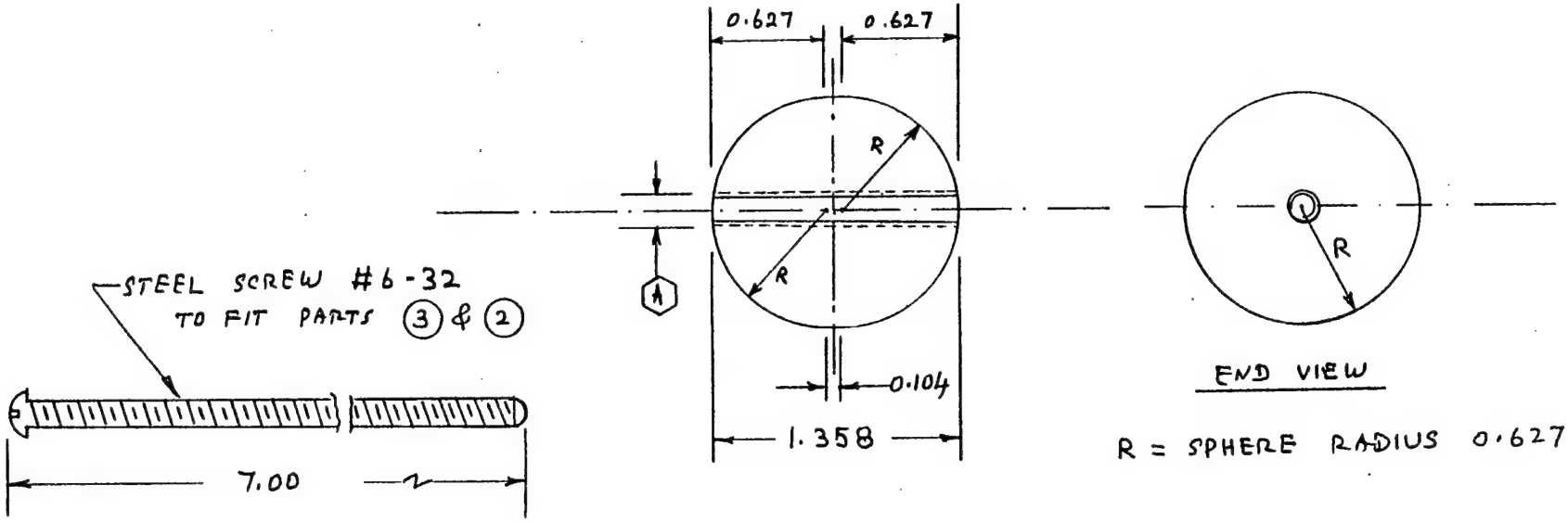

R = SPHERE RADIUS 0.627

(3.) SPHERICAL BALL & SCREW

MATL : AL 6063

QTY : ONE

FINISH : VERY SMOOTH

ALL DIMENSIONS IN INCHES ONLY
SCALE : 1:1

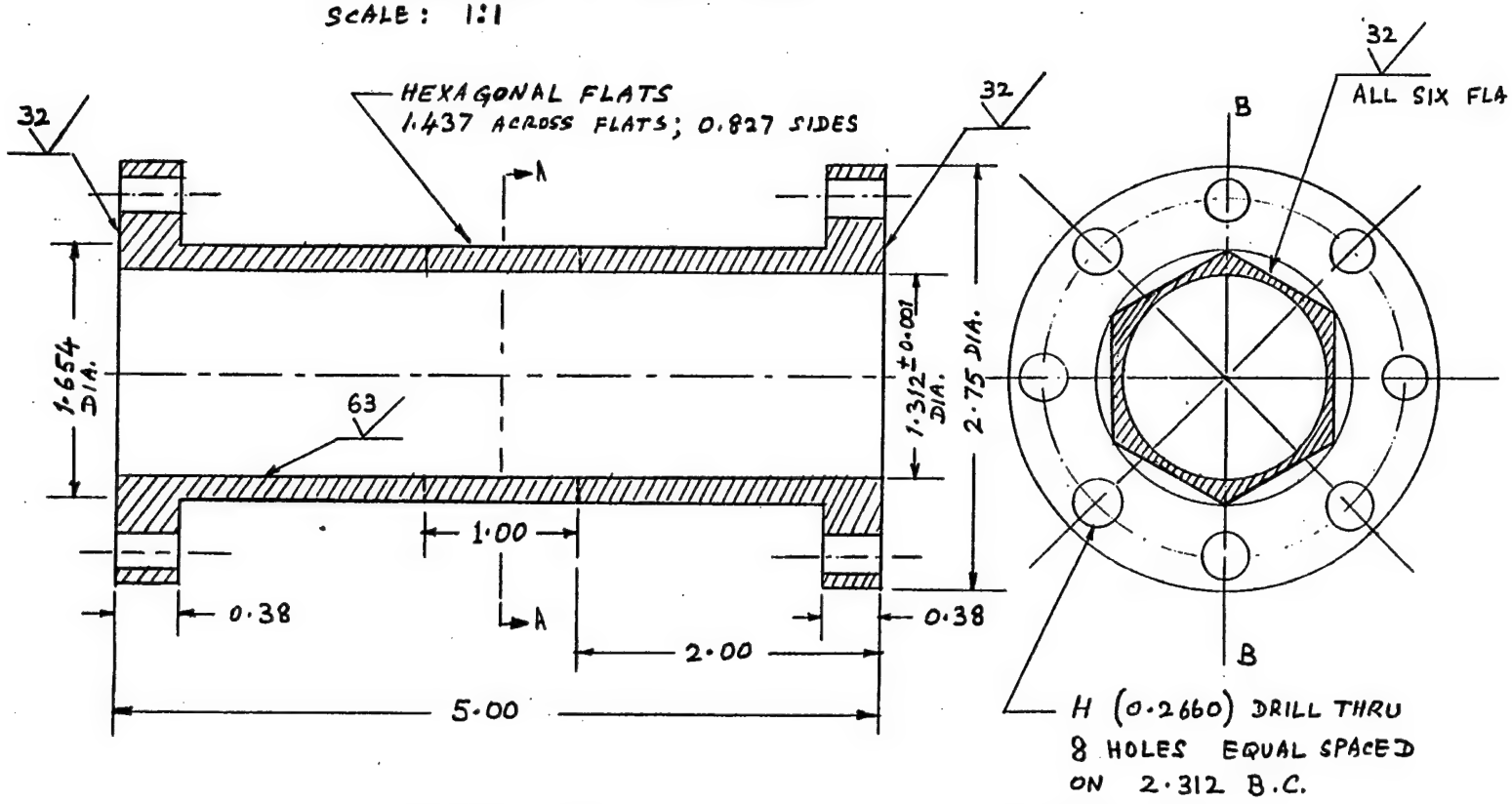

SECTION - BB

SECTION - AA

MATERIAL : COPPER
FINISH : AS SHOWN
QTY : ONE

(1) HEATER SECTION FOR VENTURI

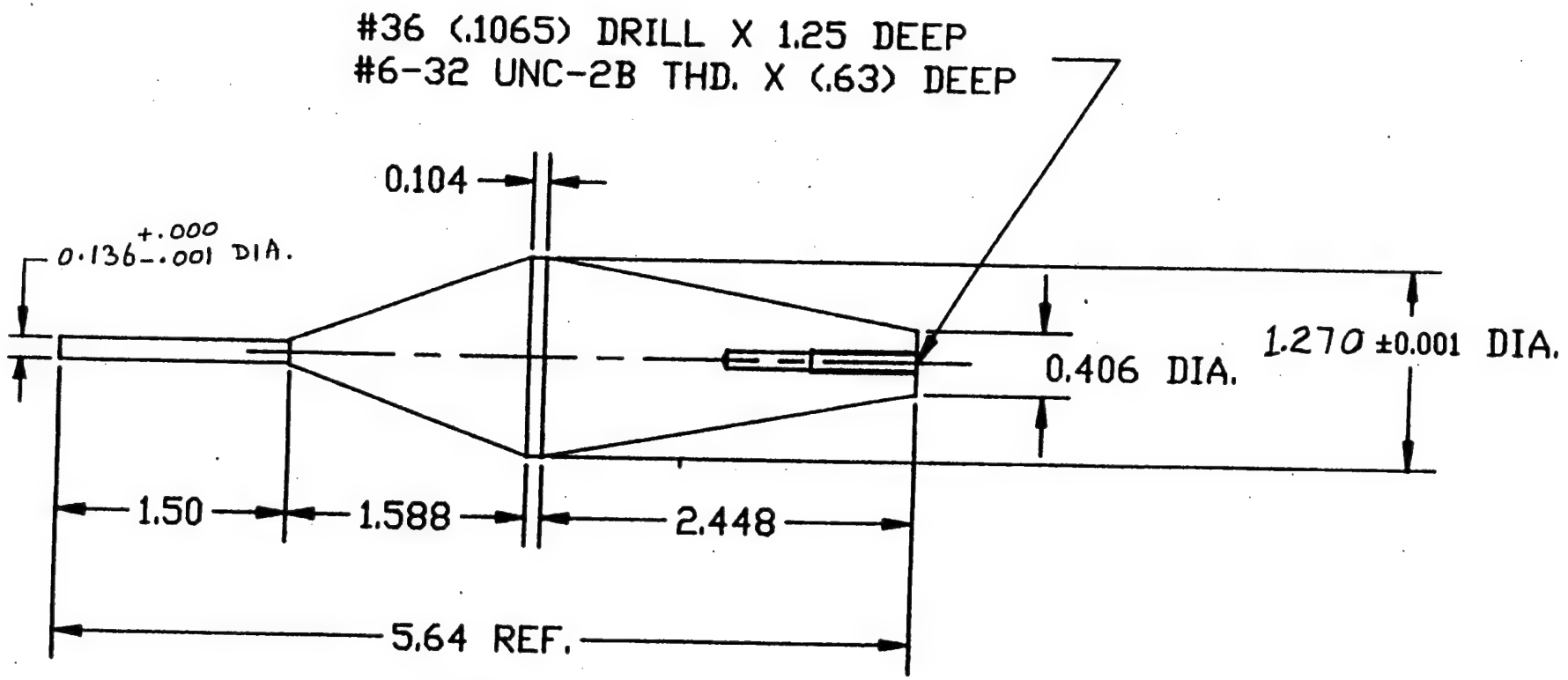

(3) BICONE 91005F-03

SCALE: 1:1

MATERIAL: SS 304

QTY: ONE

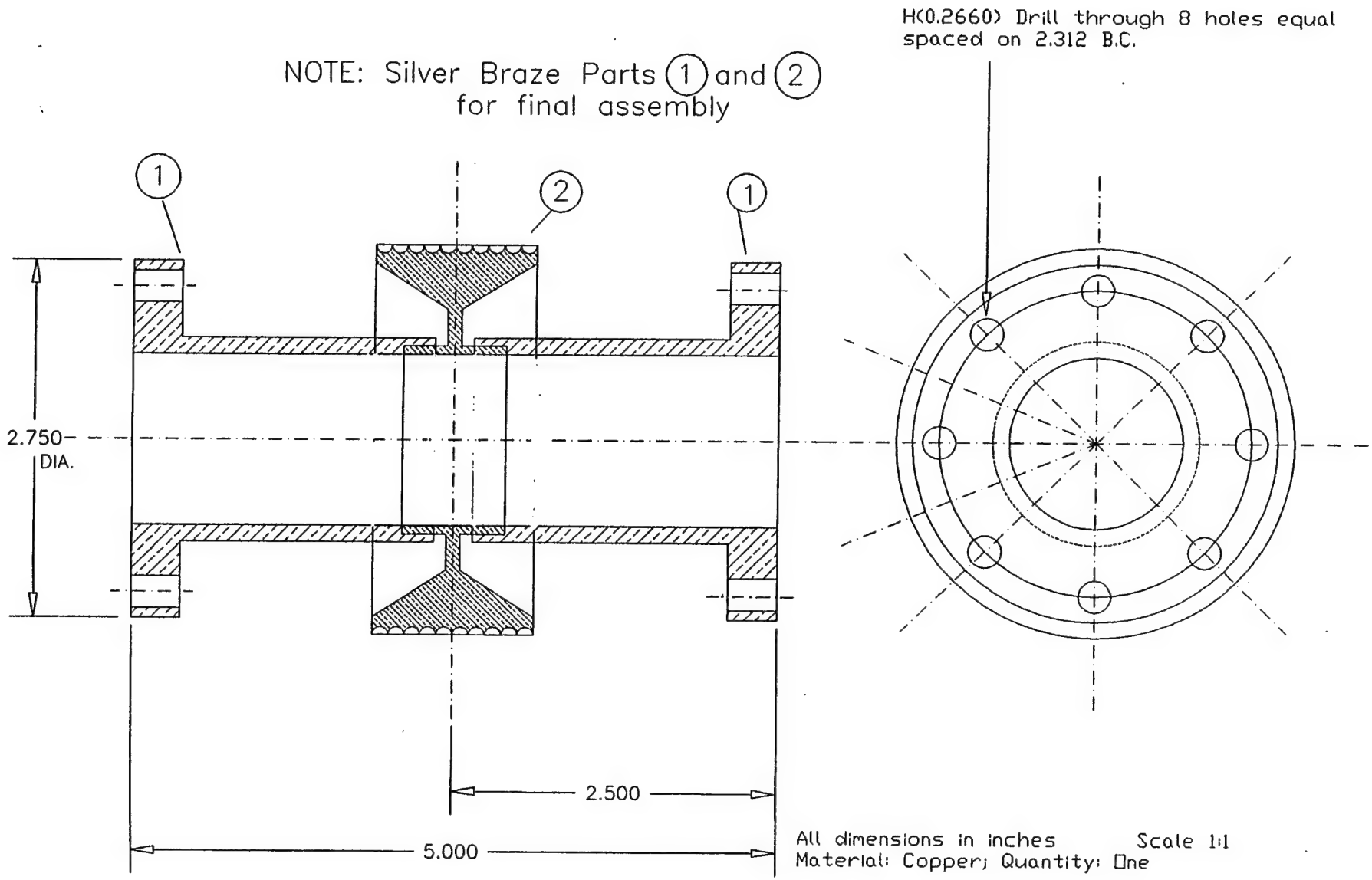

HEATER AND VENTURI TEST SECTION

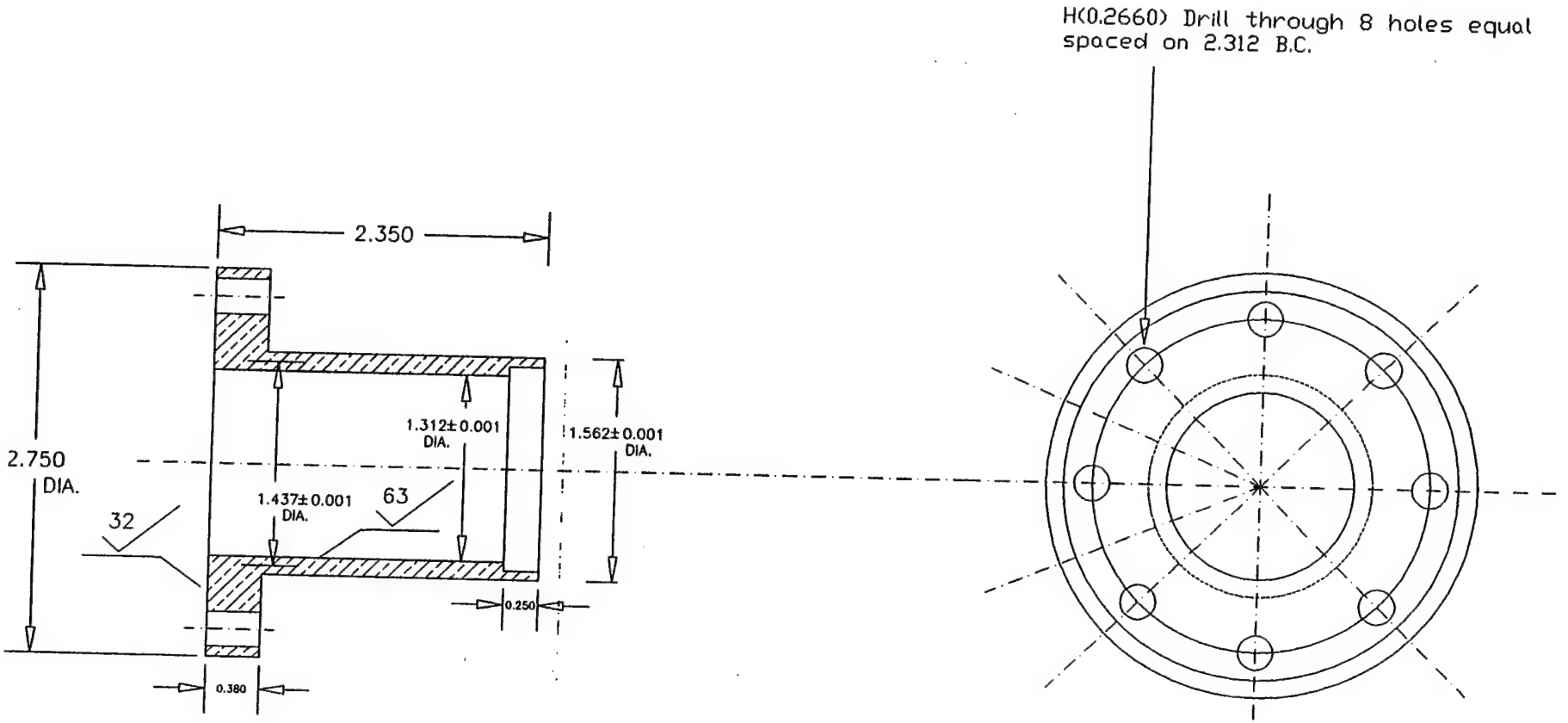

(1) VENTURI FLANGE TUBES

Quantity: Two Material: Copper

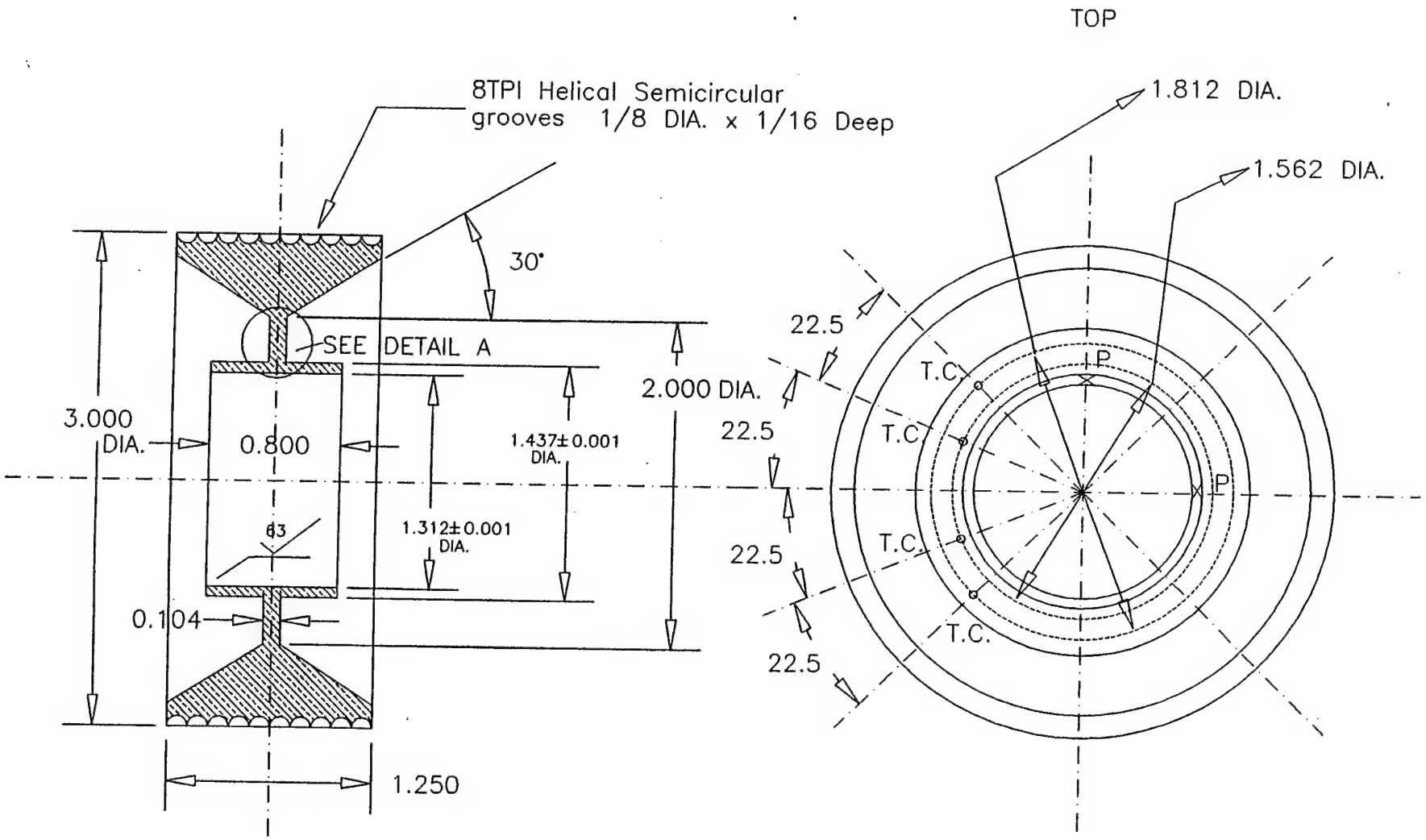

(2) VENTURI HEAT CONCENTRATOR

Quantity: One Material: Copper

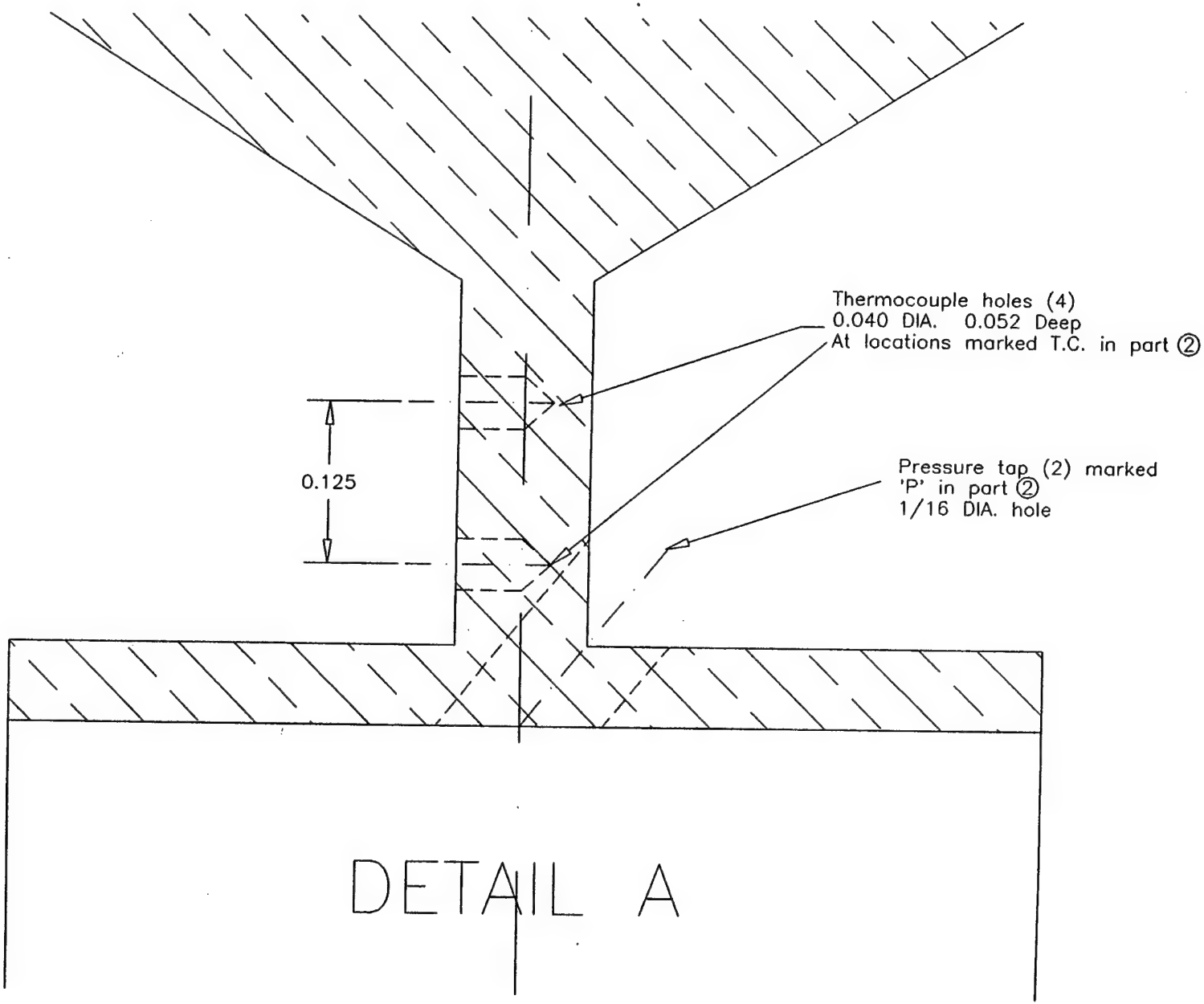
Thermocouple holes (4)
0.040 DIA. 0.052 Deep
At locations marked T.C. in part ②
Pressure tap (2) marked
'P' in part ②
1/16 DIA. hole
0.125
DETAIL A

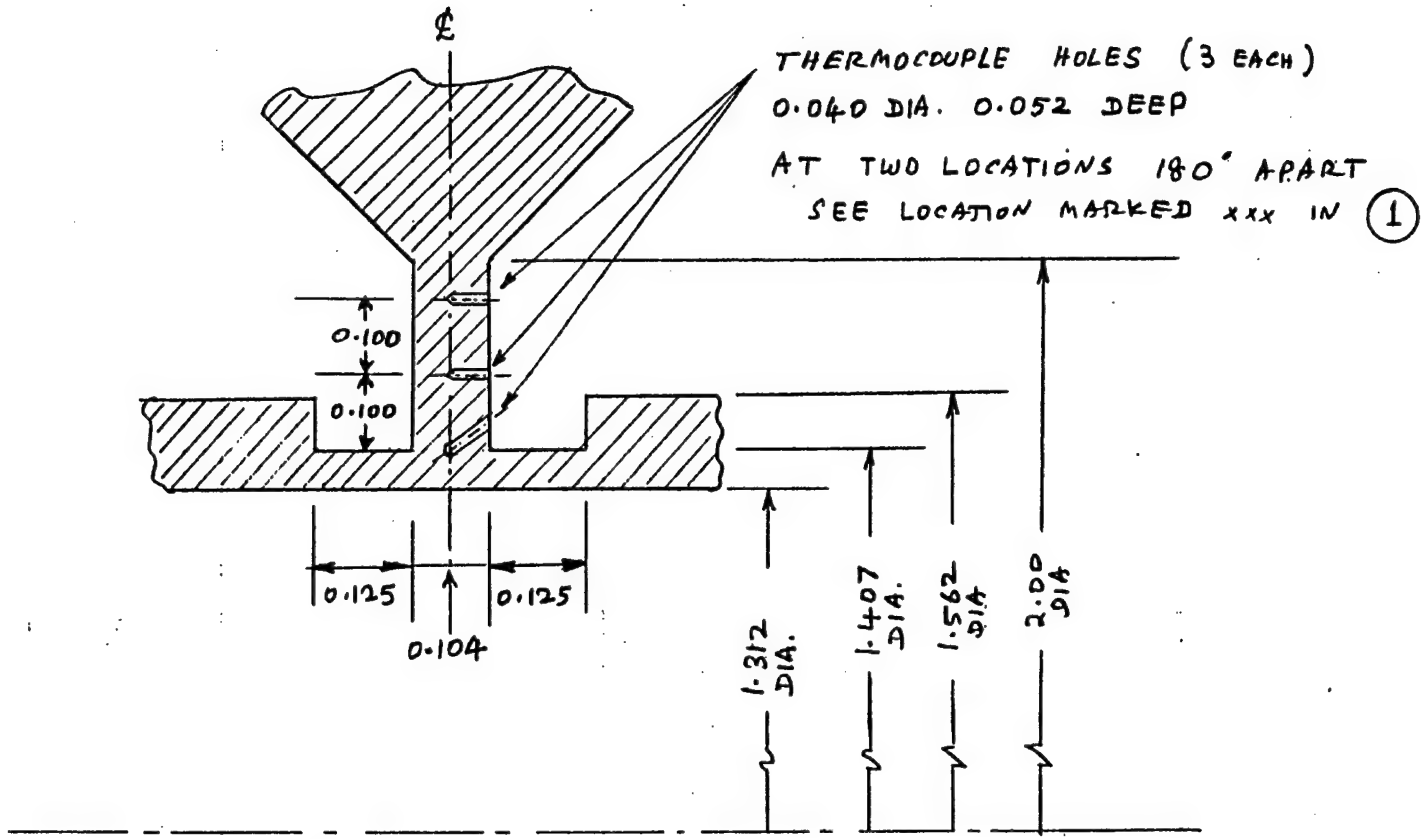

DETAIL - A

DIMENSIONS IN INCHES ONLY

SCALE : 4 : 1

FOR THERMOCOUPLE HOLES

APPENDIX B

FORTRAN CODE FOR VENTURI FLOW DATA ANALYSIS

```
      program ponn
      character*20 infile,outfile,answer,junk,date,config
      character*80 source
      real psiatop,psiasid
C*****************************************************************

      write(*,*) 'What is your TEST* input filename? (b:\test.dat)'
      read(*,714) infile
      write(*,*) 'What is your TEST* output filename? (b:\test.out) '
      read(*,714) outfile
 714  format(a20)
      open(7,file=infile,status='unknown')
      open(8,file=outfile,status='unknown')
      write(8,716) infile
  716 format(//,10x,'Input Data File Name:    ',a20)

C*****************************************************************

 5    WRITE(*,*)
      WRITE(*,*)
      WRITE(*,*) ' **** ENTER CONFIGURATION DATA ****'
      WRITE(*,*)
      WRITE(*,*) ' 1 = BICONE-1'
      WRITE(*,*) ' 2 = BICONE-2'
      WRITE(*,*) ' 3 = CIRCULAR'
      WRITE(*,*)
      WRITE(*,*) ' 9 = EXIT FROM PROGRAM'
      WRITE(*,*)
      READ(*,*) IANS
      if(ians.eq.9) goto 999
      if(ians.eq.1) goto 10
      if(ians.eq.2) goto 20
      if(ians.eq.3) goto 30
      write(*,*) 'Invalid response.  Please re-enter data.'
      goto 5

 10   continue
C************** Bicone-1 *************
c (units are inches)
      config='Bicone-1'
      dout=1.312
      din =1.255
      dhyd=dout-din
      throat=0.104
      condcu=3.8
      goto 31

 20   continue
C************** Bicone-2 *************
c (units are inches)
      config='Bicone-2'
      dout=1.312
      din =1.270
      dhyd=dout-din
      throat=0.104
      condcu=3.8
      goto 31

 30   continue
C************** Circular *************
```

```
c (units are inches)
        config='Circular'
        dout=1.312
        din =0.
        dhyd=dout
        throat=0.104
        condcu=3.8
        goto 31

 31     continue

C************** SPECIFY CONSTANTS ************************************

 35     WRITE(*,*)
        WRITE(*,*)
        WRITE(*,*) ' **** ENTER FLUID TYPE ****'
        WRITE(*,*)
        WRITE(*,*) ' 1 = WATER'
c       WRITE(*,*) ' 2 = PAO'
c       WRITE(*,*) ' 3 = TURBINE OIL'
        WRITE(*,*)
        WRITE(*,*) ' 9 = EXIT FROM PROGRAM'
        WRITE(*,*)
        READ(*,*) IANF
        if(ianf.eq.9) goto 999
        if(ianf.eq.1) goto 36
c       if(ianf.eq.2) goto 37
c       if(ianf.eq.3) goto 38
        write(*,*) 'Invalid response.  Please re-enter data.'
        goto 35

c ** water **
 36     condfld = 0.00608
        rho= 0.997
        cp = 4.186
        rnu= 9.e-7
        goto 39

c **  PAO  **
c37     condfld=
c       rho=
c       cp=
c       rnu=
c       goto 39
c
c ** turbine oil **
c38     condfld=
c       rho=
c       cp=
c       rnu=
c       goto 39
c
C********************** OTHER CONSTANTS ******************************
 39     iflowch=0
        wallthk=0.0625
        condwal=4.01
        disclen=0.104
        pi=4.* atan(1.)

C************** READ DATA FILE  ***************************************
```

```
      do 40 i=1,12
      read(7,714,end=888) junk
40    continue
      i=1
50    do 55 j=1,3
      read(7,714,end=999) junk
55    continue
      read(7,714,end=999) date
      read(7,714,end=999) junk
100   READ (7,1001,end=999) ihr,imin,isec
      write(*,*) ihr,imin,isec
      read(7,714,end=999) junk
      read(7,714,end=999) junk
      read(7,*,end=999) ival,tamb
      read(7,714,end=999) junk
      read(7,*,end=999) ival,tci1
      read(7,714,end=999) junk
      read(7,*,end=999) ival,tci2
      read(7,714,end=999) junk
      read(7,*,end=999) ival,tco1
      read(7,714,end=999) junk
      read(7,*,end=999) ival,tco2
      read(7,714,end=999) junk
      read(7,*,end=999) ival,heat5
      read(7,714,end=999) junk
      read(7,*,end=999) ival,heat6
      read(7,714,end=999) junk
      read(7,*,end=999) ival,heat7
      read(7,714,end=999) junk
      read(7,*,end=999) ival,heat8
      read(7,714,end=999) junk
      read(7,*,end=999) ival,heat9
      read(7,714,end=999) junk
      read(7,*,end=999) ival,heat10
      read(7,714,end=999) junk
      read(7,*,end=999) ival,heat11
      read(7,714,end=999) junk
      read(7,*,end=999) ival,heat12
60    do 65 j=1,7
      read(7,714,end=999) junk
65    continue
      read(7,*,end=999) ival,coil
70    do 75 j=1,9
      read(7,714,end=999) junk
75    continue
      read(7,*,end=999) ival,flow
c***** NOTE *****
      if(i.eq.1 .and. flow.lt.0.05) then
         write(*,*) flow,'  This Flow Data is INCORRECT'
         write(*,*) ' ** Enter Correct Flow Rate Data (gals/min)'
         read(*,*) cflow
         iflowch=1
      endif
      if(iflowch.eq.1) flow=cflow

      read(7,714,end=999) junk
      read(7,*,end=999) ival,tfiavg
      read(7,714,end=999) junk
      read(7,*,end=999) ival,tfoavg
```

```
          read(7,714,end=999) junk
          read(7,*,end=999) ival,tfavg
          read(7,714,end=999) junk
          read(7,*,end=999) ival,del56
          read(7,714,end=999) junk
          read(7,*,end=999) ival,del78
          read(7,714,end=999) junk
          read(7,*,end=999) ival,del910
          read(7,714,end=999) junk
          read(7,*,end=999) ival,del1112
          read(7,714,end=999) junk
          read(7,*,end=999) ival,delavg
          read(7,714,end=999) junk
          read(7,*,end=999) ival,qest
 80       do 85 j=1,19
          read(7,714,end=999) junk
 85       continue
          read(7,*,end=999) ival,htpowin
 90       do 95 j=1,19
          read(7,714,end=999) junk
 95       continue
          read(7,*,end=999) ival,psiatop
          read(7,714,end=999) junk
          read(7,*,end=999) ival,psiasid
          read(7,714,end=999) junk

          if(i.eq.1) then
          start=ihr*3600.+imin*60.+isec
          write(8,1005) config,date,ihr,imin,isec
          endif

          time=ihr*3600.+imin*60.+isec-start
          time=time/60.
c ** above calculates time from start in minutes

          write(8,1003) time

C****************** MAKE CALCULATIONS ********************
          if(i.eq.1) then
c           first convert inches to cm
            dout=dout*2.54
            din=din*2.54
            dhyd=dhyd*2.54
            wallthk=wallthk*2.54
            throat=throat*2.54
          endif
c convert flow rate from gals/min to liters/sec
          GALFLOW=flow
          flow=flow*3.7864/60.
c delta T  of coolant
          deltemp=tfoavg-tfiavg
c calculated Q
          qcal=rho*cp*flow*deltemp*1.e3
c Q est = channel 30 = qest
c Q in =htpowin * correction factor
          resis=12.48471+1.616924e-4*coil
          corfac=13.148/resis
          qin=htpowin*corfac
c Q loss
          qloss=(qin-qest)/qin * 100.
```

```
c flow c.s. area upstream
        aus=(pi*dout**2.)/4.
c flow velocity upstream
        vup=flow*1000./(aus*100.)
c upstream Reynolds number
        Reup=vup*dout*.01/rnu
c heat addition area at throat w/o conduction spread
        at1=pi*dout*throat
c heat addition area at throat w/ 45 degree conduction spread
        at2=pi*dout*(throat+2.*wallthk)
c amplification factor
        f=1./(1.-(din/dout)**2.)
c throat velocity
        vthr=vup*f
c throat Reynolds number
        Rethr=vthr*dhyd*.01/rnu
c delta T 2-w
        delt2w=qest*alog(1.562/1.312)/(2.*pi*condcu*throat)
c avg T2
        t2bar=(heat6+heat8+heat10+heat12)/4.
c wall throat temp
        twbar=t2bar-delt2w
c heat transfer coefficients
c w/o conduction spread
        hc1=qest/(at1*(twbar-tfavg))
c with conduction spread
        hc2=qest/(at2*(twbar-tfavg))
c heat fluxes
c w/o conduction spread
        q1=qest/at1
c with conduction spread
        q2=qest/at2
c throat pressure
        thrtpr=(psiatop+psiasid)/2.
c
C************** RESISTANCE DATA ************************************


        write(8,1020) dout,din,dhyd,wallthk
        write(8,1030) flow,galflow,tfiavg,tfoavg,deltemp,tfavg
        write(8,1040) vup,reup,vthr,rethr,f
        write(8,1050) qcal,qin,qest,qloss
        write(8,1060) t2bar,twbar,hc1,q1,hc2,q2
        write(8,1070) thrtpr
        i=i+1
        goto 50

 888    write(*,*) 'missing part of data file'
        goto 999

 1001   format(1x,i2,1x,i2,1x,i2)
 1003   format(10x,'Time = ',1x,f9.4,/)
 1005   format(/,10x,'Configuration: ',a20,//,10x,a20, 5x,
     +  'start time = ',i2,':',i2,':',i2,///)
 1020   format(10x,'Outer diameter      (cm)',2x,f7.4,/,
     +         10x,'Inner diameter      (cm)',2x,f7.4,/,
     +         10x,'Hydraulic diameter (cm)',2x,f7.4,/,
```

Sample Output Data for Modified Venturi Test Setup

```
Input Data File Name:     112592a.dif

Configuration: Bicone-2

"25 NOV 92"                start time = 10:10:26


Time =       .0000

Outer diameter       (cm)    3.3325
Inner diameter       (cm)    3.2258
Hydraulic diameter   (cm)     .1067
Wall thickness       (cm)     .1587

Coolant flow rate (liters/sec)      .6311
                  (gallons/min)   10.0000

Fluid inlet temp          (C)     19.8010
Fluid outlet temp         (C)     20.2780
Fluid delta T,   To-Ti    (C)       .4770
Avg fluid temperature     (C)     20.0400

Velocity    (upstream)   m/s           .7235
Reynolds #  (upstream)              26790.1600
Velocity    (throat)     m/s         11.4845
Reynolds #  (throat)                13612.9700

 Velocity amplification factor =    15.8731

 Heat Flow Calorimeter   (W)    1256.2830
 Heat Flow In Digimeter  (W)    1126.7660
 Heat Flow Actual        (W)     893.0500
 Heat Flow Losses %               20.7422


 Temp at 2 avg         (C)    55.825
 Temp at throat wall   (C)    31.129

WITHOUT CONDUCTION SPREAD
h =    29.121 W/cm**2 C    heat flux =  322.917 W/cm**2

WITH CONDUCTION SPREAD
h =    13.225 W/cm**2 C    heat flux =  146.652 W/cm**2


 Throat Pressure =    10.485 psia
```

APPENDIX C

C.1 UNCERTAINTY ANALYSIS FOR ESTIMATION OF POWER IN HEATMETER MEASUREMENTS

C.2 UNCERTAINTY ANALYSIS FOR CALORIMETRIC MEASUREMENTS

C.1 UNCERTAINTY ANALYSIS FOR ESTIMATION OF POWER IN HEATMETER MEASUREMENTS

The heat flow through the thin copper disc in the heatmeter was calculated using the experimentally measured parameters, ℓ_t and ΔT_{12}, and known property data for copper, k, using radial conduction equation.

$$Q_{12} = \frac{2\pi k \ell_t \Delta T_{12}}{\ell n (d_1/d_2)}$$

Thermal conductivity is known from standard tables with ±0.5% uncertainty. The length of the disc (ℓ_t) is measured using vernier caliper with ±0.001 inch which amounts to ±1.0% uncertainty in measuring 0.104 inch. The ΔT measurement contributed the highest level of uncertainty and it varied with the operating power level. The type T thermocouple and the Fluke datalogger used in this experiment had a combined uncertainty of ±0.3°C in the range of 20 to 200°C. This level of accuracy was obtained by calibration against a RTD secondary standard which was accurate to within ±0.03°C. The measured ΔT varied from 1.9°C to 21.2°C in the power range of 80 W to 900 W. Hence, the uncertainty for ΔT varied from 15.8% at 80 W to 1.4% at 900 W. Summarizing the individual uncertainties, we have

Parameter	Uncertainty, $u_{\Delta T}$
Thermal conductivity, k	0.5%
Length, ℓ_t	1.0%
Temperature difference, ΔT	15.8 to 1.4%

The maximum uncertainty of this experimental Q measurement was obtained by the Pythagorean summation as described in, "Mechanical Measurements," by Beckwith, Buck and Marangoni; Addison-Wesley Publishing Co., 3rd Edition 1982; pp. 268-273.

Systematic uncertainty = $\left[(1)^2 + (0.5)^2 + (1.4 \text{ to } 15.8)^2\right]^{1/2}$

The heatmeter method of power measurement in this test had the following uncertainty:

Power (W)	ΔT (°C)	$u_{\Delta T}$ (%)	Uncertainty (%)
80	1.9	15.8	15.84
200	4.7	6.4	6.5
400	9.4	3.2	3.4
600	14.1	2.1	2.4
900	21.2	1.4	1.8

C.2 UNCERTAINTY ANALYSIS FOR CALORIMETRIC MEASUREMENTS

The heat gain in the cooling water at the test section is calculated using,

$$Q_{calorimeter} = \dot{V}\rho C_p\left(T_{f,out} - T_{f,in}\right) = \dot{V}\rho C_p \Delta T$$

The property data for water, ρ and C_p are obtained from standard tables with ±0.5% uncertainty. The volume flow rate, $\dot{V}$, was measured using two flowmeters. One was a turbine type electronic flowmeter (Omega Model FP-541 and FLSC-720 system) in 0-5 gpm range and the other was a piston and spring type (Omega Model FL6316 BR) in 5-10 gpm range. The uncertainties of these meters were ±1.0% and ±4.0%, respectively. These values were manually verified by recording the time for collecting a known quantity of the fluid. The type T thermocouples and the Fluke datalogger used in this experiment had a combined uncertainty of ±0.3 °C in the range of the coolant temperature variation, 5 to 35 °C. These accuracy data were verified by calibrating against a RTD secondary standard which was accurate to within ±0.03 °C. However, the uncertainty associated with the small ΔTs of the present tests result in high percentages, namely, ±30% for ΔT = 1 °C and ±12% for ΔT = 2.5 °C. Corresponding to the power input range of 100 to 1200 W. Hence, the overall maximum uncertainty in the calorimetric measurement is calculated as $\left[(1)^2 + (0.5)^2 + (0.5)^2 + (12 \text{ to } 30)^2\right]^{0.5} = 12.1 \text{ to } 30\%$ for 0 to 5 gpm flow rate and $\left[(4)^2 + (0.5)^2 + (0.5)^2 + (12 \text{ to } 30)^2\right]^{0.5} = 12.7 \text{ to } 30.3\%$

NOMENCLATURE

A, A_1	Flow area upstream
A_e	Effective area of convection heat transfer from wall to fluid
A_t, A_2	Flow area at throat
C_p	Specific heat of fluid
D	Diameter for heater wire winding
D_h	Hydraulic diameter
d	Nichrome heater wire diameter
d_1, d_2	Diameters at thermocouple positions 1 and 2
d_i	Inner diameter of the throat annulus
d_o	Outer diameter of the throat annulus
E	Applied voltage to the heater
F	Velocity amplification factor
f	Friction factor
g	Gravitational constant
H	Head loss due to friction
$\bar{h}_c, h_1, h_2$	Average heat transfer coefficient
h,K	Overall conductance factor
k	Thermal conductivity
k_s	Thermal conductivity of solid (copper)
ℓ	Length of venturi test section
l_e	Effective heat addition length
l_t	Length of throat region
ℓ_t, ℓ_2	Length of throat region
$\dot{m}$	Mass flow rate
Nu	Nusselt number
$\bar{Nu}$	Average Nusselt number in the thermal entry length
P	Pitch of formed screw thread for heater winding
Pr	Prandtl number

NOMENCLATURE (CONT'D.)

Q_{IN}	Heat input
Q_{12}	Heat flow defined in Eq. (20) = $Q_{Heatmeter}$
Q_{in}	Heat input to heater
Q_L	Heat loss Eq. (22)
Q_o	Heat flow from wall to fluid = $Q_{Heatmeter}$
q	Heat flux
Re	Reynolds number
R_{JC}, θ_{JC}	Junction-to-case thermal resistance
R_{DF}, θ_{DF}	Device-to-fluid thermal resistance
$T_f, \bar{T}_f$	Fluid temperature; Average measured fluid temperature
$T_w, \bar{T}_w$	Wall temperature; Average measured wall temperature
t_w	Tube wall thickness at the throat
V, V_1	Upstream flow velocity
V_t, V_2	Throat flow velocity
V	Volume flow rate
v_t	Volume of fluid at throat
α, β	Cone angles of the Bicone flow constrictor
μ	Dynamic viscosity of fluid
ν	Kinematic viscosity
ρ	Density
ρ_o	Specific resistance of heater wire
Φ	Viscous dissipation per unit volume
Φ_T	Total viscous dissipation
ΔT_w	Wall temperature difference Eq. (18)
ΔT_f	Rise in fluid temperature ($T_{f,out} - T_{f,in}$)
ΔT_{2w}	Temperature difference Eq. (23)
ΔT_{wf}	Wall to fluid temperature difference ($\bar{T}_w - \bar{T}_f$) (Eq. (18)

ABBREVIATIONS

AWG	American wire gage
CHF	Critical heat flux
CVD	Chemical vapor deposition
FC	Fluorocarbon fluids series (3M Company)
gpm	Gallons per minute
IGBT	Insulated gate bipolar transistor
ID	Inner diameter
lpm	liters per minute
L/D	Length-over-diameter ratio
MCT	Metal oxide semiconductor controlled thyristor
OD	Outer diameter
PAO	Poly-Alpha-Olefin (synthetic coolant)
PHOENICS	Computational computer code licensed software by CHAM of North America, Inc.
RCD	Resistor, capacitor and diode circuit